4-2011

Geological Controls on Reservoir Quality and Geologic Carbon Sequestration Potential in the Upper Cambrian Mount Simon Sandstone

Kyle Patterson
Western Michigan University

GEOLOGIC CONTROLS ON RESERVOR QUALITY AND GEOLOGIC CARBON SEQUESTRATION POTENTIAL IN THE UPPER CAMBRIAN MOUNT SIMON SANDSTONE

by

Kyle Patterson

A Thesis
Submitted to the
Faculty of The Graduate College
in partial fulfillment of the
requirements for the
Degree of Master of Science
In Geology
Advisor: David Barnes Ph.D.

Western Michigan University
Kalamazoo, Michigan
April 2011

ACKNOWLEDGMENTS

I would like to thank my committee for their insight and patience, I would like to thank my family and friends for their support and I would like to thank Michigan Geologic Repository for Research and Education (MGRRE), for whom without the research would not have been possible.

Kyle Patterson

GEOLOGIC CONTROLS ON RESERVOIR QUALITY AND GEOLOGIC CARBON SEQUESTRATION POTENTIAL IN THE UPPER CAMBRIAN MOUNT SIMON SANDSTONE

Kyle Patterson, M.S.

Western Michigan University, 2011

The Upper (?) Cambrian Mount Simon Sandstone is an important deep saline geological carbon sequestration (GCS) target throughout the Midwest, USA. The distribution of sedimentary facies, primary mineralogy, and diagenetic alterations and the relationship to wireline log response and reservoir quality throughout the Michigan basin are not well known. This study uses rock core, thin section point counts, x-ray diffraction, inferred spectroscopy, conventional core plug porosity and permeability and pressure fall-off test data to constrain wireline log interpretations of regional geology and reservoir quality.

Prior to the permitting of a CO_2 sequestration project, documentation of a robust transient injection model is needed to predict the possible outcomes of CO_2 injection. The first step to creating a reliable transient model is creating a sound static geologic model. This study created static geologic models for two locations in Michigan using Schlumberger's Petrel. Gamma ray, wireline log porosity and wireline log estimated permeability were all modeled.

TABLE OF CONTENTS

Table of Contents - continued

CHAPTER

Table of Contents - continued

Table of Contents - continued

APPENDICES

APPENDICES

LIST OF TABLES

LIST OF FIGURES

CORE DESCRIPTIONS
Attached

CHAPTER I

INTRODUCTION

The Upper (?) Cambrian Mount Simon Sandstone is an important deep saline geological carbon sequestration (GCS) target throughout the Midwest, USA. Regional assessment and site characterization studies to date suggest that the Mount Simon may have total GCS capacity in excess of 29 Gt in Michigan and the capacity for industrial scale GCS in many areas (Barnes et al., 2009).

The objective of this study is to assemble and analyze available subsurface geological data including: conventional core, core analysis, petrographic thin sections, wireline log, x-ray diffraction (XRD), infrared spectroscopy and pressure transient data to evaluate the geological controls on the regional variability in reservoir quality and injectivity in the Mount Simon Sandstone and related strata in Michigan. This analysis will lead to a more reliable assessment of regional Mount Simon Sandstone GCS potential in Michigan including CO_2 storage capacity, injectivity, and entrapment/storage permanence potential, and provide geological characterization input data for use in numerical models simulating CO_2 injection.

The most abundant source of subsurface data in the Mount Simon Sandstone of Michigan is wireline log data collected from wells drilled into the formation. Previous research in the Mount Simon of Michigan depicts the formation as a homogenous quartzose blanket sandstone. Little detailed work has been done to refute this interpretation. Although the Mount Simon Sandstone has been subdivided into three distinct electro-facies in the Midwest (Medina et al., 2010; Barnes et al., 2009), wireline log response in this unit and related strata varies in character across the Michigan basin (Kelley 2010). The distribution of sedimentary facies, primary mineralogy, and diagenetic alterations and the relationship to wireline log response and reservoir quality throughout the Michigan basin are not well known.

Gamma Ray (GR) log response is typically interpreted to be inversely proportional to grain size and, by extension, representative of reservoir quality potential in terrigenous clastics dominated successions (Posamentier, 1999; Emery and Myers, 1996). Preliminary work in the Mount Simon (Kelley et al., 2010) suggests that: (1) in many areas spatial variation of K-feldspar content, rather than grain size, is directly correlated to GR log response, (2) GR log response is neither clearly nor consistently related to reservoir quality, and (3) previous geologic carbon storage calculations eliminating prospective reservoir rock with high (above ~50 API) GR log response and high K-feldspar content significantly underestimate regional storage capacity in the Mount Simon Sandstone in Michigan. This study correlates core, thin sections and mineralogical data to wireline logs in order to better understand the relationship between log response and reservoir quality.

Barnes et al. (2009) calculated the regional GCS capacity in the Mt. Simon Sandstone to be 29 Gt. Most of the geological characterization data used in that study was concentrated in southwestern Lower Michigan. This study investigates the regional variation in textural, mineralogical, and petrophysical properties of the Mount Simon and related strata using conventional core plug measured porosity-permeability and petrographic analysis in order to establish the relationships amongst effective porosity and wireline log data: GR, neutron porosity (NPHI) and bulk density (RHOB). These relationships are used to correlate and model the distribution of petrophysical properties.

Most, if not all successful CO_2 sequestration projects will require a transient injection model prior to permitting. The first step to creating a quality transient model is the formulation of a robust, static geologic model. Barnes et al. (2009) created a simple 2-D transient CO_2 injection model with data from the western portions of Michigan. Two 3-dimensional static models have been created in this study with Schlumberger's Petrel as a preliminary step for running transient CO_2 injection simulations.

The Michigan Basin

The Michigan Basin is nearly circular in shape, covers approximately 300,000 km^2 (Catacosinos, 1973) and has accumulated about 5 km of sediment near the center of subsidence in Bay County, Michigan (Howell, 1999). Michigan Basin strata generally dip approximately 1° or less toward the center of the basin, though there are local variations that occur due to gentle folding (Briggs, 1968). Several studies have been published concerning the mechanism driving subsidence in the Michigan Basin, however the basin's irregular rate of subsidence makes it difficult to validate a solitary subsidence mechanism. Howell and van der Pluijm (1999) suggest that the basin's change in subsidence patterns reflect the change in subsidence mechanisms.

As such it has been interpreted that there have been multiple mechanisms driving subsidence of the Michigan basin over geologic time.

Fisher et al. (1988) and Fisher (1981) suggest that reactivation of Keweenawan age grabens due to changes in regional stresses are responsible for structural deformations that took place from the beginning of the Paleozoic and culminate at the end of the Mississippian. Major uplift of many of the basin fault blocks took place in the Mississippian time, though the majority of the fault displacements ended during the deposition of the Devonian Dundee formation (Fisher, 1988). Fisher (1981) suggests that the structural trends form a rectilinear pattern parallel to sub-parallel relative to the Midcontinental Rift System. The structures are believed to have formed due to the movement of basement blocks either vertically or horizontally in response to regional stresses (Fisher, 1981).

During the Cambrian, the Michigan Basin was roughly 15° south of the equator (Blakey, 2005). The basin configuration during this time period is interpreted to be a trough-like structure with an axis oriented north-east to south-west (Barnes et al., 2009). Stratigraphic evidence indicates that the Mt. Simon sandstone was deposited unconformably on crystalline and other Precambrian rocks (Catacosinos et al., 2001). The Michigan basin had a relatively low sedimentation rate in comparison to other basins, i.e. the Appalachian or Cordilleran foreland basins (Sloss, 1988).

Stratigraphy

Mount Simon

The Mt. Simon sandstone is named after an exposure at Mt. Simon Hill in Eau Claire County, Wisconsin (Walcott, 1914). In the Michigan Basin, the Mt. Simon sandstone blankets the underlying Precambrian rocks with the exception of isolated paleo-topographic highs that were present prior to the deposition of the Mt. Simon (Figure 1) (Fisher, 1988). The Mt. Simon sandstone in Michigan's Lower Peninsula is not exposed at the surface, therefore all available lithologic descriptions in the basin are derived from well cutting samples, rock core and petrophysical logs. In western Michigan three electro-facies have been identified by Barnes et al. (2009) and Medina et al. (2009) (Figure 2): a poorly sorted lower feldspathic sandstone facies, a middle quartzose sandstone facies, and an upper feldspathic and argillaceous facies (Kelley, 2010).

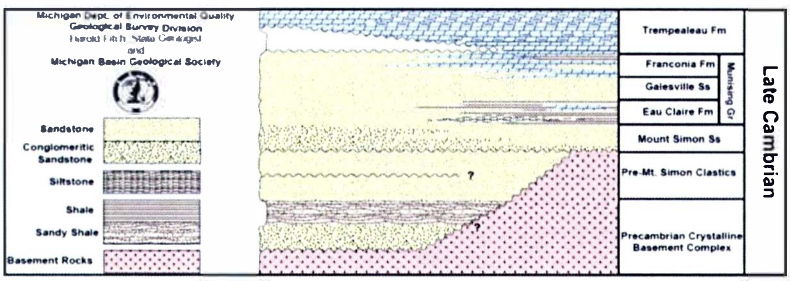

Figure 1: Lower Paleozoic stratigraphy of Michigan. Modified from Catacosinos et al. (2001). This stratigraphic column represents the variation of the lower Paleozoic strata from Michigan's Northern Peninsula (the left of the image) to center of the basin in the Lower Peninsula (the right of the image). The presence of paleotopographic highs are not represented on this image.

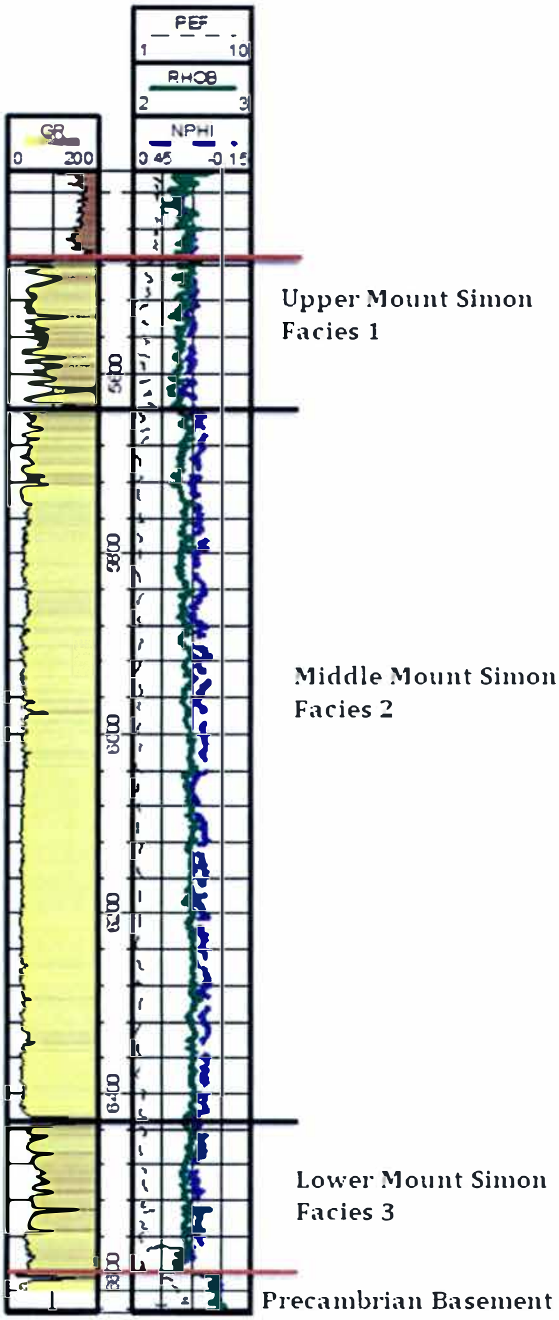

Figure 2: Wireline log facies of western Michigan. Single well cross section from the Mirant IW #1 in Ottawa County. This wireline log suite is representative for the Mount Simon in Western Michigan. The increased GR signature and NPHI curve, decreased RHOB and rapidly changing PEF curve in the Upper Mt. Simon reflects a more shale rich interval. The Middle Mt Simon is a quartzose sandstone facies with very little fluctuations in the GR, RHOB or PEF curves. The Lower Mt. Simon facies is a poorly sorted fluvial, feldspathic sandstone facies. The Lower Mt. Simon facies varies greatly throughout the basin in thickness and signature.

Driese et al. (1981) published detailed facies descriptions using data gathered from twenty-six outcrops in Wisconsin. Dreise described three depositional facies and suggests that the base of the Mt. Simon sandstone consists of laterally discontinuous sequences of braided fluvial and marine foreshore deposits. The succession is transitional up section into a mid-tidal flat facies at the top of the formation. Relative to the outcrops of Wisconsin, spatially isolated core descriptions in the Michigan basin provide a lower resolution and less comprehensive understanding of Mount Simon depositional systems. Core studies presented in this study suggest that the Mt. Simon Sandstone of the Michigan basin has similar depositional facies to the outcrops in Wisconsin described by Driese et al. (1981). However the character and thickness of these lithofacies and their petrophysical properties vary from east to west across the Michigan Basin, and are not directly correlative with the Mt. Simon in Wisconsin.

Eau Claire

The Eau Claire Formation immediately overlies the Mount Simon, and is a potential the primary confining interval for Mount Simon CO_2 injection projects. The Eau Claire Formation is an argillaceous sandstone, siltstone and/or dolomitized carbonate rock that is in gradational contact with the top of the Mt. Simon Sandstone (Cottingham, 1990; Runkel et al. 2007; Catacosinos, 1973). The Eau Claire varies in log response, lithologic character and thickness across the Michigan Basin. Historically the boundary between the Mount Simon and Eau Claire was considered to be marked by an abundance of thinly bedded shales that contain trilobites, a decrease in sand size and/or the presence of glauconite (Cottingham, 1990; Catacosinos, 1973). The Eau Claire Formation in the west is identified in wireline logs by a high GR signature that is attributed to the presence of clay, glauconite and/or potassium feldspar, whereas the Eau Claire in the southeastern portions of the Michigan Basin is identified by a high bulk density signature (RHOB) associated with dolomite.

Previous Research

Briggs (1968) used data from brine-disposal wells in St. Clair County to document the waste water injection potential for the Mt. Simon Sandstone. Briggs (1968) suggests that the best reservoir facies grade laterally into more carbonate-prone facies to the south and reservoir quality decreases proportionally as dolomite percentages increase.

Odom (1975) documented the inverse relationship of detrital potassium feldspar abundance and grain size and related this relationship to depositional environment in the basal sand units of the Upper Mississippi Valley, including the Mount Simon Sandstone. Odom (1975) found that feldspar and glauconite concentrations are higher in low energy shelfal environments, whereas high energy littoral environments are predominantly quartz arenite deposits. Odom (1975) proposed a hydrodynamic model suggesting that feldspars experience more physical abrasion whilst passing through high energy depositional environments, and are then sorted and deposited in the lower energy (finer grained) shelfal environments.

Runkel et al. (2007) applied sequence stratigraphic concepts to the lower Paleozoic sandstones in central North America (Mount Simon included) and suggest that the laterally extensive distribution of shallow marine sandstones can be produced by a system with low subsidence rates in conjunction with low sedimentations rates and widespread shallow bathymetry.

Barnes et al. (2009) published results on a regional geologic storage capacity and site characterization study for the Mt. Simon Sandstone of the Michigan Basin. The total storage capacity was calculated to be 29 Gt. The reservoir quality rock is discriminated from nonreservoir quality rock by using log data with the following filters: a GR signature less than 50 American Petroleum Institute (API) units, bulk density (RHOB) between 2.3 and 2.8, neutron porosity (NPHI) of .10 or above and depth intervals between 2600 and 6500 ft. Depths less than 2600 feet in the Michigan Basin do not have sufficient pressure to keep CO_2 in the supercritical state. Rocks below 6500 ft have unusable porosity and permeability due to burial diagenesis (Barnes et al., 2009; Medina et al., 2010). Barnes et al. (2009) documents that the Mount Simon is no shallower than the 2600 ft in Michigan; the necessary depth to keep CO_2 in the supercritical state. Below 6500 ft burial diagenesis is generally thought to reduce reservoir quality to noninjectable levels (Barnes et al., 2009; Medina et al., 2010).

Kelley (2010) suggests that the GR cut-off of 50 API may not be an appropriate indicator of reservoir quality in the Mt. Simon in the eastern portions of the Michigan basin where potassium feldspar concentrations are apparently higher. By raising the GR cut-off to 100 API the state storage capacity is recalculated to be to 42.1 Gt. Kelley (2010) also documents the general lithologic variability in the Mount Simon from west to east across the basin. He suggests that there are potentially multiple source rock provenances, including the Wisconsin Arc to the west and the Grenville Front to the east. Variations in primary mineralogy across the basin may be a result of varying source rock provenances (Kelley, 2010).

Medina et al. (2008) suggests that log-derived porosity can be used to estimate permeability based on core plug measured porosity to permeability correlations. In the Mount Simon these correlations tend to be poor due to multiple pore type geometries. Kelley (2010) demonstrated the value of interpreting depositional facies as a means to further constrain porosity/permeability relationships in the Mount Simon, and found that grouping data by facies greatly improved the porosity/permeability correlations, and in turn the ability to better predict permeability from log derived porosity.

Fishietto (2009) described depositional facies for the Mount Simon Sandstone in the northern Illinois Basin. The study suggests that the Mount Simon was a transgressive sandstone from the base of the formation to nearly the top of the formation, at which point there was a substantial drop in water depth. The uppermost sandstone unit suggests a significantly shallower marine environment of deposition. Water depth then increased from the upper Mount Simon into the Eau Claire Formation (Fishietto, 2009).

CHAPTER II

DATA AND METHODOLOGY

This study uses data from 66 wells with digital wireline logs, 10 wells with core, 16 wells with conventional core plug analysis and 18 wells with pressure fall-off tests (Figure 3). Available conventional core is limited, therefore the spatial distribution of reservoir data derived from petrophysical analysis is greatly enhanced through core to wireline log correlations and analysis of wireline log data. Core, thin section petrography, XRD, infrared spectroscopy and pressure fall-off test data are correlated to wireline logs to constrain log interpretations.

Wireline Log Data

Core data is very sparse in the Mount Simon study area. With only 10 cored wells basin wide, correlation of core to wireline logs to make geologic interpretations of reservoir quality greatly enhances the resolution of available data. The digital wireline logs used in this study are courtesy of Michigan Geologic Repository for Research and Education (MGRRE). This study uses digital gamma ray (GR), neutron porosity (NPHI), bulk density (RHOB), photo electric factor (PEF), (calculated) density porosity (DPHI) and the porosity average (PHIA). The PHIA log is a computed average of the NPHI and DPHI logs.

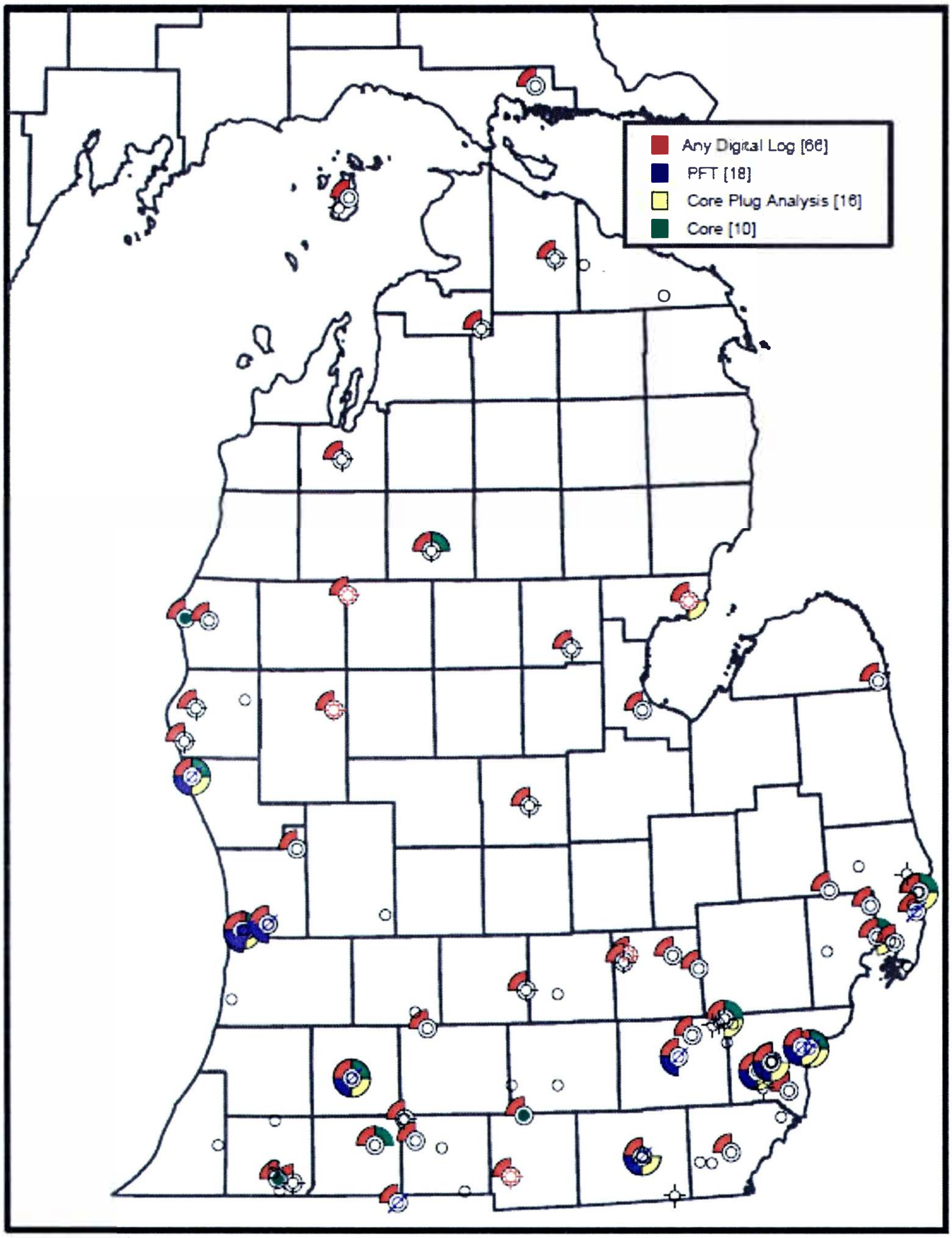

Figure 3: Attribute map with available data. This study incorporates data from 101 wells penetrating the Mt. Simon Sandstone in Michigan; 66 have digital logs. This map illustrates the distribution of data. It is important to note that there is very poor core coverage (green) in the Mount Simon.

Core Data

Figure 4 illustrates the vertical and spatial distribution of available conventional core. It is important to note that the basal feldspathic and conglomeritic sandstone wireline log facies identified by Barnes et al. (2009) and Medina et al. (2010) is only cored in the Lloyd Cupp 1-11 well, St. Joseph County, Michigan. The wireline log signature in the Angell & Kehrl 1-12 (and surrounding wells) has limited core to constrain wireline log interpretations. The three Consumer's Power wells in the east have nearly complete core data, but limited wireline log data for core to log correlations.

The Lloyd Cupp 1-11, Angell & Kehrl 1-12, Semet-Solvay #2 and the Consumers Power Company 139 cores have been described in detail for this study. Core descriptions are attached as Core Descriptions (1 - 4). The Doornbos et al. 5-30, Dupont Montague #1, BASF Chemetron D-1 and the Upjohn cores were viewed to develop depositional environment interpretations for wireline log facies. For detailed descriptions of the Doornbos et al. 5-30, Dupont Montague #1, BASF Chemetron D-1 and the Upjohn cores, see Kelley (2010).

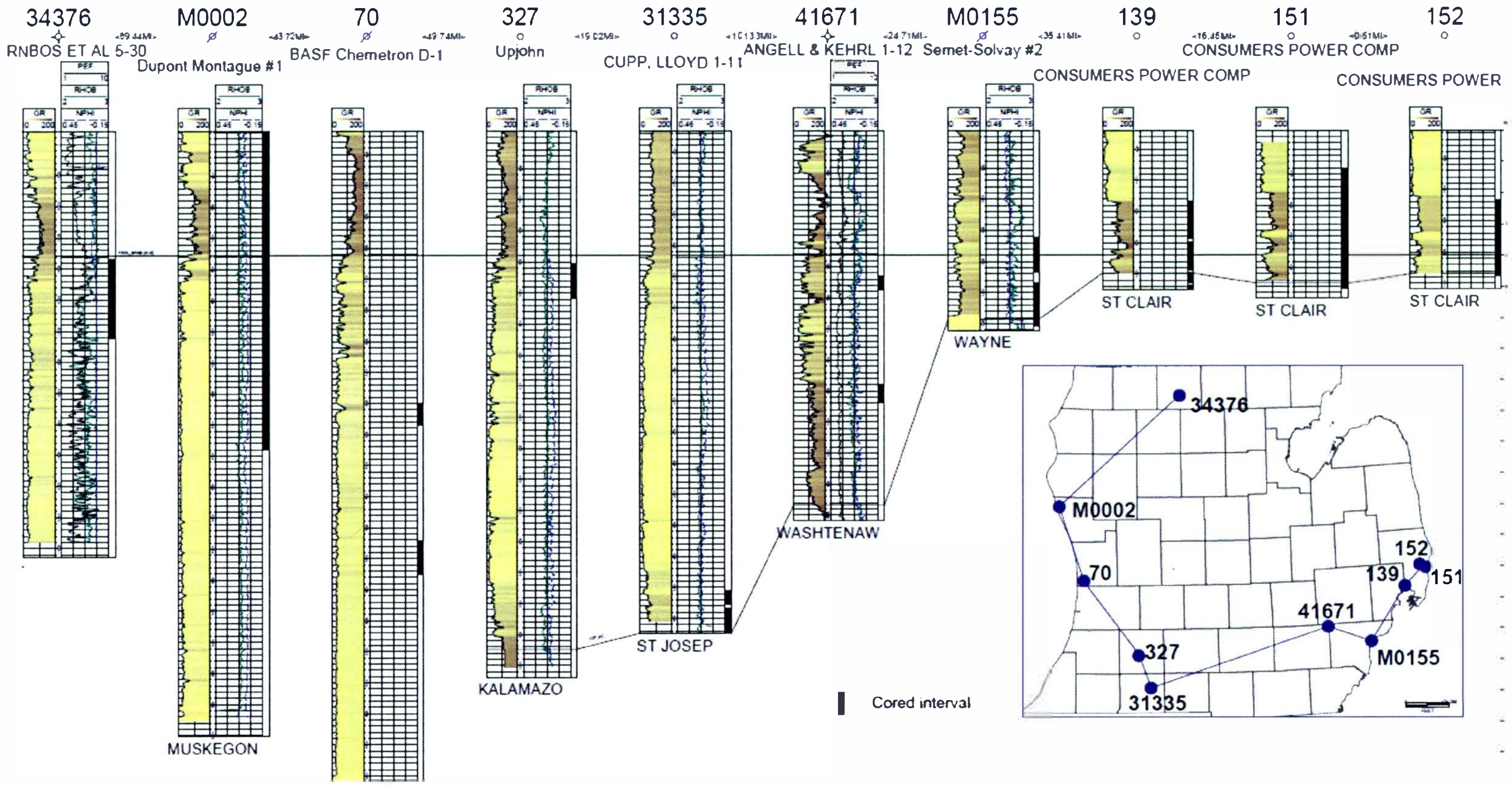

Figure 4: Core distribution. All of the cored intervals available to this study are marked with a solid black indicator. As demonstrated in the cross-section, the Mount Simon has very limited core to constrain geologic interpretations. Core to wireline log correlations are essential to understand the regional geologic setting.

Thin Section Data

Fifty-eight thin sections were characterized with petrographic point count data In the course of this study. Estimates of volumetric mineral compositions were made using 200 to 250 point counts. Seventy-five to 150 grains were measured to obtain grain size and grain sorting data. Some of the point count data was taken from Briggs (1968) and Kelley (2010) (Appendix 32). Feldspar stains were used to help identify potassium feldspar. Carbonate minerals were stained on a slide by slide basis with Alizarin red S to discriminate calcite versus dolomite, and ferroan versus non-ferroan dolomite (Tucker, 1988). Thin section observations are attached; Plate 1 through Plate 11.

X-ray Diffraction Data

X-ray diffraction (XRD) data was obtained for 5 samples to establish gross mineralogical composition (Appendix 34). Appendices 17-21 contain interpreted mineralogy from the XRD. Powdered whole rock samples were examined, and detrital orthoclase and quartz signals dominate the dataset. Chlorite, biotite, hematite, muscovite and dolomite were identified in this analysis (Table 1). Clay mineral separates were not analyzed.

Table 1: XRD mineral identifications.

Well	Facies	Depth	Mineral Identification
Angell & Kehrl 1-12	4	5478'	Chlorite grp., Biotite, Orthoclase, Quartz
Angell & Kehrl 1-12	5	5660'	Muscovite, Orthoclase, Hematite, Quartz
Lloyd Cupp 1-11	3	5021.5'	Muscovite, Orthoclase, Quartz, Hematite
Lloyd Cupp 1-11	3	5052'	Muscovite, Orthoclase, Quartz
Semet-Solvay #2	6	4001'	Chlorite grp., Orthoclase, Quartz, Dolomite

Infrared Spectroscopy

Analytical Spectral Device FieldSpec3 was used to gather shortwave to near infrared reflectance spectroscopy data for 10 samples to identify the iron oxides speciation (for instrument specifications see Appendix 35). Samples 1 cm in diameter were illuminated with artificial lighting from a Hi-Bright Contact Probe. The spectral reflectance was measured between 350 to 2500 nm with a 2151 channel instrument. Sample interpretations are attached as Appendices 7 - 16. In Appendices 7 - 16 the test samples are marked with thick solid black lines. Mineral signatures are plotted in thinner colored and dashed lines. The focus of this analysis was to identify iron oxide speciations (Table 2). Clay mineral identifications were more difficult to confirm. Hematite, chlorite, orthoclase and possibly goethite, illite and kaolinite were identified using infrared spectroscopy. Infrared spectral signatures were taken from the USGS Spectral Lab Library (http://speclab.cr.usgs.gov/).

Table 2: Infrared spectroscopy mineral identifications.

Well	Facies	Depth (MD)	Positive Identifications	Possible Identifications
Angell & Kehrl 1-12	4	5478'	Chlorite	Illite, Kaolinite
Angell & Kehrl 1-12	4	5478'	Hematite	Orthoclase
Angell & Kehrl 1-12	5	5660'	Hematite	
Angell & Kehrl 1-12	5	5669'		Hematite
Semet-Solvay #2	6	4001'	Hematite, Dolomite	Orthoclase
Semet-Solvay #2	6	4038.7'		Goethite, Hematite
Semet-Solvay #2	6	4099'	Dolomite	Goethite
Lloyd Cupp 1-11	3	5021.5'	Hematite	Orthoclase
Lloyd Cupp 1-11	3	5024'	Hematite	Orthoclase
Lloyd Cupp 1-11	3	5065'		Goethite

CHAPTER III

GEOLOGIC CHARACTERIZATION

Wireline Log Facies

One of the main goals of this study is to use wireline logs to interpret petrophysical properties and relate these properties to geologic interpretations throughout the basin. This study identified 6 wireline log facies and constrains interpretations of the wireline logs with available core data. Wireline Log Facies 1, 2 and 3 are only observed in west Michigan, and are consistent with the wireline log facies described in Barnes et al. (2009) and Medina et al. (2010). Wireline Log Facies 4, 5, 6 and 6b are only present in the east and have not been previously discussed in the literature.

Wireline Log Facies 1

Wireline Log Facies 1 is the uppermost portion of the Mount Simon in west Michigan, and is characterized by a relatively high saw toothed GR signature, often above 30 to 40 GR API units (Figure 2). The NPHI log is to the right of the RHOB log, which is consistent with a sandstone lithology. Facies 1 and 2 have a gradational contact that varies in character across the basin, which can make identifying a distinct facies boundary difficult. Facies 1 is typically mottled argillaceous sandstone that consists of scattered brachiopod fossils, syneresis cracks, burrows cross bedding, planar bedding and thin shale layers. The argillaceous intervals are correlated to the GR highs. Wireline Log Facies 1 was predominantly deposited in the lower shoreface environment (below the fair wave base) (Kelley, 2010).

Wireline Log Facies 2

Wireline Log Facies 2 is the thickest log facies in the Mount Simon. Facies 2 is located in western Michigan and is characterized by a constant low GR signature, often around 25 GR API units (Figure 2). Wireline Log Facies 2, for this study, is always found stratigraphically between Facies 1 and 3. Wireline Log Facies 2 is a quartz arenite with low angle cross bedding, planar bedding, clay drape laminations, scour surfaces, skolithos burrows and conglomeritic intervals. Wireline Log Facies 2 is interpreted to have been formed in a variety of marine environments including; tidally restricted foreshore, upper shoreface and lower shoreface (Kelley, 2010).

Wireline Log Facies 3

Wireline Log Facies 3 is found at the base of the Mount Simon in west Michigan, and is characterized by a saw tooth GR log response that varies significantly and often reads higher than 50 API (Figure 2). Wireline Log Facies 3 is a poorly sorted argillaceous braided fluvial/alluvial fan deposit In the Lloyd Cupp 1-11 and is similar to facies described by Driese (1981) (Core Description 1). The core photographs in Core Description 1 illustrate the abundance of poorly sorted, clay rich, and cross bedded intervals present. Wireline Log Facies 3 is texturally and compositionally immature. Compositionally the Facies 3 is very similar to the underlying porphyritic Precambrian granite rock.

Wireline Log Facies 4

Wireline Log Facies 4 is only present in east Michigan and is the uppermost facies of the Mount Simon in this area. It is characterized by a relatively low GR signature (compared to subjacent Facies 5), often between 25 and 100 API. The NPHI log is to the right of the RHOB log, consistent with a sandstone lithology on the basis of point count data. Facies 4 is a dolomitic subarkosic sandstone. It is interpreted to be a storm dominated shallow marine/tidal deposit (Core Description 2). High energy tempestite bedding is common in the upper portion of the core, and often incorporates intraclasts from the underlying strata.

Wireline Log Facies 5

Wireline Log Facies 5 is located in east Michigan only and is subjacent to Facies 4. Facies 5 is characterized by a relatively high GR signature, mostly greater than 75 API units. The NPHI log is to the right of the RHOB log suggesting a sandstone lithology. Wireline Log Facies 5 is interpreted to be a storm dominated marine deposit (Core Description 2). Multiple tempestite packages have been identified in the Angell & Kehrl 1-11 core (Core Description 2). Land organisms did not evolve until after the Cambrian (Mayr, 1963), so the presence of burrows in conjunction with brachiopod fossils in core representing Wireline Log Facies 5 is indicative of a marine environment. Wireline Log Facies 5 has potassium feldspar abundances that range from 28.5 to 45.5 % by volume, averaging 36.5% from point count data (Appendix 32). Carbonate percentages in Facies 5 range from 0 to 9% by volume, and average 2.6%.

Wireline Log Facies 6

Wireline Log Facies 6 is present in the southeastern Michigan only, and is characterized by a relatively low GR signature, often lower than 50 API. The RHOB log is to the right of the NPHI log, consistent with a dolomitic composition. Facies 6 ranges from a poorly sorted arkosic fluvial deposit to a well to moderately sorted, cross bedded and burrowed arkosic marine deposit with gross carbonate abundances ranging from 0 - 51% (Core Description 3). Primary carbonate grains are difficult to discern in either hand samples or thin section.

Wireline Log Facies 6b

Wireline Log facies 6b is difficult to identify in logs, but may prove to be very important when injecting CO_2 in southeast Michigan. Facies 6 is characterized by a decrease in GR, an increase in the RHOB and increase in the PEF logs. The RHOB of is to the right of the NPHI, consistent with a dolomitic lithology. Wireline Log Facies 6b consists of thin dolomitic intervals 3" to 9" thick observed in the core of the Semet Solvay #2, Angell & Kehrl 1-12 and the Consumer Power Company 139 wells. These intervals are difficult to correlate long distances (>10 miles) with wireline logs, but can be correlated short distances (<1 mile). The dolomitic intervals may result from large storm events transporting carbonate grains from the southeast, though there is little rock data available to further investigate this hypothesis. Becker et al. (1978) documented oolitic beds >200 ft in thickness in the Eau Claire Formation in the southern Indiana carbonate belt (Runkle et al., 2007). These dolomitic storm deposits(?) may result in vertical compartmentalization of the reservoir and secondary capping intervals, which would increase the storage efficiency of the formation (NETL, 2007), but hamper injectivity.

Depositional Model: Southeast Michigan

Walker (1985) described a storm dominated, shallow marine depositional system (Figure 5) in which the further landward sediment tends to be coarser grained, more bioclast-rich and have more rip-up clasts than distal correlative sediment. Textural and compositional observations made in the Angell and Kehrl 1-12, Semet Solvay #2 and the Consumers Power Company 139 in southeast Michigan suggest that the strata were deposited in a storm dominated marine environment (Core Descriptions 2-4). In eastern Michigan the Mt. Simon is interpreted to be a regressive sandstone. The three observed cores are more bioclast (carbonate) rich, have more rip-up clasts and evidence of sub-aerial exposure near the top of the cores, which based on Walker (1985), are suggestive of a shoaling upward sequence. Furthermore, based on Blakely's (2005) paleogeographic map (Figure 6), the Angell and Kehrl 1-12 is the most distal core and the Consumers Power Company 139 is the most proximal core. The Angell and Kehrl 1-12 has the least carbonate content and is the finest grained; the Consumers Power Company 139 is the coarsest grained and has more bioclasts (carbonate). Blakely's (2005) paleogeographic map is also consistent with Walker's (1985) depositional model (Figure 6).

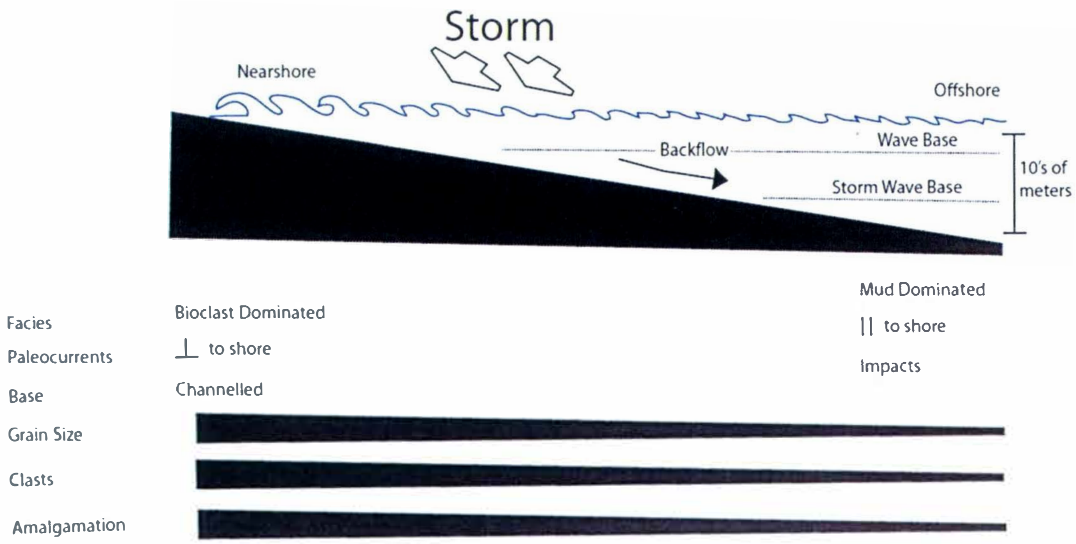

Figure 5: Depositional model for the Mount Simon in eastern Michigan. Modified from Walker (1985). Walker's storm dominated shallow marine model is consistent with the observations made from the core in southeastern Michigan. The abundances grain size, rip-up clasts and bioclast increase landward.

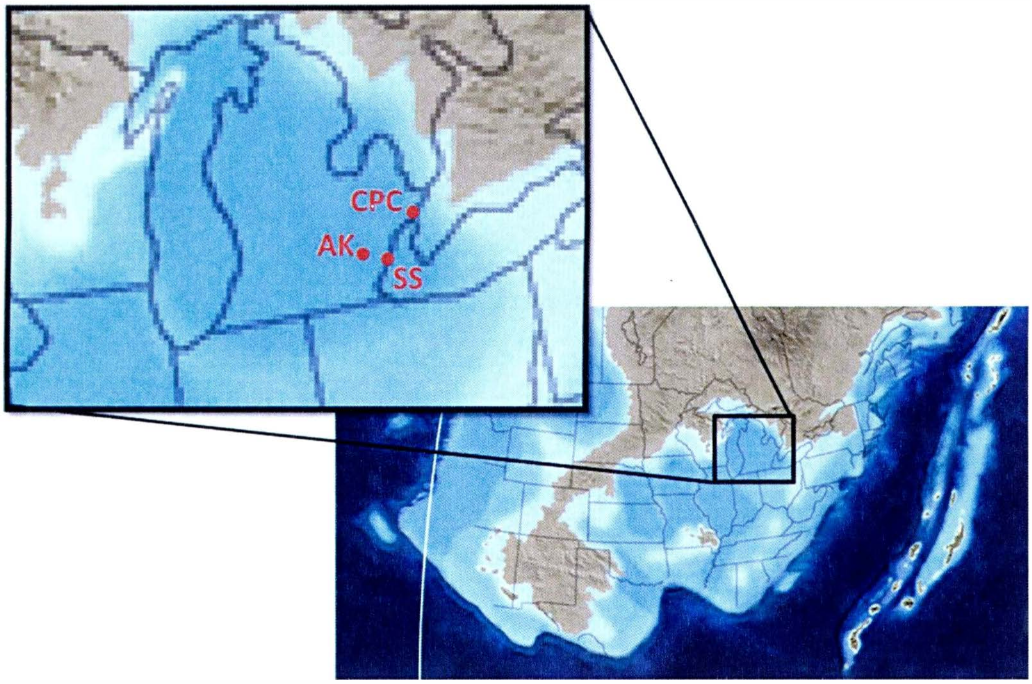

Figure 6: Paleogeographic map of Michigan during the Cambrian. Modified from Blakely (2009). Three well locations are marked on this image: CPC = The Consumers Power Company 139, SS= the Semet-Solvay #2 and the AK= the Angell & Kehrl 1-12.

Variations in Mount Simon: West vs East

Kelley (2010) recognized lateral variation in primary mineralogy and wireline log signatures in the Mount Simon in a general east-west direction across Michigan and Ohio. Figure 4 documents the change in wireline log signature from west to east across the Michigan Basin. Baranoski (2010, and in review) also recognized a similar west to east lateral variation in the Mt. Simon of Ohio and southeastern Michigan. The Ohio study has proposed that these eastern lithofacies are correlative to the Eau Claire Formation of the Michigan Basin and the Conasauga Formation of the Appalachian Basin, and thus should not be called the Mt. Simon. This section documents the differences in primary mineralogy, and in turn wireline log signature, between the Mount Simon in western Michigan versus eastern Michigan.

Variations in Primary Mineralogy

Table 3 shows general mineralogy differences between the Mount Simon in the western and eastern Michigan. Note that the Mount Simon in the east has significantly higher feldspar and carbonate abundances. The differences in primary mineralogy between the west and the east are reflected in wireline log signatures as described above.

Table 3: Mineralogical differences between western and eastern Mount Simon. Abundances are in percent. *=Mount Simon Intervals no greater than 6500' deep, the depth at which quartz diagensis is thought to destroy porosity and permeability (Barnes et al., 2009; Medina et al., 2010)

	Detrital Quartz	Detrital K-Spar	Carbonate	Quartz Overgrowths	Total Authigenic Minerals including CO_3's
West	65.88	4.85	0.47	5.20	15.98; *12.43
East	51.02	18.91	13.41	1.50	17.19

Variations in Wireline Log Signature

In the west, the wireline facies from base to the top are Facies 3, 2 and 1 from bottom to top. The character and thickness of each Facies varies throughout the basin, but the stacking pattern is always identifiable and consistent (Figure 2). In the east, there is no consistent stacking pattern of wireline logs facies. Also, the wireline log signatures in the east have much greater lateral variability compared to log facies in the west.

Figure 7 is a map with representative GR logs. The thickness and character of each wireline log facies varies throughout the basin. To the west of the red line on the map, every GR log displays the upwards Facies 3, 2 and 1 stacking pattern. To the east of the red line the stacking patterns are not consistent.

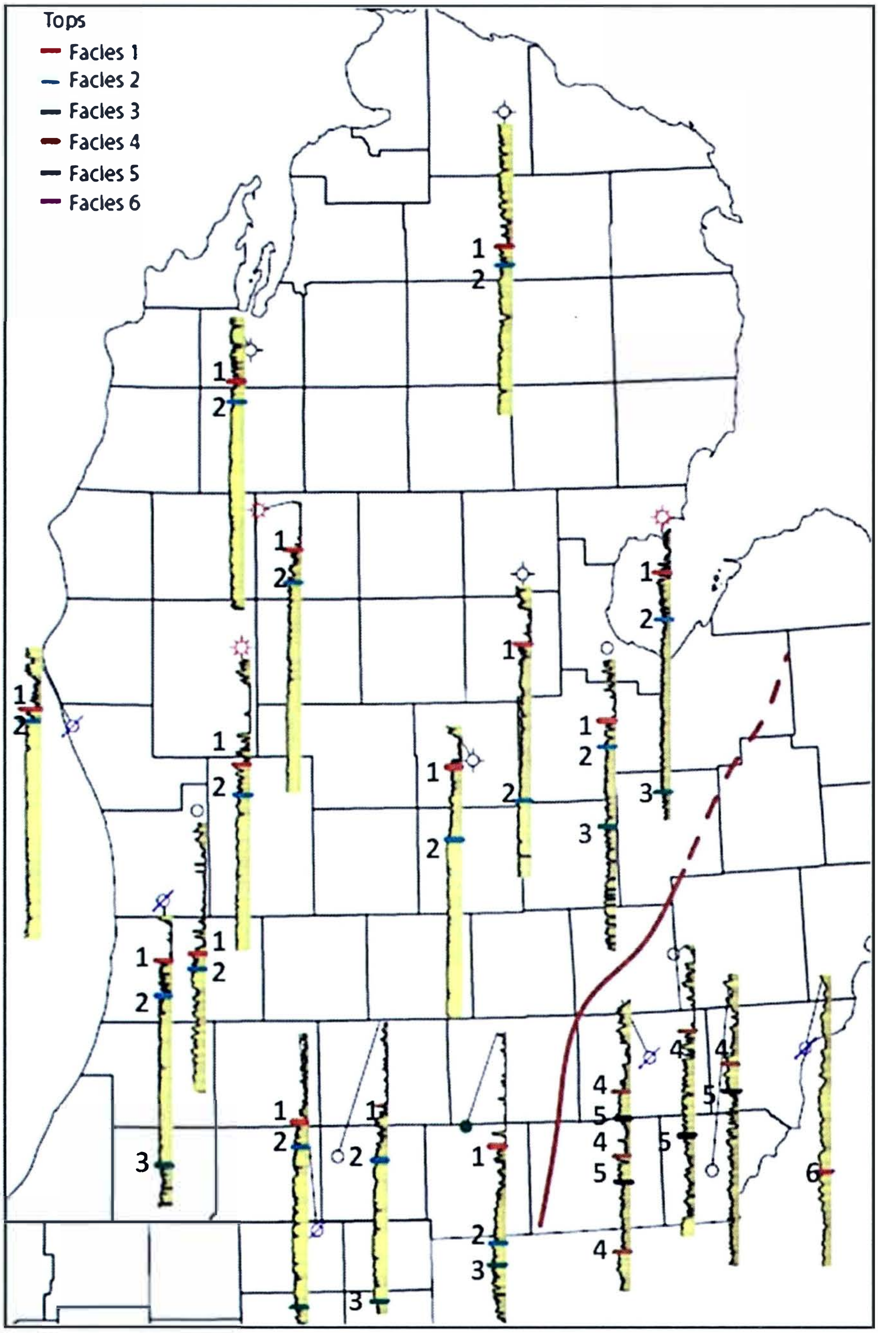

Figure 7: Boundary between the western and eastern Mount Simon. Note the wells to the east of the red line do not have the three facies stacking pattern, furthermore, they tend to have a much higher GR signature.

Variation and Interpretation of the Eau Claire Depositional System

The Eau Claire Formation also changes in character from northeast to southwest across Michigan, similar to the Mount Simon (Figure 8). The Eau Clair in northwest Michigan has low GR signature in conjunction with a NPHI/RHOB crossover, consistent with a sandy lithology. The Eau Claire gradationally changes in character from the northwest of the basin toward the center of the basin where the Eau Claire has a high GR and NPHI signature and is interpreted to be argillaceous and/or more K-spar rich. An abrupt change in log signature occurs between the center of the basin and southeast Michigan. The wireline log signature in southeast Michigan has a lower GR, high PEF and high RHOB signature, which is characteristic of a dolomitic lithology.

A general interpretation of the regional depositional system of the Eau Claire Fm in Lower Michigan is that the formation is sandier in the northwest because it is proximal to clastic source areas in the Wisconsin highlands. Rock data in the Mount Simon and Eau Clair in southeastern Michigan is interpreted to be a storm dominated, low sediment supply distal carbonate shelf deposit (Core Descriptions 1-3), which is not consistent with a northwesterly sourced single polarity basin.

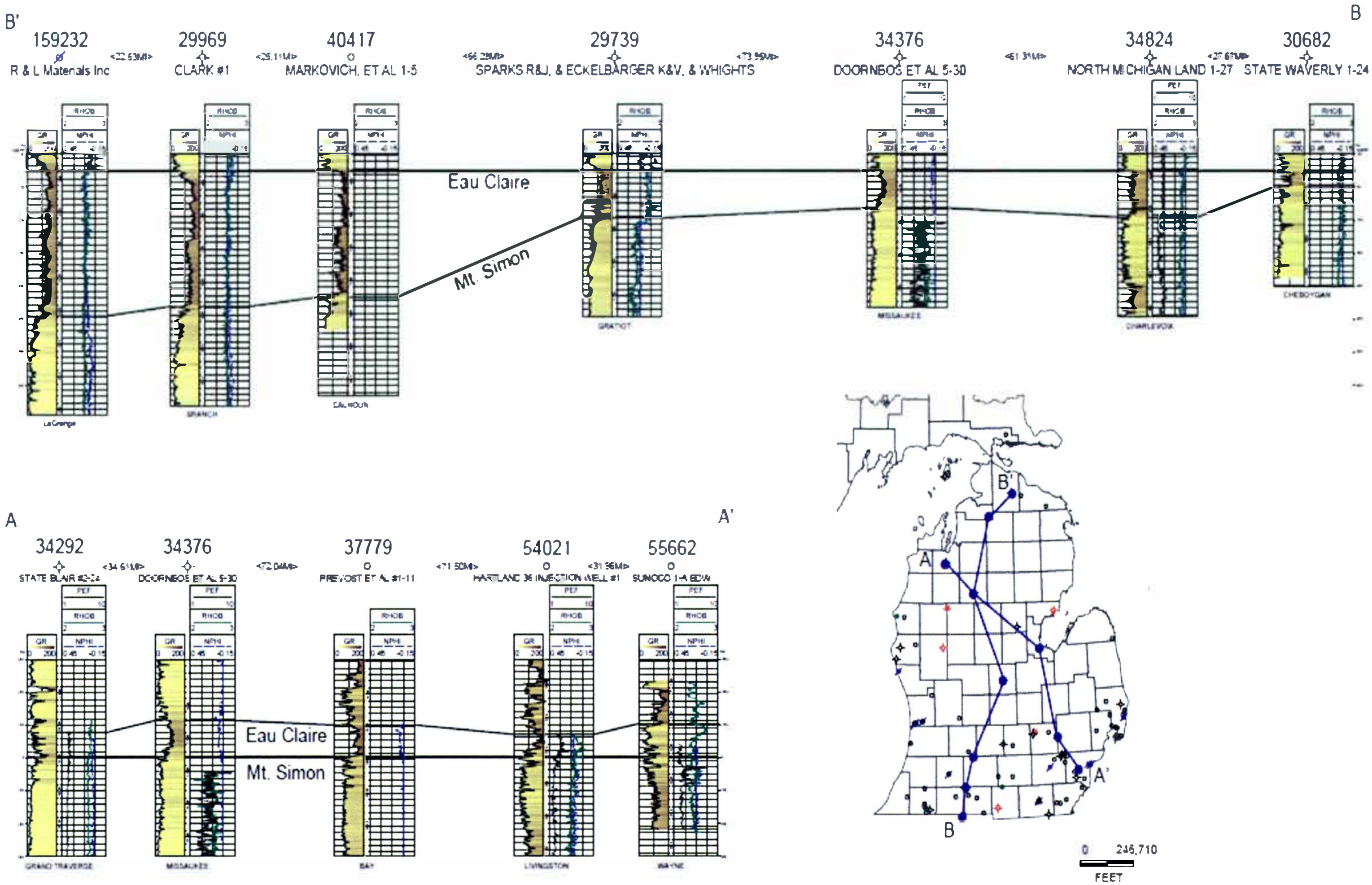

Figure 8: Cross-sections of the Eau Claire demonstrating regional variability.

The Significance of Potassium Feldspar

Feldspar and Grain Size Relationships

Odom (1975) suggests that feldspar concentrations are inversely proportional to grain size in the Mount Simon Sandstone of the Upper Mississippi Valley. As discussed earlier, this relationship is expected because feldspar is more easily mechanically broken down into smaller fragments relative to quartz, and is then hydraulically sorted and concentrated in more distal lower energy environments (Odom, 1975). Figure 9 is a plot of potassium feldspar concentrations versus grain size for the core data from the Angell & Kehrl 1-12, Semet Solvay #2 and the Consumers Power Company 139. The potassium feldspar concentration and grain size correlation in the Angell & Kehrl 1-12 has an R^2 value of .70. The Semet Solvay #2 and Consumers Power Company 139 plots show almost no correlation; R^2=.174 and .010, respectively. Based on Blakey's (2005) paleogeographic interpretation (Figure 6) and the core descriptions discussed previously (Cores Descriptions 1-3), the Angell and Kehrl 1-12 is the most distal well from the potential source area to the east, and shows an inverse grain size to feldspar relationship. Sediment in a storm-dominated shallow marine environment is more amalgamated and poorly sorted in the more proximal environments (Walker, 1985). This is also observed in the Mount Simon cores in southeast Michigan. Because the sediment is more poorly sorted in the more proximal environments, it would be expected that the more proximal strata would have a less predictable relationship between potassium feldspar concentrations and grain size.

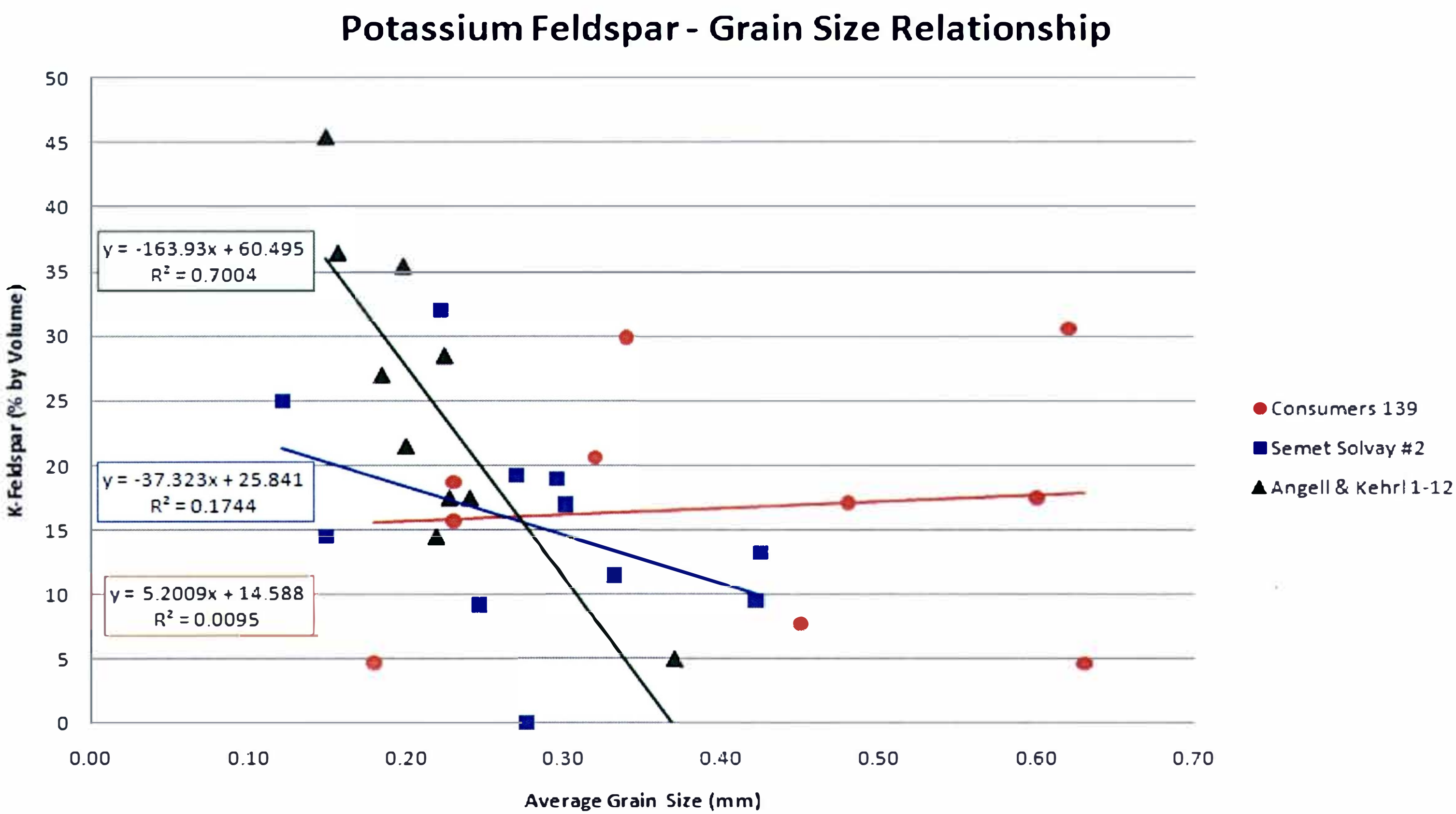

Figure 9: Feldspar to grain size correlations. Odom (1975) suggests that grain size is inversely proportional to feldspar abundance. This interpretation is consistent with the Angell and Kehrl 1-12 well, but not the Semet Solvay #2 or the Consumer Power Company 139.

Feldspar and Gamma Ray Relationships

Gamma Ray (GR) log response is typically interpreted to be inversely proportional to grain size and, by extension, representative of reservoir quality potential in terrigenous clastics dominated successions (Posamentier, 1999; Emery, 1996). Figure 10 is a plot of GR versus measured porosity from conventional core plug analysis and shows no correlation between porosity and the GR log. Point count data indicates that the high GR response in the east is a function of the abundance of potassium feldspar (Figure 11).

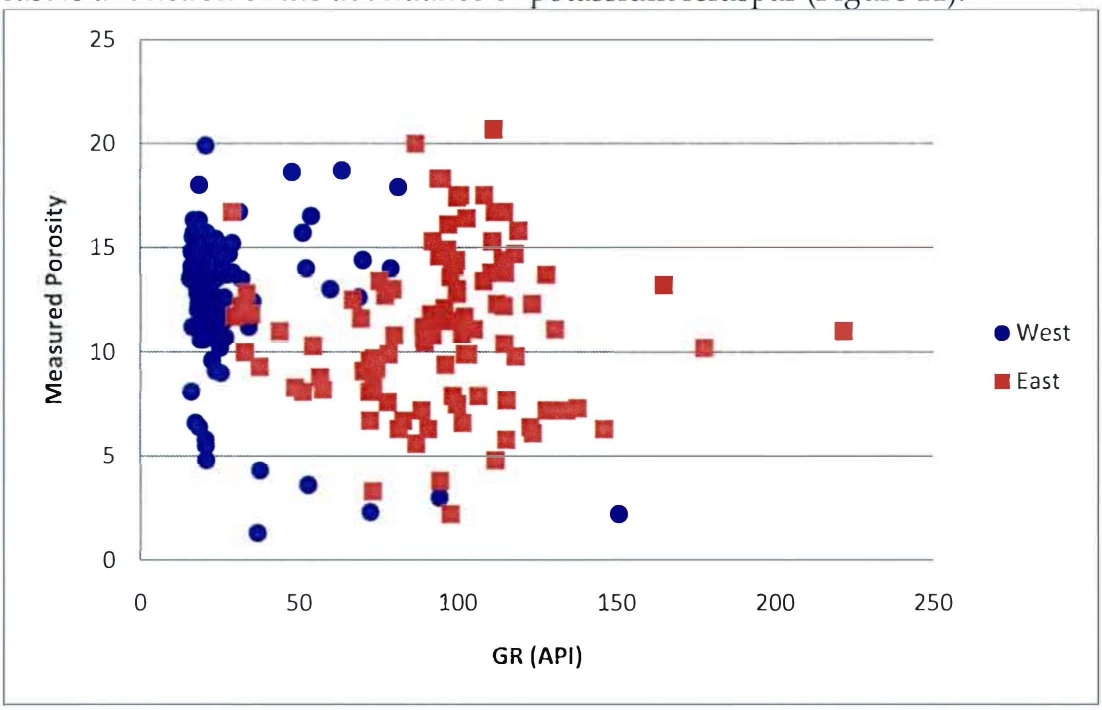

Figure 10: Plot of measured porosity versus gamma ray (API). There is no correlation between GR and core plug porosity in both the western and eastern Mount Simon.

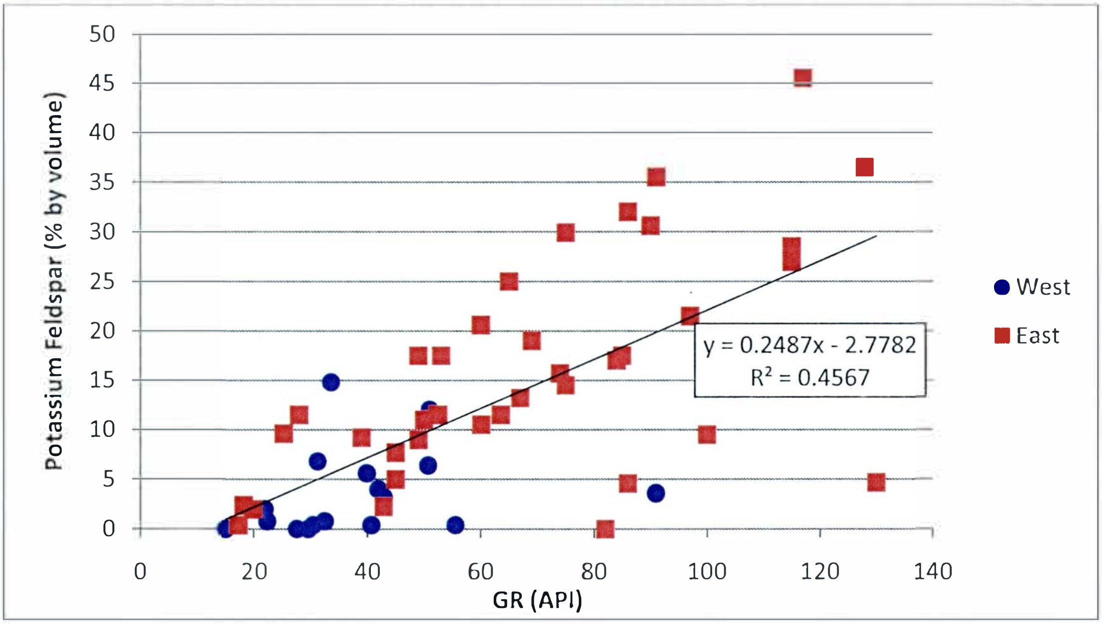

Figure 11: The relationship between potassium feldspar content and the gamma ray log (API). The increase in GR signature in the eastern parts of the Michigan is attributed in large part to an increase in potassium feldspar. The line of best fit includes all points graphed.

Because the GR log is proportional to the abundance of potassium feldspar in the rock (Figure 11), and rocks with more potassium feldspar have a higher fraction of porosity that results from the dissolution of primary detrital grains (Figure 12), the GR log, in some instances may be used as a proxy for the percentage of porosity that is secondary dissolution porosity. This relationship is only true in areas where increases in the GR log are caused by an increase in potassium feldspar. Brennan et al. (2010) suggests that reservoirs with small pore throats and large pores (i.e. dissolution pores) would result in higher CO_2 storage efficiency factors as a result of the immiscible fluid flow properties. Locating reservoirs that will have a higher potential for capillary retention may significantly increase the permanent storage confidence for a CO_2 reservoir.

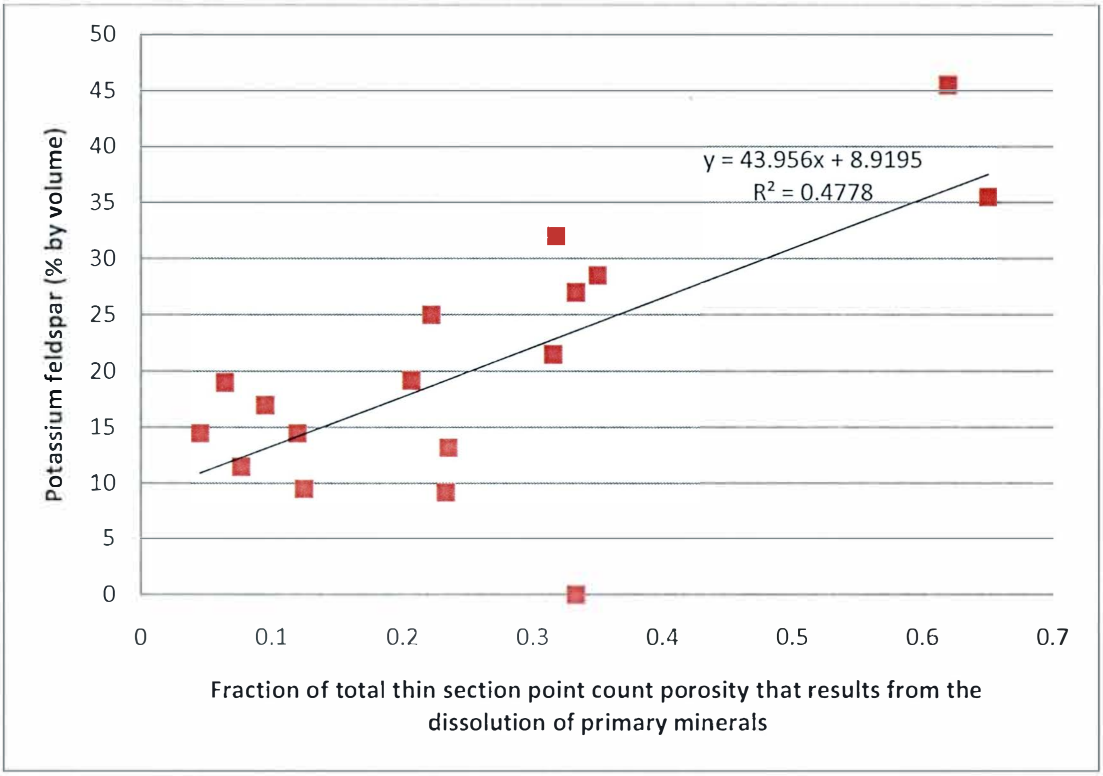

Figure 12: The relationship between feldspar abundance and dissolution porosity. There is a correlation between the amount of potassium feldspar in the rock and the amount of dissolution porosity.

Gamma Ray, Feldspar and Permeability

Odom (1975) suggests that feldspar abundance is inversely proportional to grain size; this is observed in the Angell and Kehrl 1-11 well. It is known that permeability is a function of grain size in clastic sedimentary rocks (Pettijohn et al., 1987). Because increases in the GR log are proportional to potassium feldspar abundances (Figure 11) and in some locations potassium feldspar content is inversely proportional to grain size. In regions where this potassium feldspar is inversely proportional to grain size, such as near the Angell and Kehrl 1-12, the GR log response may also be used as a qualitative assessment for permeability.

Core to Wireline Log Correlations

A goal of this study is to create static geologic models as a preliminary step for running CO_2 injection models. Because there is not enough rock core to make a static geologic model entirely from rock data, porosity and permeability values are estimated from wireline logs. The methodology used to estimate porosity and permeability from wireline logs is demonstrated in the following pages.

There is significant mineralogical and textural variation between all of the log facies, 1-6. Core porosity to wireline correlations were done for each of the wireline log facies (Table 4). Table 4 compares the ability of the NPHI, NPHI+3 and PHIA logs to estimate plug measured porosity. Facies 6b does not have enough data for the analysis and was excluded from the table. Equation 1 is used to calculate the standard deviation of the difference between the plug measured porosity and the log estimated porosity. The lower the value is, the better the log based porosity transformation method does at estimating true (plug measured) porosity. The best plug porosity to wireline log porosity correlations plot for each facies is attached in Appendices 4-6.

Equation 1:

$$\textit{Core to Log correlation value} = \sqrt{\frac{\sum_{i=1}^{n}(\Phi_i - L_\Phi)^2}{n-1}}$$

Where,

Φ = Core measured porosity

L_Φ = Log estimated porosity

n = Number of samples

Table 4: Quantification of core to wireline log correlations. Equation 1 is used to calculate each logs ability to estimate true porosity. The lower the value the better the log estimates porosity.

	Used log correlation	NPHI	NPHI+3	PHIA
Facies 1	NPHI+3	3.80	2.95	3.18
Facies 2	NPHI+3	3.79	2.14	2.31
Facies 3	PHIA	4.74	6.96	3.47
Facies 4	PHIA	3.85	4.89	2.82
Facies 5	PHIA	3.23	4.10	3.15
Facies 6	N/A	5.53	7.45	3.60

Establishing Porosity to Permeability Relationships

Porosity to permeability transformation equations have been developed for wireline log Facies 1-6 (Appendices 1-3), and are used to estimate permeabilties from wireline log data. The best fit curve for each facies is plotted on Figure 13. Discrimination of lithofacies within each wireline log facies could result in more accurate porosity to permeability transformations, but because interbedded lithofacies cannot be identified in wireline logs, this exercise could not be done.

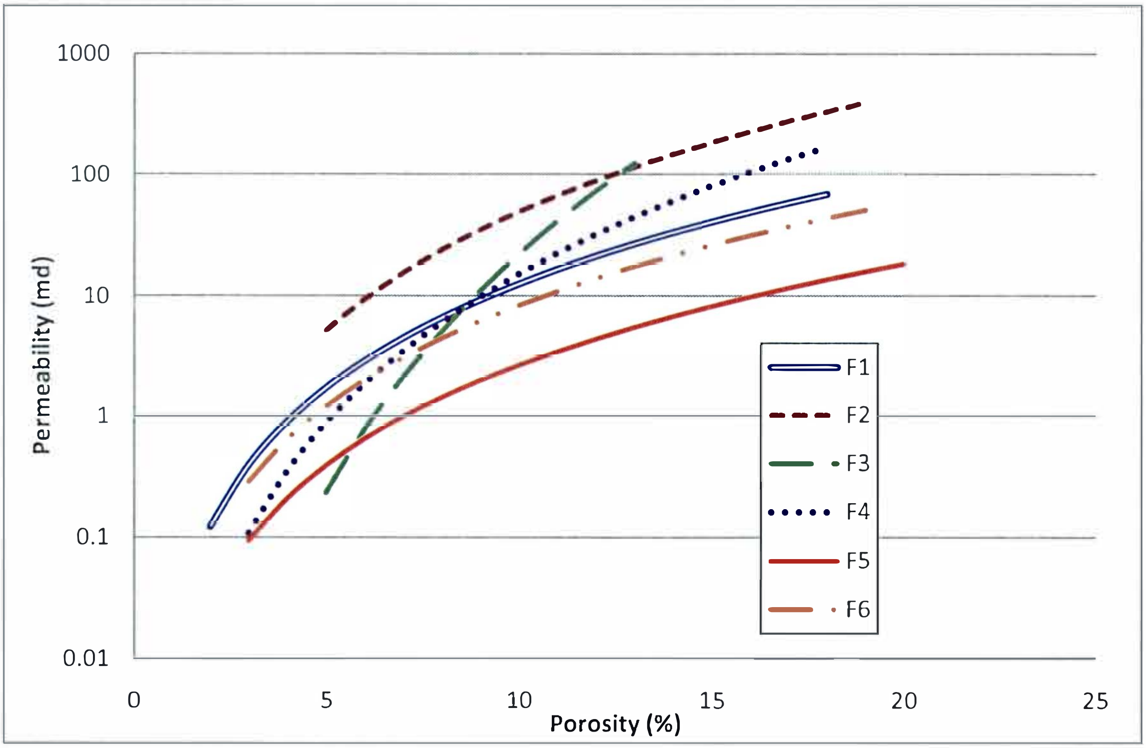

Figure 13: Best fit curve from the porosity to permeability plot for each of the facies.

The porosity/permeability curves suggest that Facies 2, the main injection target in western Michigan, has the highest average permeability (Figure 13). The trend line for Facies 3 is oblique to the trend line of the other facies. As discussed above, Facies 3 has significant vertical heterogeneity as well as grain size variations. Subdividing Wireline Log Facies 3 into two lithofacies with less grain size variations would likely result in better correlation coefficients, and trend lines that follow the shape of the other Facies. The porosity/permeability curves suggest that Facies 5 has the lowest average permeability of all the Facies, which is consistent with grain size observations. In Facies 5, the finest grained facies in eastern Michigan, permeability is a function of grain size (Pettijohn et al., 1987)

CHAPTER IV

PRESSURE FALL-OFF TESTS

One of the difficulties with creating a static geologic model is understanding how to upscale and quantify the data such that it is useful for the transient modeler. In this analysis pressure fall-off test (PFT) data is correlated to wireline log properties of wells as a means to better calibrate the static geologic model. PFT data measures the reservoir permeability in the vicinity of an injection interval. Anomalous reservoir permeabilities that are not predicted by core data or wireline logs may be attributed to features outside the scope of the wellbore, i.e high permeability flow pathways or the horizontal compartmentalization of the reservoir (EPA, 2002). The downside to the PFT is that it cannot be used to locate or identify the features contributing to the anomalous permeabilities.

Pressure fall-off tests (PFT) are used to monitor the hydraulic properties of flow units in the vicinity of a wellbore (Silin, 2005). Pressure fall-off tests are administered by injecting fluid into the formation at a known rate (q) for a defined time period (EPA, 2002). The reservoir adjacent to the borehole becomes over-pressured, and when injection is stopped, the rate at which the reservoir pressure decreases is fit to a curve. By estimating the slope of the pressure fall-off curve on a Horner Plot, the hydraulic conductivity of the reservoir can be estimated with the equation below (EPA, 2002):

Equation 2: $$K = \frac{162 * q * \mu * B}{h * m}$$

Where,

K = intrinsic permeability (md)

q = the average injection rate (Barrel/Day)

μ = the viscosity of the injectate

B = the formation fluid factor

h = the height of the injection interval (ft)

m = the estimated slope of the fall-off curve (psi/cycle)

Possible Sources of Error in Pressure Fall-off Tests

The accuracy and consistency of PFT results should be considered when using the data to calibrate models. While reviewing the PFT reports at the Michigan Geologic Survey it became clear that there are at least three major mechanical and judgment mistakes that can result in bad permeability calculations. (1) The height (*h*) of the injection interval for the intrinsic permeability (*K*) calculation in wells with large open-holes (~300+ ft) is often decreased for the calculation. *h* is the height of the effective reservoir, and if the engineer thinks the lower part of the injection interval does not accept significant quantities of injectate, the lower part of the injection interval is not included in the K calculation. The error occurs in trying to determine what intervals of the reservoir will accept versus will not accept injectate. (2) Many of the pumping rates are very inconsistent, and an average of the pump rate

(q) is used in the permeability calculation. PFT calculations are based on a constant injection rate, and an estimated constant (q) could cause the results to be slightly if not significantly off. (3) Estimating the slope of the PFT could also be a source of error. In some cases it was observed that the errors with the pressure gauges were causing a scatter of the PFT data, and as a result, the accuracy of the calculated *m* was poor.

Table 5 is calculated permeabilities from the Subsurface Mechanical Integrity Test (1999) for the 373 Parke-Davis well. The PFT data is compiled from the 1993, 1996, 1998 and 1999 tests. Note that the permeability results range from 70 md to 117 md. There is no trend suggesting that the well quality is improving or degrading over the 6 years, so it is reasonable to assume that the data spread represents the inherent testing error. The 1998 test suggests a permeability that is 60% higher than the 1993 tests. When multiple tests were available for the same well, the average permeability value was assigned as the PFT calculated K.

Table 5: Investigation of the error in the PFT analysis. Below are the results of 4 PFT on the same well over a 6 year period.

Comparison of Parke-Davis 373 PFT Results				
Year	**1993**	**1996**	**1998**	**1999**
k	70	98	117	76
kh	51,892	72,488	86,454	56,551

Available Data

There are 25 waste injection wells that have injected nearly 6 billion gallons of waste into the Michigan Mount Simon Sandstone since the early 1960s. Of these 25 injection wells, 17 wells have PFT data complete enough to calculate reservoir transmissivity (Appendix 31). Figure 18 is compilation of all of the available PFT permeability data with the corresponding GR log and injection interval for the Mount Simon. It is clear that the hydraulic conductivity for the Mount Simon in the west is higher than the hydraulic conductivity for the Mount Simon in the east. Furthermore data in the east suggests that the Knox sequence (formations above the Mount Simon) may have comparable injection potential compared to the Mount Simon Sandstone (Figure 18).

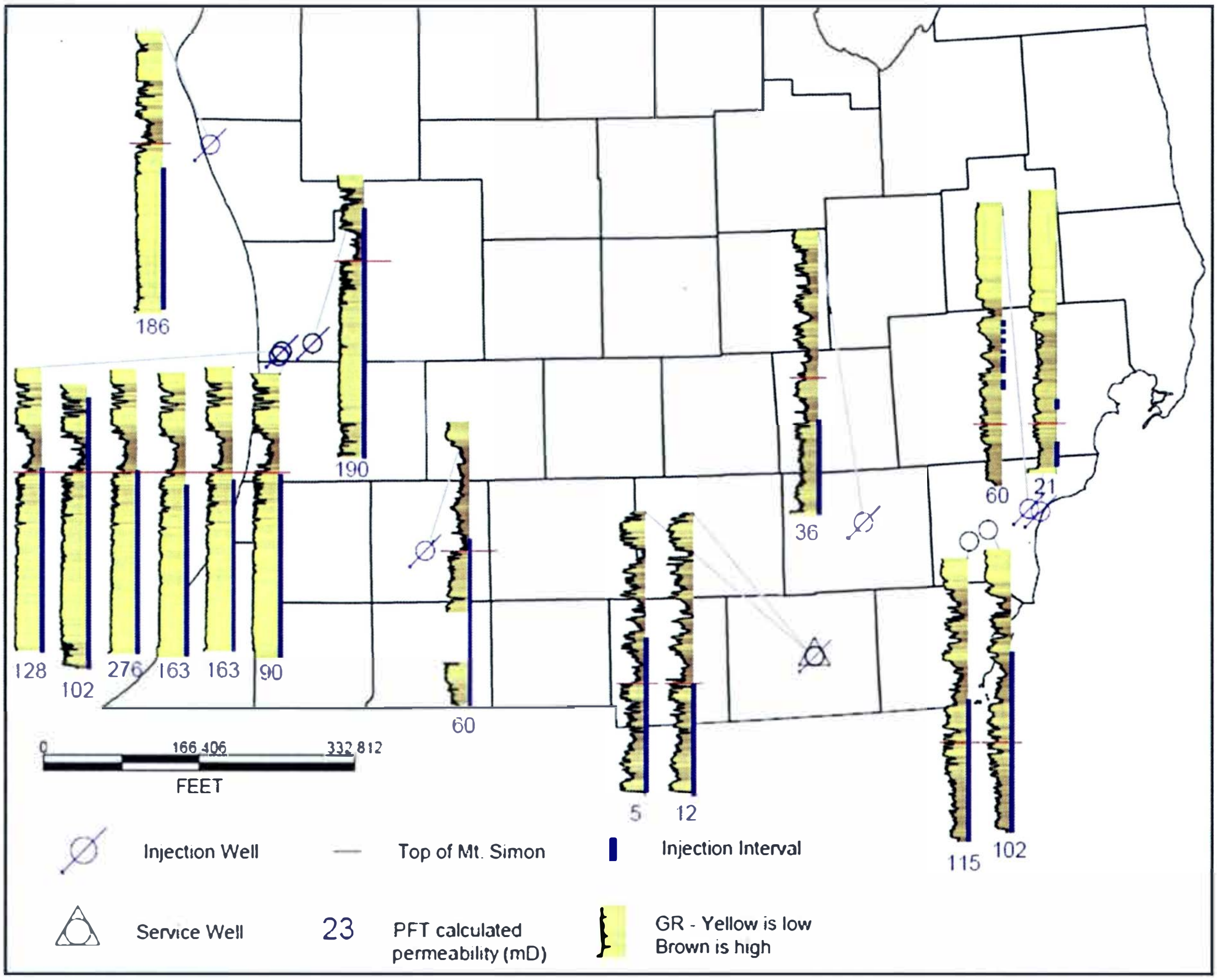

Figure 18: Distribution of pressure fall-off tests. This map documents the distribution of pressure fall-off tests and reservoir permeabilities.

Correlating PFT to Core Data

The Semet-Solvay #2 is an exceptionally good well to compare reservoir permeability calculated from core plugs to PFT calculated permeability. Figure 19 contains the wireline log data, core plug porosity, measured permeability and the perforated injection intervals for the Semet-

Solvay #2. This well has a core plug permeability measurement taken every one foot for nearly the entire waste injection interval. The core plug permeabilities in the injection interval yield an average reservoir permeability of 12.86 md. The reservoir permeability calculated from the PFT is 35.8 md. PFT for the Semet-Solvay #2 estimates reservoir permeability nearly 3 fold higher than core plug permeabilities. The significantly higher PFT permeability may result from high permeability flow pathways undetected by the core plug, or the inherent error associated with estimating permeabilities in both PFT and conventional core plugs.

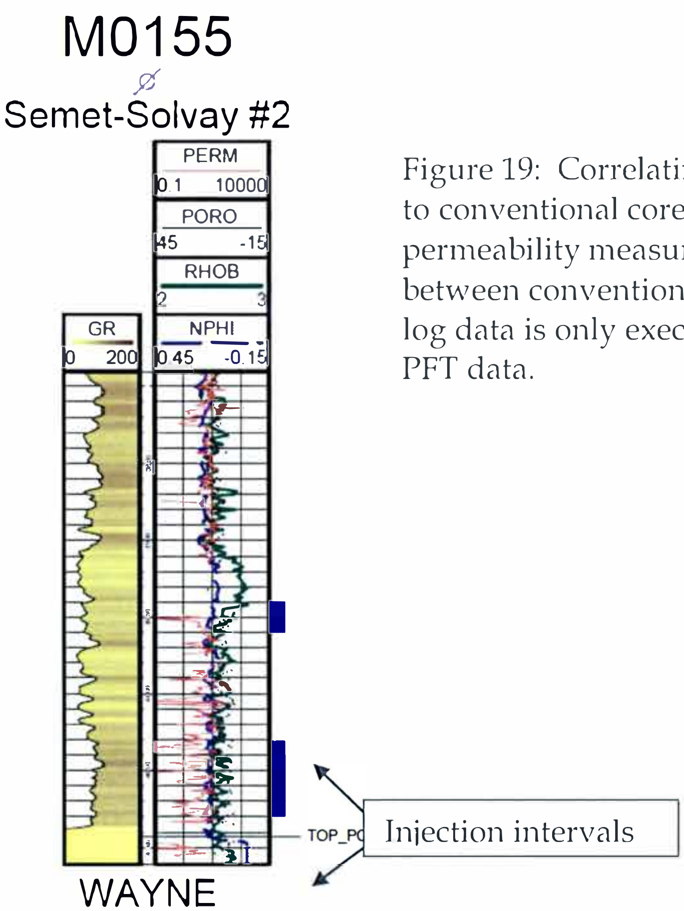

Figure 19: Correlating pressure fall-off test data to conventional core plug porosity and permeability measurements. The correlation between conventional core plug data to wireline log data is only executed for the intervals with PFT data.

Correlating PFT to Wireline Logs

With limited core data, understanding the correlation between wireline logs and PFT results is essential to maximizing the usefulness of the dataset. Core plug porosity and permeability data was used to create porosity and permeability transformations for each of the Facies (Chapter 3 and Appendix 1-3). As discussed earlier, core to wireline log correlations were done to determine which porosity log transformation best estimates porosity for each Facies (Table 4). Using the established porosity/permeability transformations (Appendix 1 - 3) and the wireline log porosity estimations from Table 4, the hydraulic conductivity for each injection interval was calculated. These results were compared to the calculated PFT permeabilities in Table 6 (Equations 4 and 5). Equation 5 is used to calculate the PFT correction factor shown in Table 6.

Equation 3:

$$WLL_k = \frac{\left(\sum_{i=1}^{n_{f1}} .0167 * \Phi_{f1}{}^{2.8769}\right) + \left(\sum_{i=1}^{n_{f2}} .0283 * \Phi_{f2}{}^{3.2401}\right) + \left(\sum_{i=1}^{n_{f3}} .00005 * \Phi_{f3}{}^{.2102}\right)}{n_{f1} + n_{f2} + n_{f3}}$$

WLL_k=	Wireline log permeability
Φ_{f1} =	Porosity sample in Facies 1
n_{f1} =	Number of porosity samples in Facies 1
Φ_{f2} =	Porosity sample in Facies 2
n_{f2} =	Number of porosity samples in Facies 2
Φ_{f3} =	Porosity sample in Facies 3
n_{f3} =	Number of porosity samples in Facies 3

Equation 4:

$$PFT\ Correction\ Factor = \frac{PFT\ K}{WLL_K}$$

Table 6: PFT to wireline log correction factor. PFT data can be used to constrain wireline log permeability estimations by using a correction factor. The correction factor is calculated by dividing PFT K by the well average log K.

UWI	Well Log K	PFT K	PFT to Wireline Log Correction factor
21121000027000	27	186	6.89
21139003737000	120	90	0.75
21139000537000	128	128	1.00
21139001297000	145	163	1.12
21139004707000	147	190	1.29
21139001307000	168	163	0.97
21139000517000	334	276	0.83

Using this methodology the wireline log permeability calculations can be weighted to more accurately match the results of the pressure fall-off test. Table 7 contains results of calculated well log permeabilities constrained using the PFT correction factor (Equation 6). This methodology constrains the interval permeability data estimated from the wireline logs by the PFT results.

Equation 5:

$$PFT\ constrained\ K = PFT\ Cor.Factor * Well\ log\ K\ at\ each\ interval$$

Table 7: Wireline log permeabilities constrained by the PFT correction factor.

UWI	Depth	NPHI	NPHI+3	Wireline log permeability	PFT-constrained Permeability
.	.	.	.	.	.
.	.	.	.	.	.
.	.	.	.	.	.
21139000517000	5057	0.195	23	940	781
21139000517000	5058	0.184	21	734	609
21139000517000	5059	0.179	21	656	544
21139000517000	5060	0.172	20	560	465
21139000517000	5061	0.16	19	427	355
21139000517000	5062	0.181	21	686	569
21139000517000	5063	0.193	22	899	746
21139000517000	5064	0.188	22	803	667
21139000517000	5065	0.176	21	613	509
21139000517000	5066	0.197	23	984	817
.	.	.	.	.	.
.	.	.	.	.	.
.	.	.	.	.	.
21139000517000	5521	0.147	18	319	264
21139000517000	5522	0.163	19	457	379
21139000517000	5523	0.18	21	671	557
21139000517000	5524	0.187	22	785	652
21139000517000	5525	0.174	20	586	486
21139000517000	5526	0.156	19	390	324
21139000517000	5527	0.134	16	238	197
21139000517000	5528	0.137	17	254	211
21139000517000	5529	0.151	18	349	289
21139000517000	5530	0.152	18	357	296
.	.	.	.	.	.
.	.	.	.	.	.
.	.	.	.	.	.

CHAPTER V

STATIC GEOLOGIC MODELS

Prior to the permitting of a CO_2 sequestration project, documentation of a robust transient injection model is needed to predict the possible outcomes of CO_2 injection. The first step to creating a reliable transient model is creating a sound static geologic model. This study used Schlumberger's Petrel 2010 to model two potential injection zones that vary in size and complexity. Model 1 is located in Ottawa County, and is close to the CO_2 point sources in western Michigan (Figure 21); the model area is about 1.4 square miles (Figure 20). Model 2 occupies approximately 6,492 square miles (Figure 20). Model 2 has three potential injection zones with varying petrophysical properties; Facies 1, Facies 2 and Facies 3. Both of the models are located in western Michigan because the Mount Simon in the west is much less complex and has more storage potential than the Mount Simon in the east (Kelley 2010; Barnes et al., 2009).

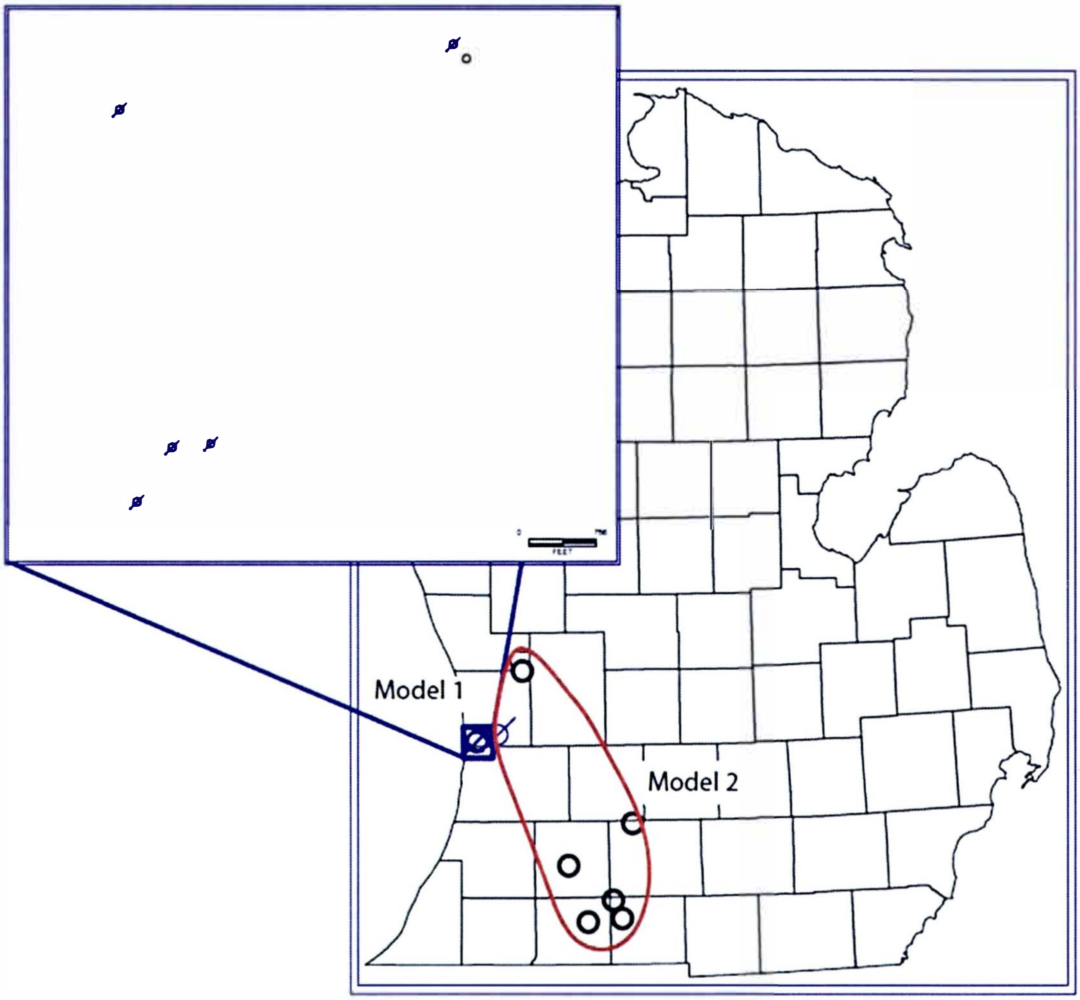

Figure 20: Location map for the two geostatic models. The map above illustrates the locations of the wells used in two static geologic models created for this study.

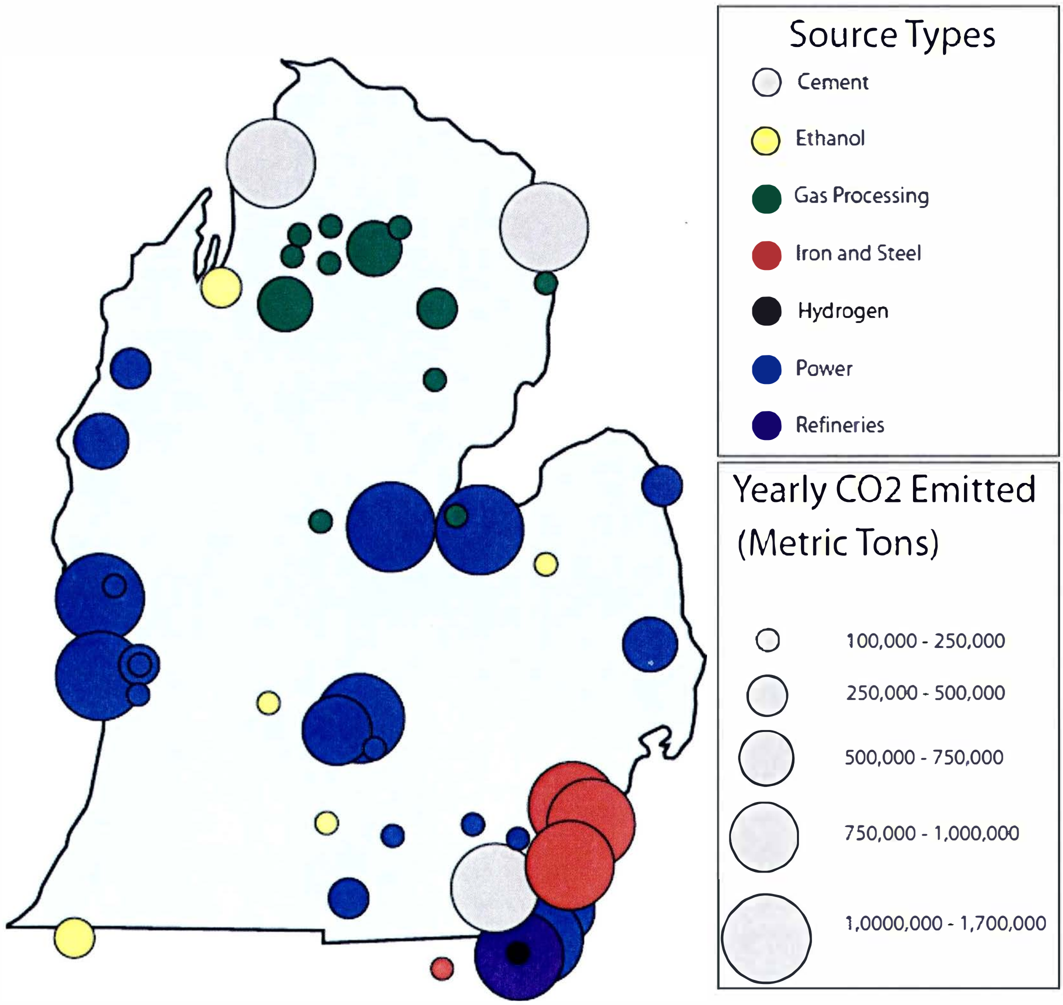

Figure 21: Distribution of point sources for CO2 pollution in Michigan.

Models

Model 1

Model 1 (Appendices 22-25) is located in Ottawa County and is composed of data from 5 wells. These wells were chosen for static modeling because they have the highest density of data in the entire dataset. Additionally, the wells modeled include the Deep Well M007 (21139000707000), for which Barnes et al. (2009) modeled a 20 year injection. The wells were not drilled deep enough to incorporate Facies 3, so only Facies 1 and 2 are modeled. These two Facies are expected to accept an overwhelming majority of the injectate. Porosity was estimated from the wireline logs by using the NPHI+3 for both Facies 1 and 2 (Table 4, Appendix 4). The porosity to permeability transformations are found in Appendix 1. Using the techniques discussed above, the PFT data was used to constrain/calibrate permeability estimations for each of the 5 wells. The model parameters and results are tabulated in Appendices 22-24.

GR, NPHI+3 and wireline log estimated permeabilities were all modeled in Petrel. Figures 22 is a 3-D model of GR, where the warmer colors are higher GR API signatures. There is a clear distinction between Facies 1 and 2. Facies 1 has a higher GR signature. Figure 23 is a 2-D slice of the 3-D permeability model. Warmer colors represent higher permeabilities. Figure 23 demonstrates the lower permeability in Facies 1 relative to Facies 2.

There was not enough data to create a meaningful variogram; the sill and the nugget values were left at the default parameters. The range at which data would be extrapolated or interpolated between data points was picked based on the minimum distance needed to interpolate between the wells with the largest distance between them. Wireline log features in Facies 1 and 2 can be traced from well to well quite consistently and predictably. The algorithm used to interpolate and extrapolate data between wells should reflect this level of lateral continuity. As such, the simple kriging method was chosen. Considering that the basal sands can extend vast spatial areas with little depositional variation (Runkel, 2007), and this model area is a very small portion of the depositional system, this system was not treated as an anisotropic, and depositional strike and dip were not taken into consideration.

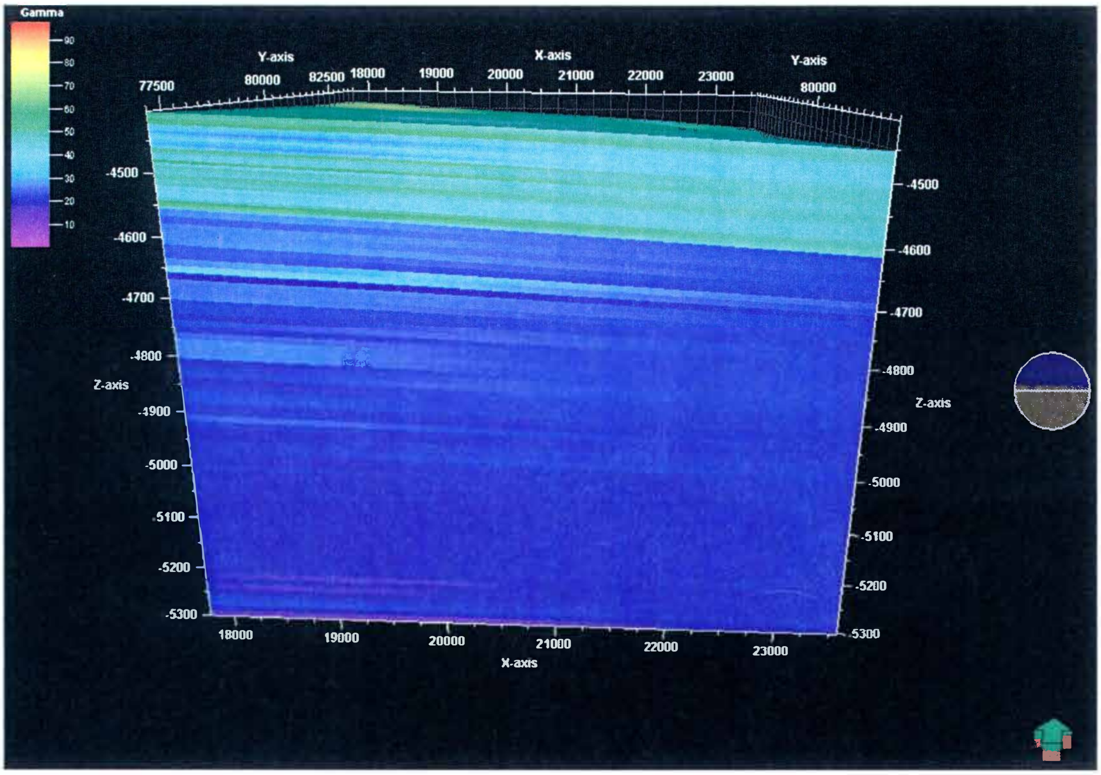

Figure 22: Model 1: a realization of the 3-dimensional distribution of gamma ray (API) signals.

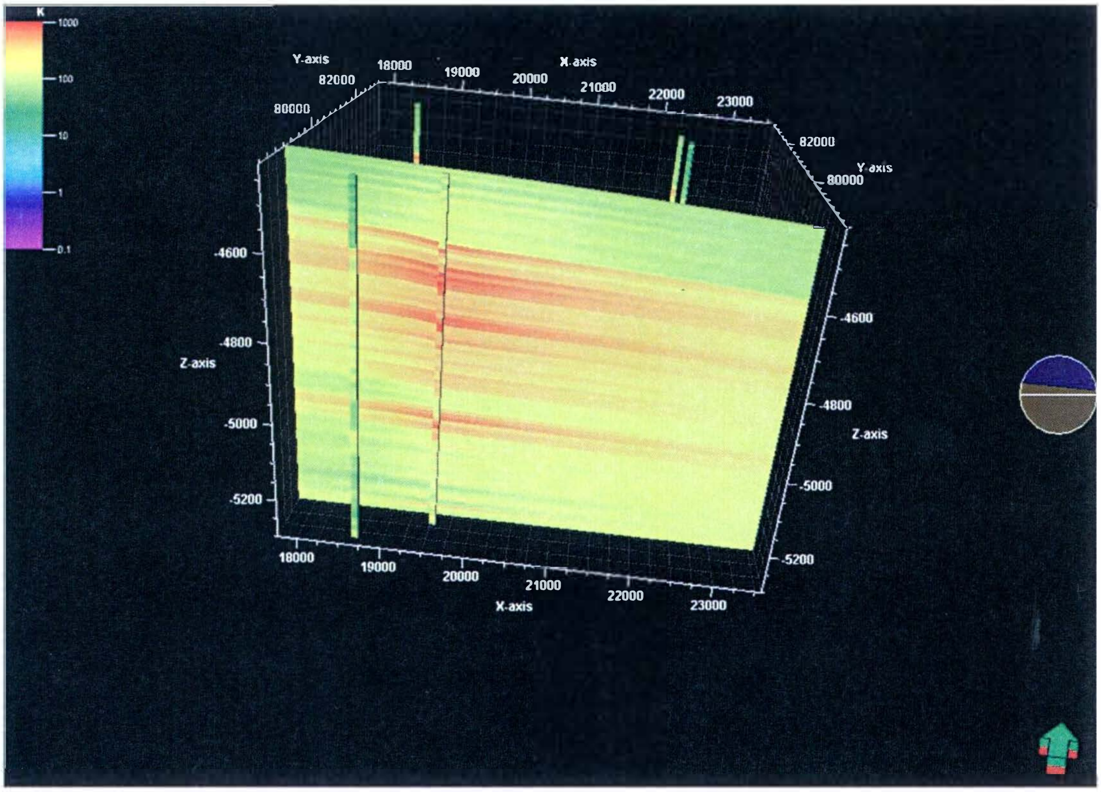

Figure 23: Model 1: permeability constrained by PFT data. The above picture is a cross-section through Model 1 illustrating the distribution of PFT constrained permeability. Note that Facies 1 has relatively lower permeability than Facies 2.

Model 2

Model 2 (Appendices 25-27) is a multicounty model that covers about 6,492 square miles and has a volume of about 6,881 cubic miles. Petrel was used to model GR, NPHI+3 and wireline log permeability. PFT data was not available to constrain/calibrate permeability estimations. There was not enough data to create a meaningful variogram, so the sill and the nugget values were left at the default parameters. The range at which data would be extrapolated or interpolated between data points was picked based on the minimum distance needed to interpolate between the wells with the largest distance between them. Similar to Model 1, the petrophysical properties for Facies 1 and 2 were interpolated and extrapolated with the simple kriging algorithm.

Facies 3 is interpreted to be a braided fluvial and alluvial fan deposit (Core Description 1). Facies 3 exhibits tremendous vertical heterogeneity in core. The simple kriging function was used on Facies 1 and 2 because these facies are interpreted to have laterally continuity on a regional scale. Facies 3 is expected to have very limited lateral continuity, and might be better modeled with a kriging algorithm that reflects the random spatial variability of this Facies. The Gaussian kriging function was chosen as the interpolation and extrapolation algorithm for Facies 3 because it most accurately captures the random spatial variability of the depositional system (Figure 25).

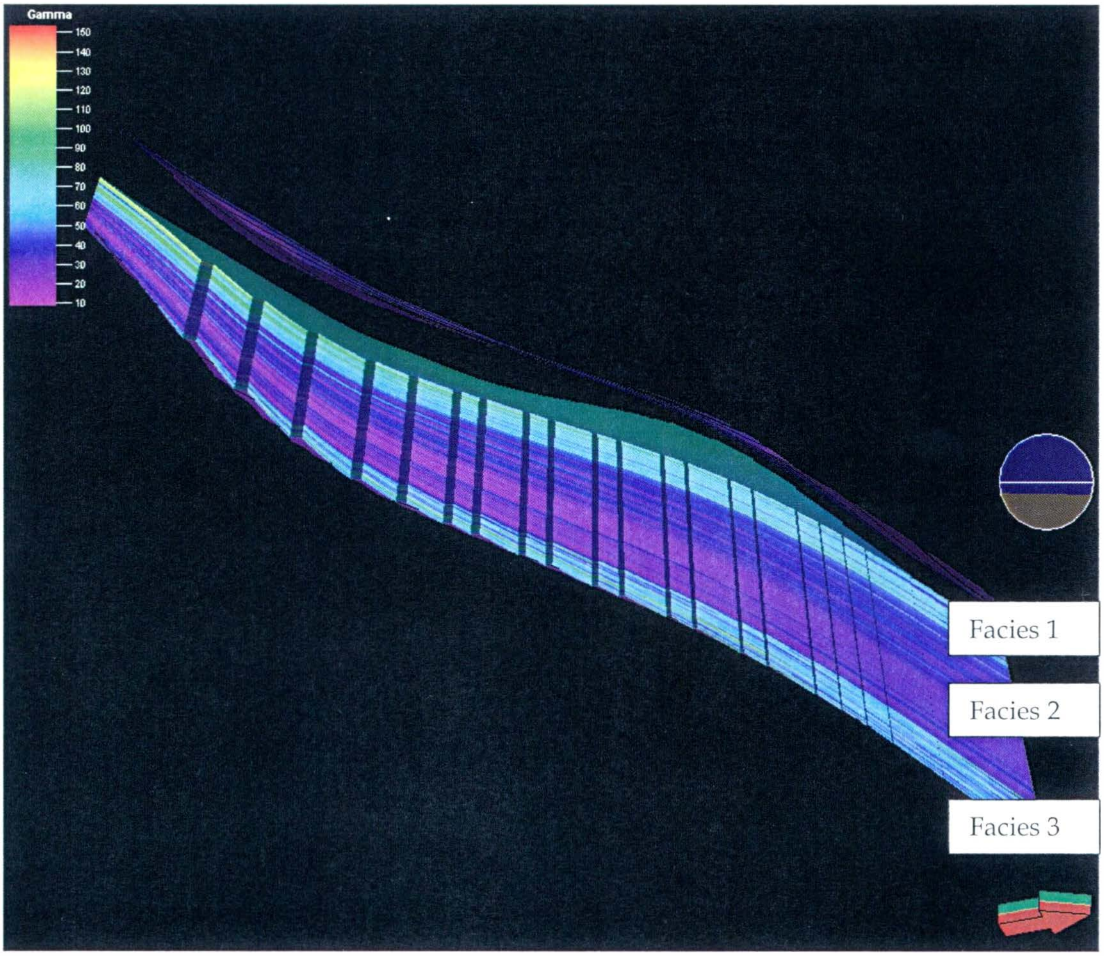

Figure 24: Model 2: gamma ray interpretation. Vertical exaggeration is 100X. This illustrates that there is clear distinction between Facies 1, 2 and 3 when viewing the interpreted GR data. This model is bound by the Precambrian on the bottom and the top of the Eau Claire on the top. The Eau Claire is pictured in the above image.

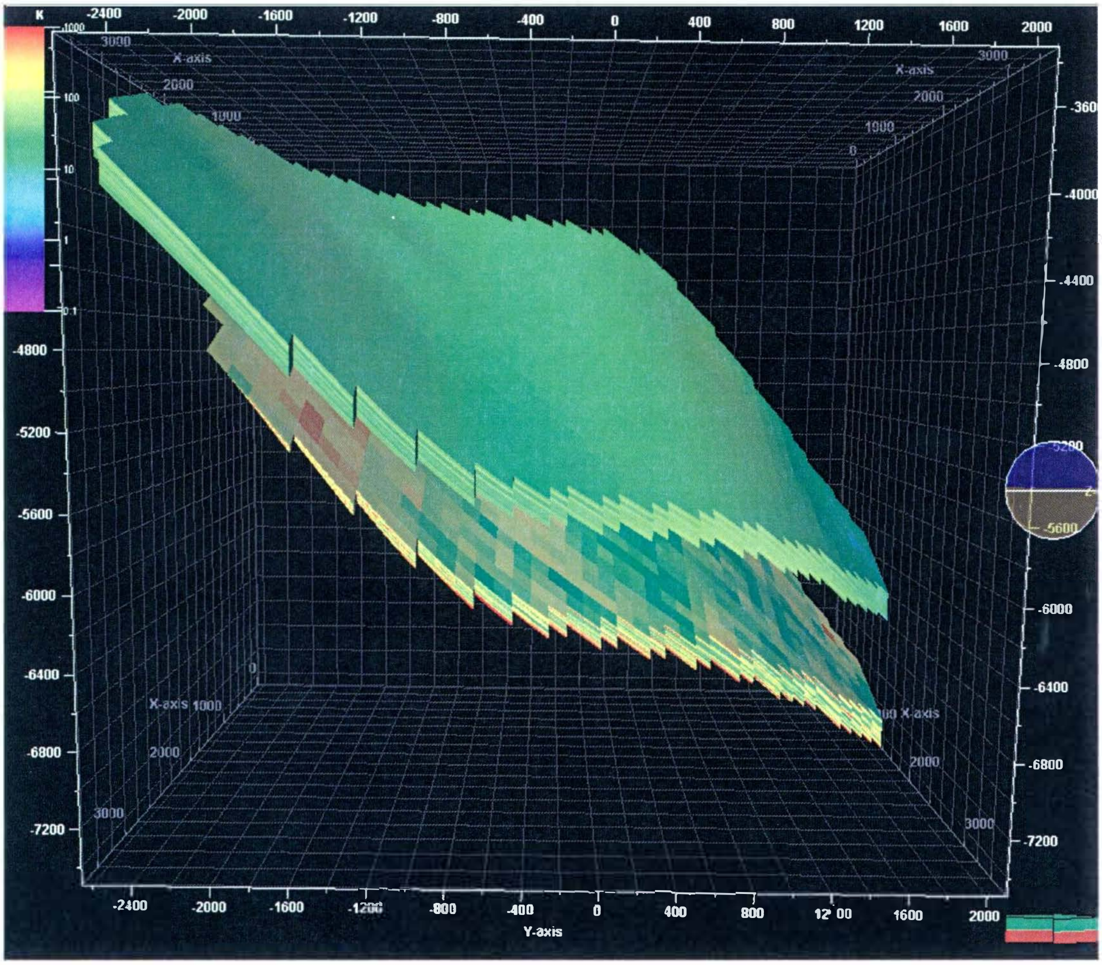

Figure 25: Model 2: a visual comparison between kriging and the Gaussian random function. Facies 2 is not pictured in this image. The purpose of this image is to demonstrate the difference between the simple kriging algorithm (the upper unit -Facies 1) and the Gaussian random simulation (the lower unit - Facies 3)

CHAPTER VI

RESULTS AND CONCLUSIONS

- The Lloyd Cupp #1-11 is the only studied rock core that penetrates Wireline Log Facies 3 and the Precambrian crystalline basement rock. The textural immaturity of Facies 3 identified in core, in addition to a petrographic thin section comparison between the textures and compositions of the minerals in Facies 3 and the Precambrian Basement suggests that the Wireline Log Facies 3 is derived from the local Precambrian Basement.
- Odom (1975) suggests that feldspar concentrations are inversely proportional to grain size in the Mount Simon Sandstone of the Upper Mississippi Valley due to the relative ease at which feldspar is abraded and then subsequently hydraulically sorted. Point count data from this study indicates that Odom's feldspar to grain size relationship only holds true in some areas, especially sections of the Mount Simon Sandstone dominated by more distal marine shelf facies.
- The gamma ray (GR) log response is typically interpreted to be inversely proportional to grain size and representative of reservoir quality potential in terrigenous clastics dominated successions (Posamentier, 1999; Emery, 1996). Kelley, et al. (2010) suggested that in eastern Michigan the variation of K-feldspar content, rather than grain size and clay content is directly correlated to GR log response. As a result the GR log response is not clearly nor consistently related to reservoir quality. This study found that the GR log may potentially be used as a qualitative assessment of permeability based on the following relationships: (1) the GR log signature is proportional

to the K-feldspar content of the rock (Figure 11), (2) in some regions the abundance of feldspar is inversely proportional to grain size (Figure 9) and (3) finer grained sandstones have smaller pore throats, and in turn lower permeabilities (Pettijohn et al., 1987). In areas analogues to the Angel and Kehrl 1-12 well, where potassium feldspar concentrations are shown to be inversely proportional to grain size, the GR log might be used as a qualitative assessment permeability.

- Baranoski (2010, and in review) recognized a west to east lateral variation in the Mount Simon of Ohio and southeastern Michigan in wire line log signature and mineralogy, and suggests that these eastern lithofacies should not be called the Mount Simon. Data from this study supports Baranoski's (2010) interpretation. The eastern Mount Simon has significantly more potassium feldspar, carbonate and iron oxides.
- Pressure fall-off test data can be used to help constrain permeability interpretations from wireline log suites. Using pressure fall-off tests helped in the development of more geologically sound 3-D static models that mapped the distribution of permeability.
- The best means to estimate porosity from wireline logs varies for each individual facies. Porosities from relatively homogenous facies such as Facies 2 or Facies 4 can be fairly accurately estimated from wireline logs, but extremely heterogeneous facies such as Facies 6 should be further subdivided for more accurate core to wireline log correlations.
- Two 3-D static models were created in Schlumberger's Petrel. The models illustrate differences in petrophysical properties between each of the modeled facies.

CHAPTER VII

DISCUSSION AND SEQUESTRATION CONSIDERATIONS

It is important to note that the models created in this study are just one of many possible realizations, and the data attributed to each cell probably varies significantly relative to the actual rock properties. However, this does not mean the models are not of use. Using these static geologic models as the geologic framework for transient injection models will help gain insight into potential injection volumes, injection rates, and the distribution and intensity of pressure plumes.

Recent work in the CO_2 sequestration community suggests that low permeability rocks may result in significantly higher volumes of CO_2 trapped permanently as a residual fluid (Brennan et al., 2010). Furthermore, rocks with small pore throats and large pores may prove to be the most effective at retaining CO_2 after the plume moves through (Brennan et al., 2010). As discussed earlier, Wireline Log Facies 5 has as much as 40% of the porosity that results from the dissolution of primary framework grains, predominantly potassium feldspar (Plate 1-3). Future studies might find that the nature of the pore network in Facies 5 may prove to be the lowest risk permanent storage injection zone in the Mount Simon.

Fisher et al., (1988) documented the presence of a Precambrian paleotopographic high in Livingston County, Michigan, on which the Mount Simon was not deposited. A cross-section for this feature is attached as Appendix 28. Leetaru and McBride (2009) used seismic data in the Illinois Basin to identify numerous Precambrian paleotopographic highs, which in many cases drastically reduces the thickness of the overlain Mount Simon Sandstone. The basement topography is not well known in Michigan and should be investigated with seismic data prior to the implementation of any CO_2 injection project.

CHAPTER VIII

FUTURE RESEARCH

Kelley (2010) and this study suggest that the variation in primary mineralogy in the Mount Simon Sandstone across the Michigan basin is a result of a variation in source rock provenance. Zircon dating could be done to constrain source rock provenance interpretations (Anderson, 2005).

Preliminary work was done with chemical equilibrium calculations to investigate the mineralogical changes that result after injecting massive amounts of CO_2. XRD, petrographic work and infrared spectroscopy were all done to characterize mineral speciations. The mineral data gathered in this research could be used as input data for geochemical equilibrium calculations as a means to better understand the potential reactions that will occur when CO_2 enters the system.

The Eau Claire Formation is the primary confining unit for the Mount Simon Sandstone. A more rigorous geologic investigation into the Eau Claire is needed to understand the spatial variation in lithology and petrophysical properties of the unit across the basin. Furthermore, injectivity into the Mt. Simon will be highly dependent on the strength of the cap rock, as such mechanical testing and modeling should be done on the Eau Claire to quantify the stress at which the cap will fracture.

This study created two 3-D models in Schlumberger, Petrel. Using these 3-Dl models as the framework for transient injections models will greatly enhance our understanding of the Mount Simon as a potential injection target.

The correlation coefficients for the porosity to permeability transformations and the standard deviations for the wireline log porosity estimations are both poor. Additional models should be created to estimate the lowest and highest possible realizations for the distribution of porosity and permeability to better understand the potential suite of realizations that could occur during injection.

REFERENCES

Aigner, T., 1982, Calcareous tempestites: storm-dominated stratification in Upper Muschelkalk limestones (Triassic, SW-Germany), in Einsele, G., and Seilacher, A. eds., Cyclic and Event Stratification: Berlin Springer-Verlag, p. 180-198

Anonymous, Subsurface Inc., 1999, unpublished mechanical injection report for Park-Davis Holland Michigan, available at the Michigan Geological Survey, Environmental Quality Division

Anderson, T., 2005, Detrital zircons as tracers of sedimentary provenance: limiting conditions from statistics and numerical simulation, Chemical Geology, v216, p. 249-270

Baranoski, M. T., (in review), revised Cambrian sub-Knox lithostratigraphy for the Ohio region: subsurface correlation and lithostratigraphy of the Cambrian Mount Simon Sandstone, Eau Claire Formation, Sandusky Formation and Conasauga Group: (unpub.) Ohio Division of Geological Survey, Columbus, Ohio.

Baranoski, M. T., 2010, (email communication), Ohio Division of Geological Survey, Columbus, Ohio, mark.baranoski@dnr.state.oh.us.

Barnes, D. A., D. H. Bacon, and S. R. Kelley, 2009, Geological sequestration of carbon dioxide in the Cambrian Mount Simon Sandstone: Regional storage capacity, site characterization, and large scale injection feasibility, Michigan Basin: Environmental Geosciences, v. 16, no. 3, p. 163–183

Becker, L. E., Hreha, A. J., and Dawson, T. A., 1978, Pre-Knox stratigraphy in Indiana, State of Indiana Department of Natural Resources Geologic Survey, p. 57

Blakey, R., 2005, Paleogeography of North America, http://jan.ucc.nau.edu/~rcb7/globaltext2.html, accessed January, 2011

Brennan, S.T., Burruss, R.C., Merrill, M.D., Freeman, P.A., and Ruppert, L.F., 2010, A probabilistic assessment methodology for the evaluation of geologic carbon dioxide storage: U.S. Geological Survey Open-File Report 2010–1127, p. 31

Briggs, L. I., 1968, Geology of subsurface waste disposal in Michigan Basin, in J. E.Galley, ed., Subsurface disposal in geologic basins—A study of reservoir strata: AAPG Memoir 10, p. 128–153

Catacosino, P.A., 1973, Cambrian lithostratigraphy of the Michigan Basin, American Association of Petroleum Geologistm v. 57, no. 12, p. 2404-2418

Catacosinos, P. A.,W. B.Harrison III, R. F. Reynolds, D. B. Westjohn, and M. S. Wollensak, 2001, Stratigraphic lexicon for Michigan: Michigan Department of Environmental Quality, Geological Survey Division, Bulletin, v. 8, p. 56.

Cottingham, J. T., 1990, Cambrian–Early Ordovician sequence stratigraphy and Mount Simon Sandstone petrology—Michigan Basin: M.S. thesis, Western Michigan University, p. 1–95

Doveton, J. H., 1994, Geologic log analysis using computer methods, Tulsa, Oklahoma, USA: The American Association of Petroleum Geologists, p. 30

Driese, S. G., C.W. Byers, and R. H. Dott Jr., 1981, Tidal deposition in the basal Upper Cambrian Mt. Simon Formation in Wisconsin: Journal of Sedimentary Petrology, v. 51, no. 2, p. 367–381

Emery, D, & Myers, K. J., 1996, Sequence stratigraphy, Malden, Massachusetts, USA: Blackwell Publishing Company. p.67

EPA Region 6, 2002, UIC Pressure falloff guidelines, http://www.epa.gov/region6/water/swp/uic/guideline.pdf

Fisher, J.A., 1981, Fault patterns in southeastern Michigan, M.S. thesis, Michigan State University

Fisher, J. H., and Barratt, M. W., Droste , J. B., and Shaver, R. H. 1988, Michigan basin, *in* Sloss, L. L., ed., Sedimentary cover – North American Craton: U.S.: Boulder, Colorado, Geological Society of America, Geology of North America, v. D-2, p. 361-381

Fishietto F. E., 2009, Lithofacies and depositional environments of the Cambrian Mount Simon Sandstone in the Northern Illinois Basin: implications for CO_2 sequestration: M.S thesis, Purdue University, p. 1-87

Howell, P. D. and van der Pluijm B. A., 1999, Structural sequences and styles of subsidence in the Michigan basin: Geological Society of America Bulletin, v.111, no. 7, p. 974-991

Kelley S. R., 2010, Geologic control on reservoir quality for carbon sequestration in the Mount Simon Sandstone, Michigan Basin, USA, M.S. Thesis, Western Michigan University

Kelley S. R., Patterson K. J. and Barnes D. A., 2010, Geological Controls on Mount Simon Sandstone Reservoir Quality and Geological Carbon Sequestration Potential in the Michigan Basin, USA: Conventional Core, Petrographic, and Petrophysics Analysis, AAPG 2010, Annual Convention and Exhibit, online Abstract.

Leetaru, H. E., & McBride, J. H., 2009, Reservoir uncertainty, Precambrian topography, and carbon sequestration in the Mt. Simon sandstone, Illinois basin. Environmental Geosciences, v. 16, no. 4, p. 235–243.

Medina, C. R., D. A. Barnes, and J. A. Rupp, 2008, Depth relationships in porosity and permeability in the Mount Simon Sandstone of the Midwest region: Applications for carbon sequestration: Eastern Section Meeting of the AAPG, Pittsburg, Pennsylvania, October 14, 2008, online Abstracts.

Maynr, E., 1963, Population, species and evolution, USA: Belknap Press of Harvard University Press, p. 356-360

National Energy Technology Laboratories (NETL), 2007, Carbon Sequestration Atlas of the United States and Canada, U.S Department of Energy Office of Fossil Energy

Odom, I. E., 1975, Feldspar-grain size relations in Cambrian arenites, upper Mississippi Valley: Journal of Sedimentary Research, v. 45, no. 3, p. 636–650

Pettijohn, F. J., Potter, P. E., & Siever, R., 1987, Sand and sandstone, West Hanover, MA: Springer-Verlag, p. 87

Posamentier, H. W., & Allen, G. P., 1999, Siliciclastic sequence stratigraphy: concepts and applications, Tulsa, Oklahoma, U.S.A: Society for Sedimentary Geology, p, 175-180

Plummer, P.S., Gostin, V.A., 1981. Shrinkage cracks; desiccation orsynaeresis? Journal of Sedimentary Petrology, 51, 1147–1156

Pratt B. R., 1997 Syneresis cracks: subaqueous shrinkage in argillaceous sediments caused by earthquake-induced dewatering, Sedimentary Geology, 117, p. 1-10

Runkel, A.C., Miller J. F., McKay R. M., Palmer A. R., and Taylor J. F., 2007, High-resolution sequence stratigraphy of lower Paleozoic sheet sandstones in central North America: The role of special conditions of cratonic interiors in development of stratal architecture: Geological Society of America Bulletin, v. 119, no. 7/8, p. 860–881

Silin, D., Tsang C., and Gerrish H., 2005, Replacing annual shut-in well tests by analysis of regular injection data: field-case feasibility study, Development in Water Science, v. 52, p. 139-149

Sloss, L. L., 1988, Tectonic evolution of the craton in Phanerozoic time, *in* Sloss, L. L., ed., Sedimentary cover – North American Craton: U.S.: Boulder, Colorado, Geological Society of America, Geology of North America, v. D-2, p. 25-50

Tucker, Maurice. 1988. Techniques in Sedimentology. London, UK: Osney Mean, Oxford, p. 98-100

Walcott, C.D., 1914, Dikelocephalus and other genera of the Dikelocephalinae, Smithsonian Misc. Collections, v. 57, p.345-415

Walker, R., 1985, Deposition of sand in shallow seas and application to reservoirs in the Western Interior Seaway, RMS-SEPM Short Course, Febuary 20-21, p. 35-80

Plate 1: The Angell Kehrl #1-12

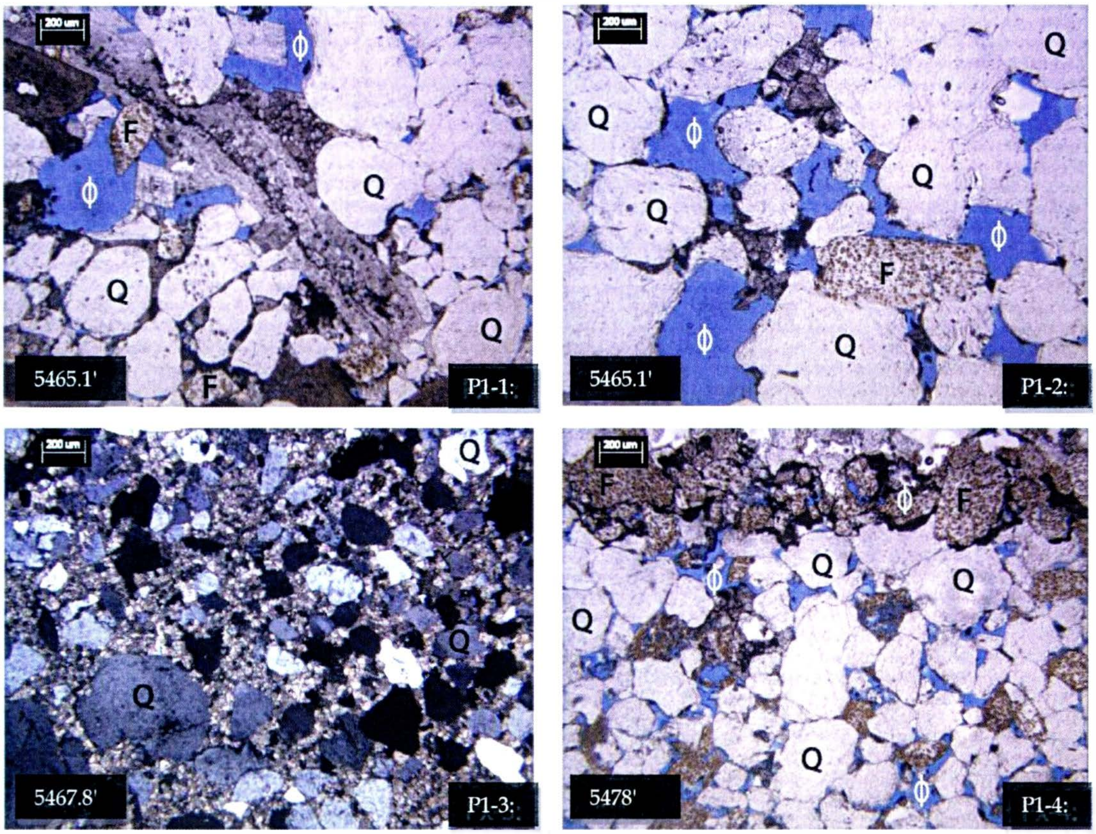

P1-1: Plane-polarized light (PPL) - Poorly sorted sandstone with carbonate cement and unidentified bioclasts. **P1-2: PPL** - Large irregular pore shapes suggest dissolution porosity **P1-3: Cross-polarized-light (XPL)** - Moderate to poorly sorted sandstone suspended in a matrix of carbonate cement. **P1-4: PPL –** There is both intergranular and dissolution porosity in this sample. Iron oxide minerals are proximal to the concentration of feldspar. Intervals of concentrated K-spar extended throughout this entire sample.

Plate 2: The Angell Kehrl #1-12

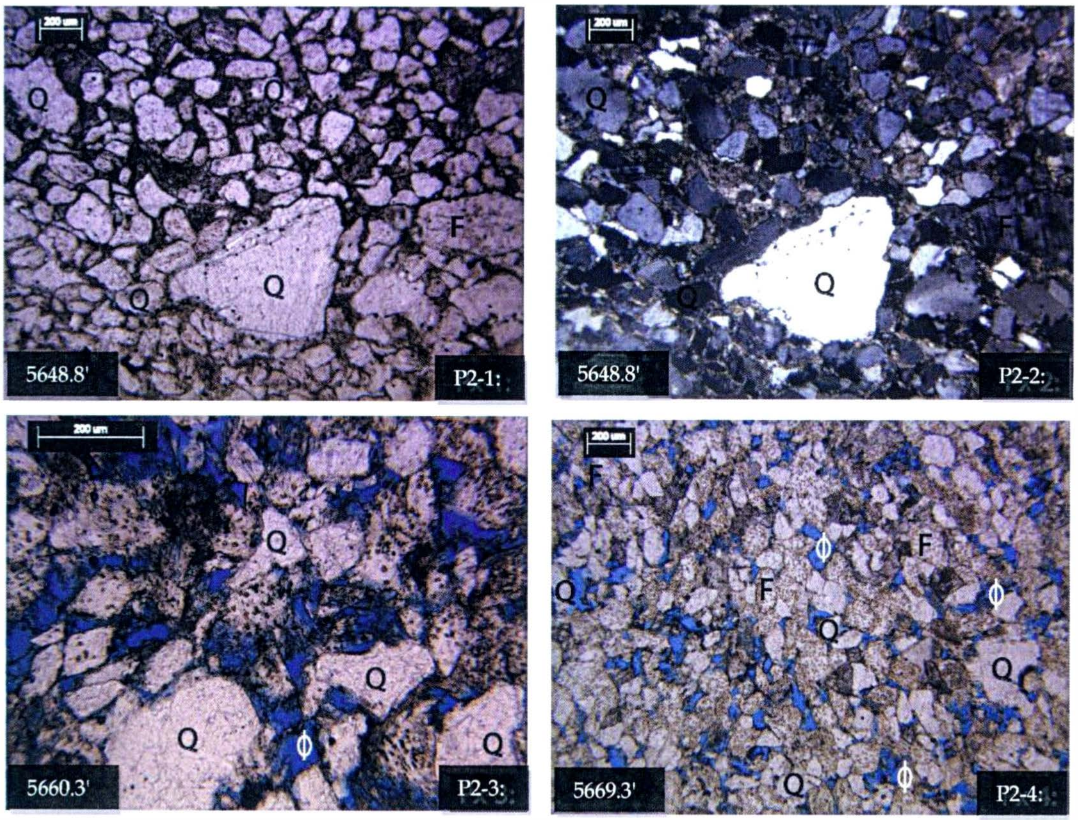

P2-1: PPL & P2-2: XPL - Clay and carbonate cements are segregated; clay is pictured on the bottom and carbonate is pictured on the top. **P2-3: PPL** - The porosity in this picture is predominantly a result of the potassium feldspar dissolution. **P2-4: PPL** - The porosity pictured above is both intergranular and dissolution.

Plate 3: The Angell Kehrl #1-12

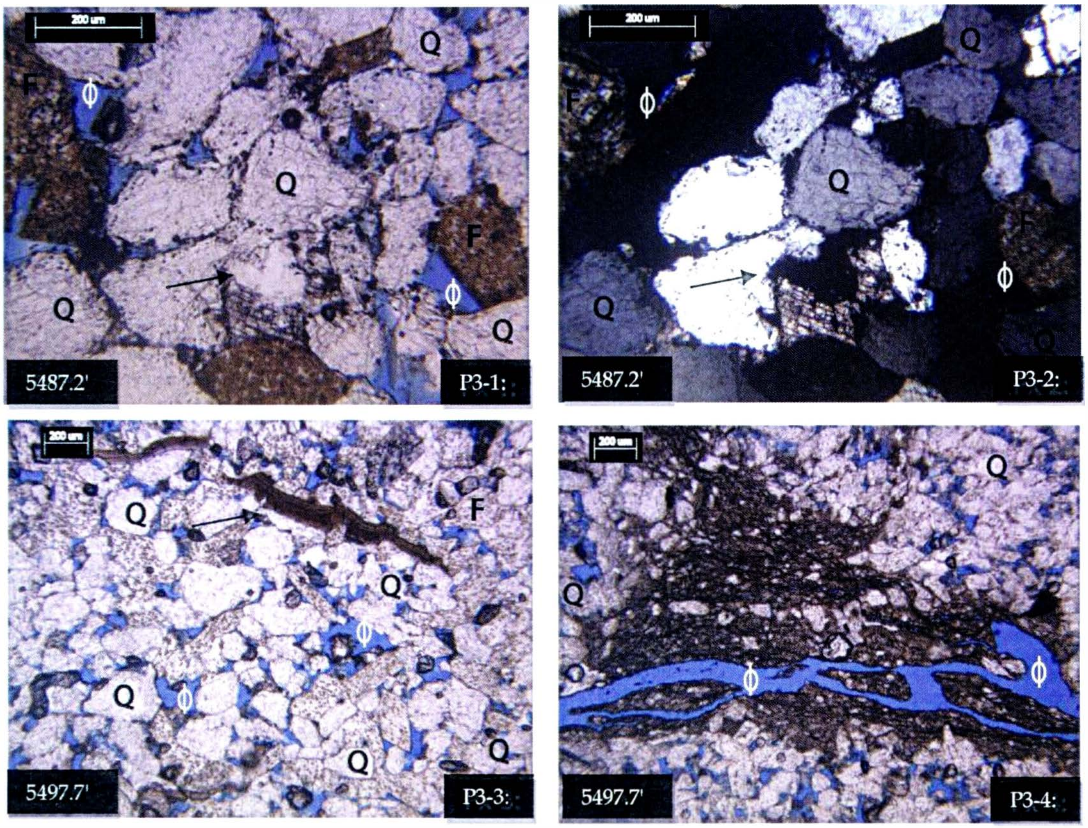

P3-1: PPL - P3-2: XPL - Partial dissolution of carbonate cement (marked by arrow). **P3-3: PPL** - Intergranular porosity and dissolution porosity. The bioclast in the top center of the photo (marked by an arrow) is fractured and deformed from compaction. **P3-4: PPL** - Diagenesis is much more severe along the fracture. Horizontal fracture porosity is prevalent in this sample.

Plate 4: The Lloyd Cupp #1-11

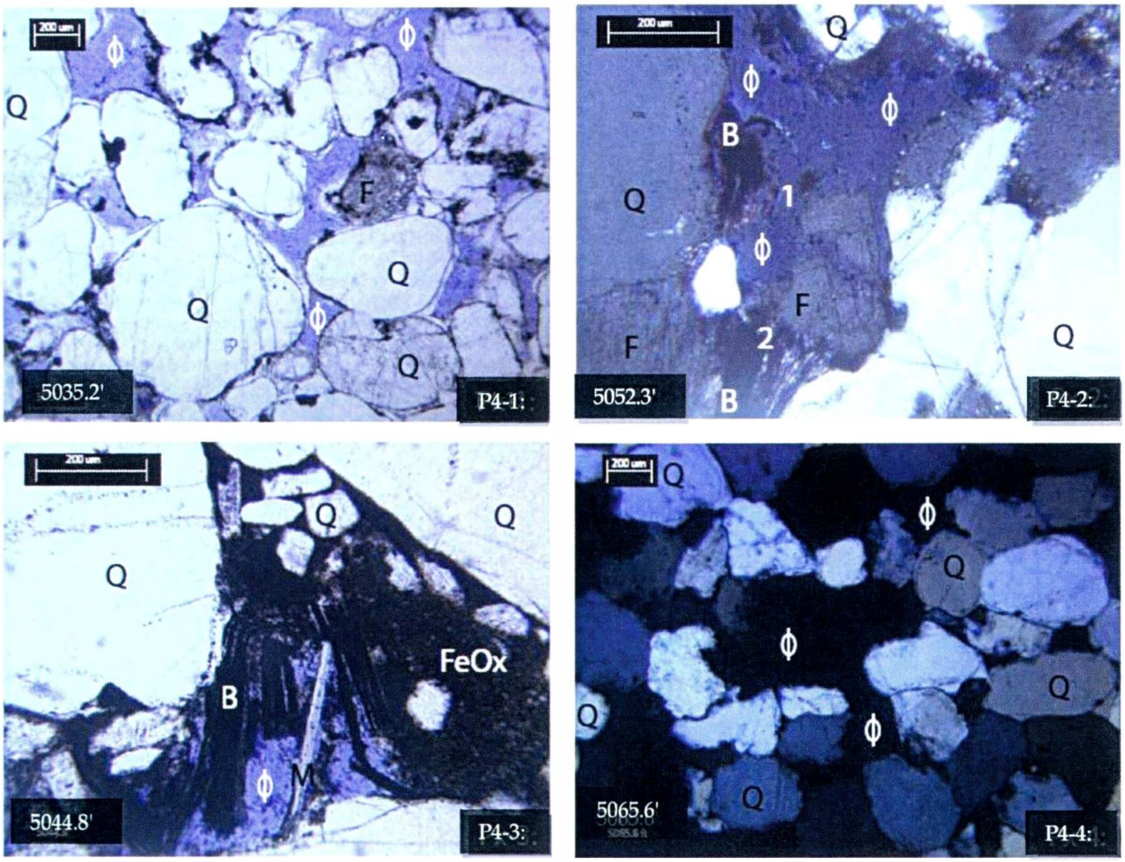

P4-1: PPL - Well rounded quartz grains with rims possibly of iron oxide, that if thick enough will deter quartz overgrowths from forming. Quartz overgrowths are present on grains with very thin iron oxide (?) dust rims. **P4-2: XPL** - Porosity formed from the dissolution of feldspar and biotite in area 1. A biotite crystal is mechanically separted by the growth of illite (?) in area 2. **P4-3: PPL** - It is common to see iron oxide cement in close proximity to weathered biotite as demonstrated in this picture. Muscovite is frequently observed in Lloyd Cupp #1-11, but is often mechanically deformed from compaction. The muscovite sample pictured above is unique for this well. **P4-4: XPL** - This sample is an example of the pre Mount Simon quartz arenite observed throughout the Midwest. Porosity is destroyed by mechanical and chemical compaction and quartz cementation. This picture shows the pressure dissolution and quartz cementation.

Plate 5: The Lloyd Cupp #1-11

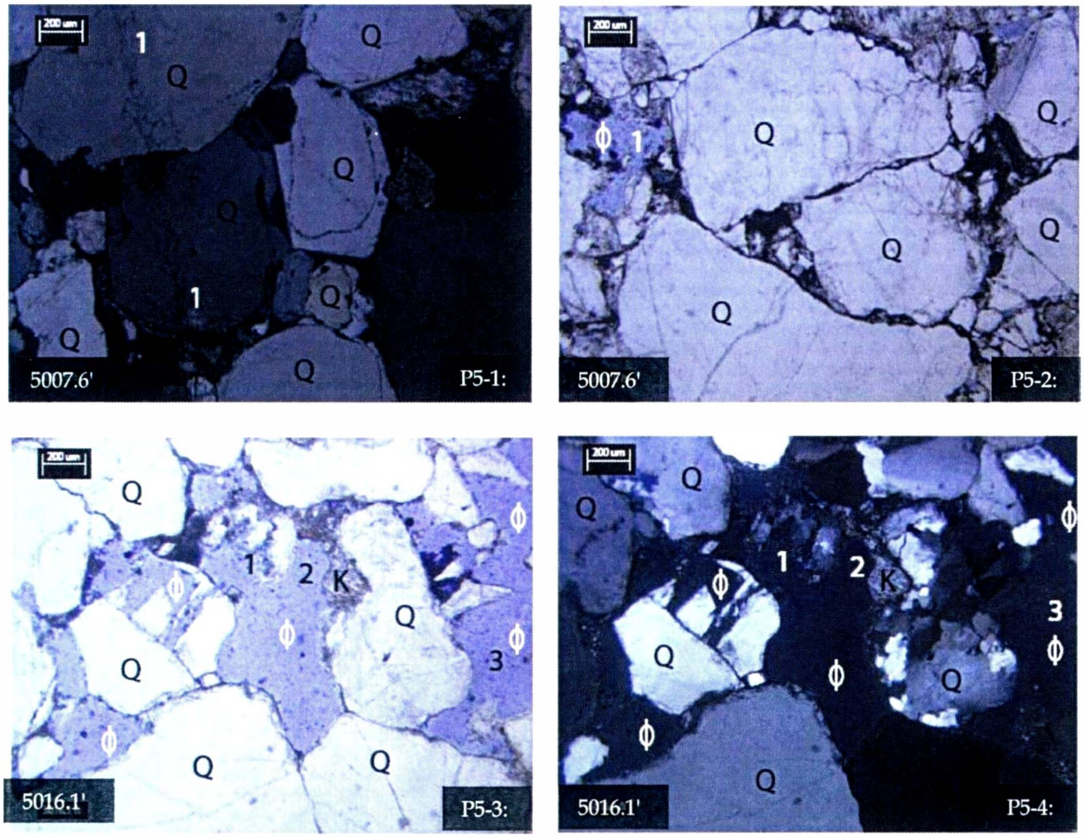

P5-1: XPL - Intervals in the Lloyd Cupp #1-11 that only have sparse iron oxide cement often have large quartz overgrowths that destroy primary porosity as illustrated in the above picture. **P5-2: XPL** -Area 1 is an irregular likely pore that formed from the dissolution of a mineral. The quartz minerals in this picture have undulating faces suggesting that pressure solution of these grains has taken place. Mechanical and chemical compaction along with iron oxide cementation has eliminated nearly all porosity in this sample. **P5-3: PPL and P5-4: XPL** – Secondary porosity constitutes a major portion of the porosity in the less compositionally mature samples of the Lloyd Cupp #1-11. Area one is the dissolution of a polycrystalline quartz grain and area two is secondary porosity resulting from the dissolution of a K-feldspar grain. The irregular shape of the pore at area 3 would suggest that it is a secondary pore.

Plate 6: The Lloyd Cupp #1-11

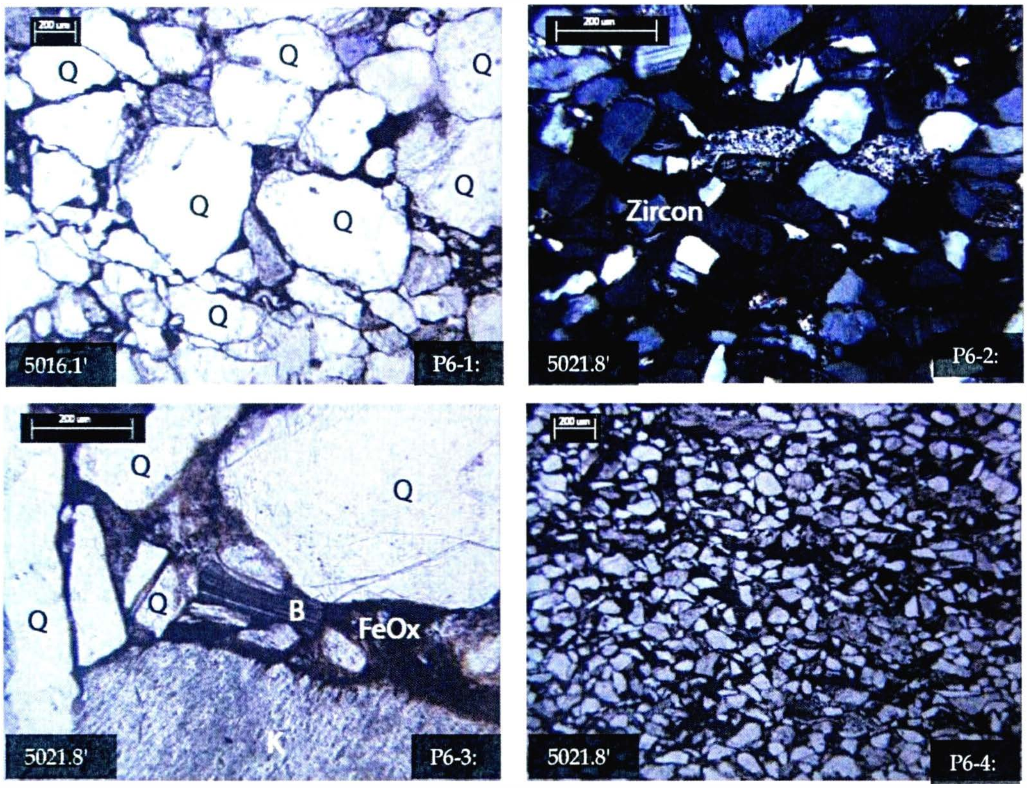

P6-1: PPL - A qualitative assessment suggests that loss of inter granular volume (IGV) by mechanical and chemical compaction is greatest in the poorly sorted intervals of the Lloyd Cupp Lloyd #1-11. This loss of IGV is illustrated in the above picture. **P6-2: XPL** - Zircons are present in the Lloyd Cupp #1-11, and are often associated with relatively smaller and compositionally immature intervals. **P6-3: PPL** – The K-feldspar is partially dissolved. In all of the thin sections described biotite was always proximal to iron oxide cement. **P6-4: PPL** - Very fine grained to silt sized intervals are compositionally immature and entirely cemented with iron oxide cement.

Plate 7: The Lloyd Cupp #1-11: Precambrian Basement

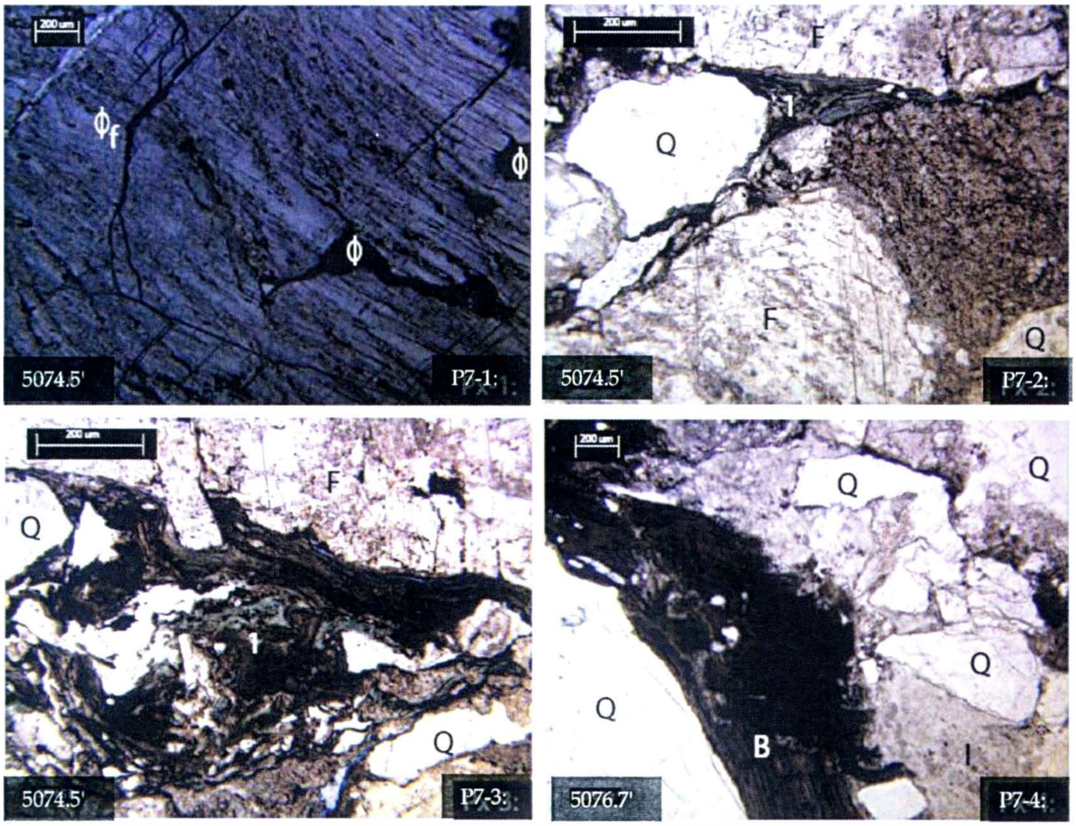

P7-1: XPL - Large feldspar phenocryst with partial dissolution and fracture porosity, some fractures and dissolution pores are filled with authigenic illite. **P7-2: PPL** - Retrogradational alteration of biotite to chlorite (location 1). **P7-3: PPL** -Retrogradational alteration of biotite to chlorite (location 1). **P7-4: PPL** - Dark brown to black biotite similar to the biotite in the above Mount Simon Sandstone.

Plate 8: The Lloyd Cupp #1-11: Precambrian Basement

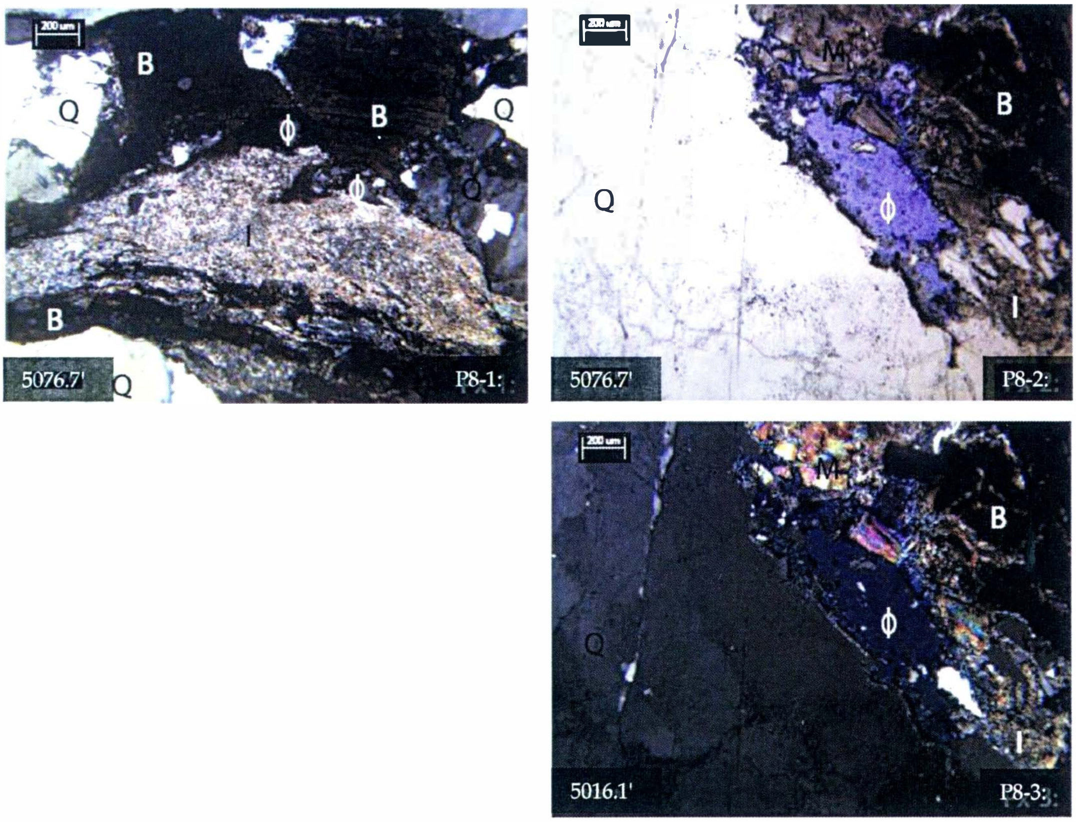

P8-1: XPL - Monocrystalline and polycrystalline quartz, biotite and illite are visible in this picture. The authigenic illite is a product of the weathered feldspars. **P8-2: PPL & P8-3: XPL** – A quartz phenocryst, secondary porosity, biotite, muscovite and illite are present in this picture.

Plate 9: Semet-Solvay #2

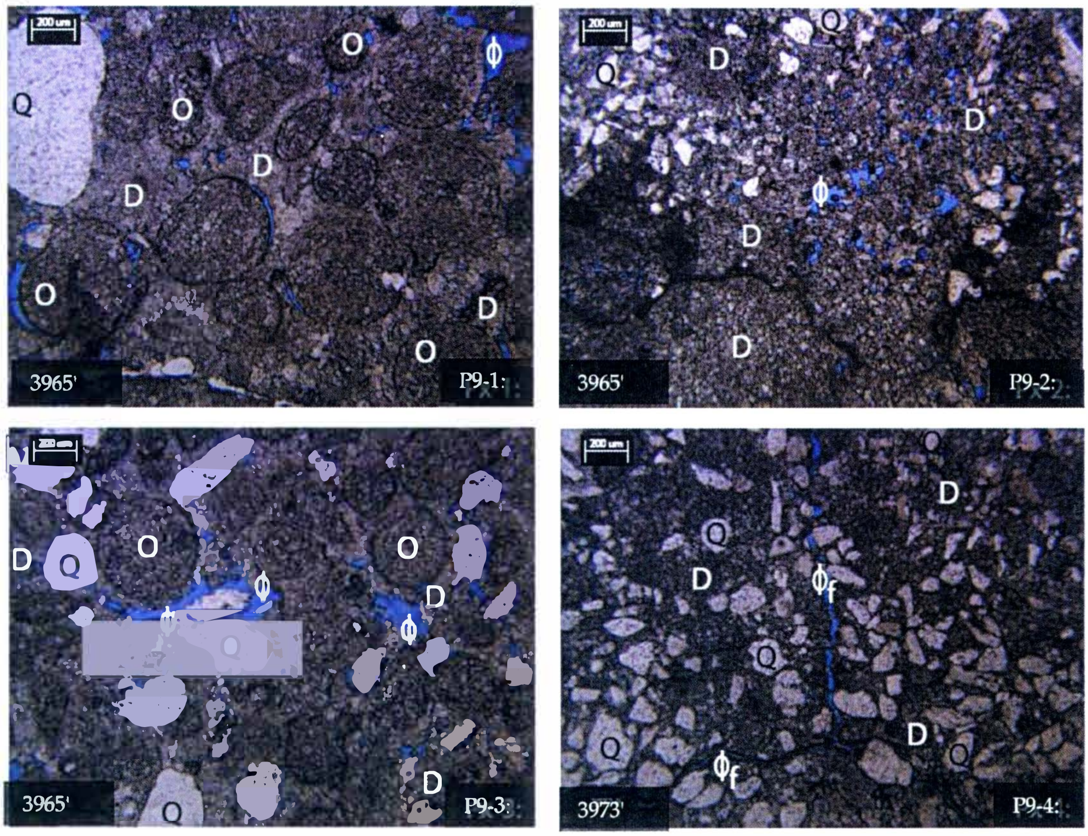

P9-1: PPL – The ooids in this core have been diagenetically altered to dolomite; detrital quartz grains are suspended in a microcrystalline dolomite. **P9-2: PPL** – Porosity is present between the microcrystalline dolomite rhombs and the detrital quartz grains. Primary depositional fabrics are difficult to discern. **P9-3: PPL** – Intergranular porosity is present between the framework of diagenetically altered ooids and detrital quartz grains. Dolomite rhombs have grown into many of the open pores. **P9-4: PPL** – Multiple perpendicular fractures span the entire length of this thin section. Diagenesis along the fractures confirms that the fractures are not artifacts from the process of sampling. The detrital quartz grains pictured are suspended in a matrix of crystalline dolomite. Fracture porosity is the sole porosity in this sample.

Plate 10: Semet-Solvay #2

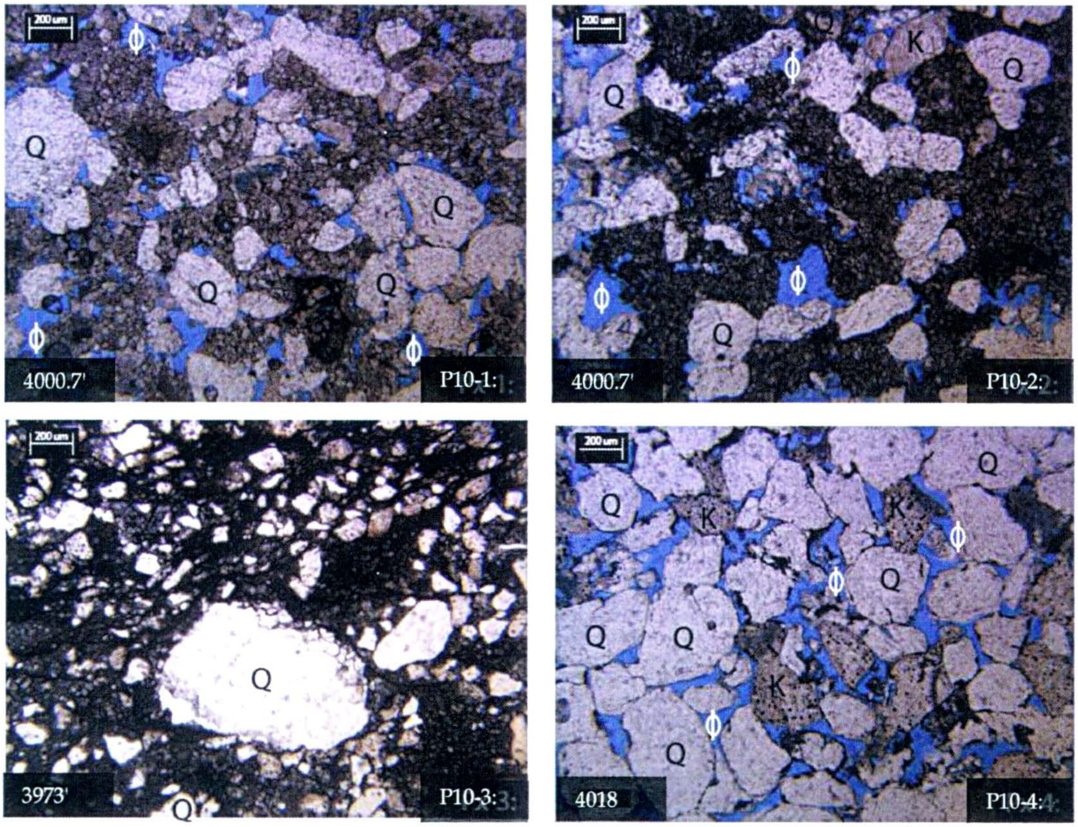

P10-1: PPL – Unstained dolomite from the same slide as P10-2. **P10-2: PPL** – The dolomite stain suggests that the sample is iron rich dolomite. **P10-3: PPL** – Poorly sorted mudstone with no porosity. **P10-4: PPL** – Well sorted arkosic sandstone with small quartz overgrowths, intergranular porosity, dissolution porosity and sparse iron oxide cementation.

Plate 11: Semet-Solvay #2

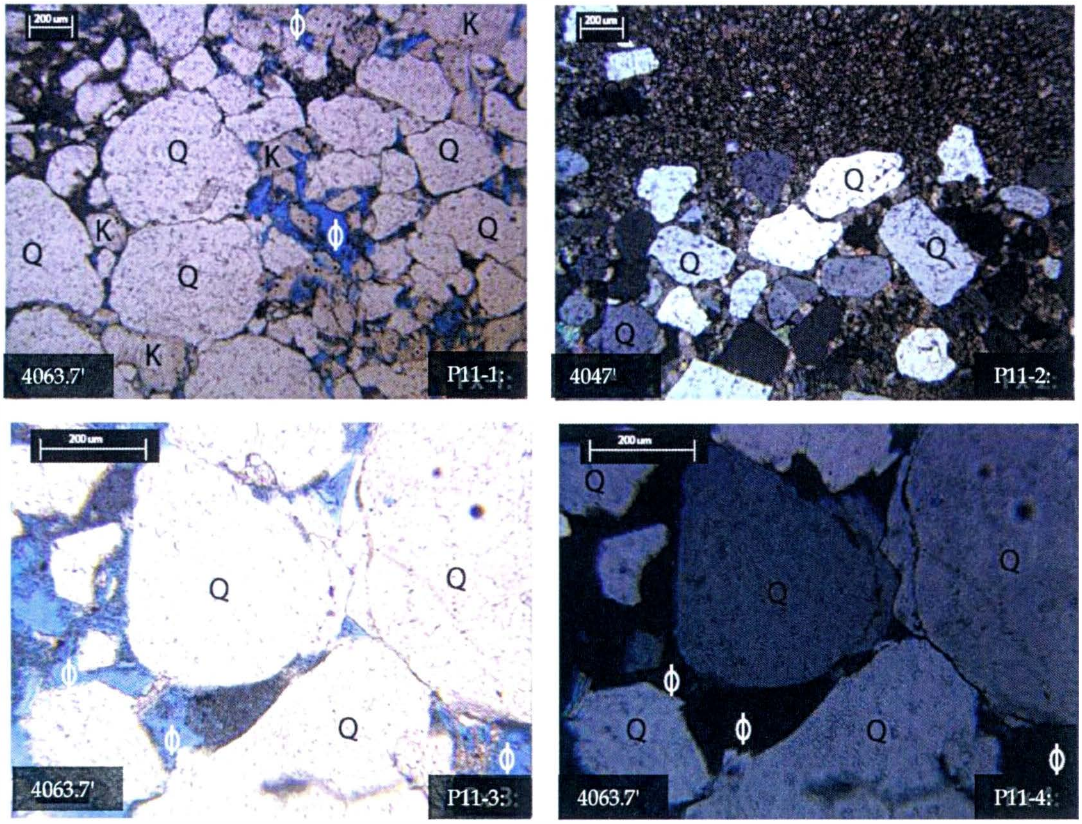

P11-1 :PPL – Quartz pressure solution results in the loss of intergranular volume. Porosity in the sample is mostly from the dissolution of feldspars. **P11-2: PPL** – Sharp contact between carbonate dominated and siliciclastic dominated facies. The dolomite above the clastics is microcrystalline, while the dolomite crystals mixed with the clastics are much larger. **P11-3: PPL and P11-4: XPL** – Dissolution of K-spar results in dissolution porosity and clay. Quartz overgrowths are present

Plate 12: Semet-Solvay #2

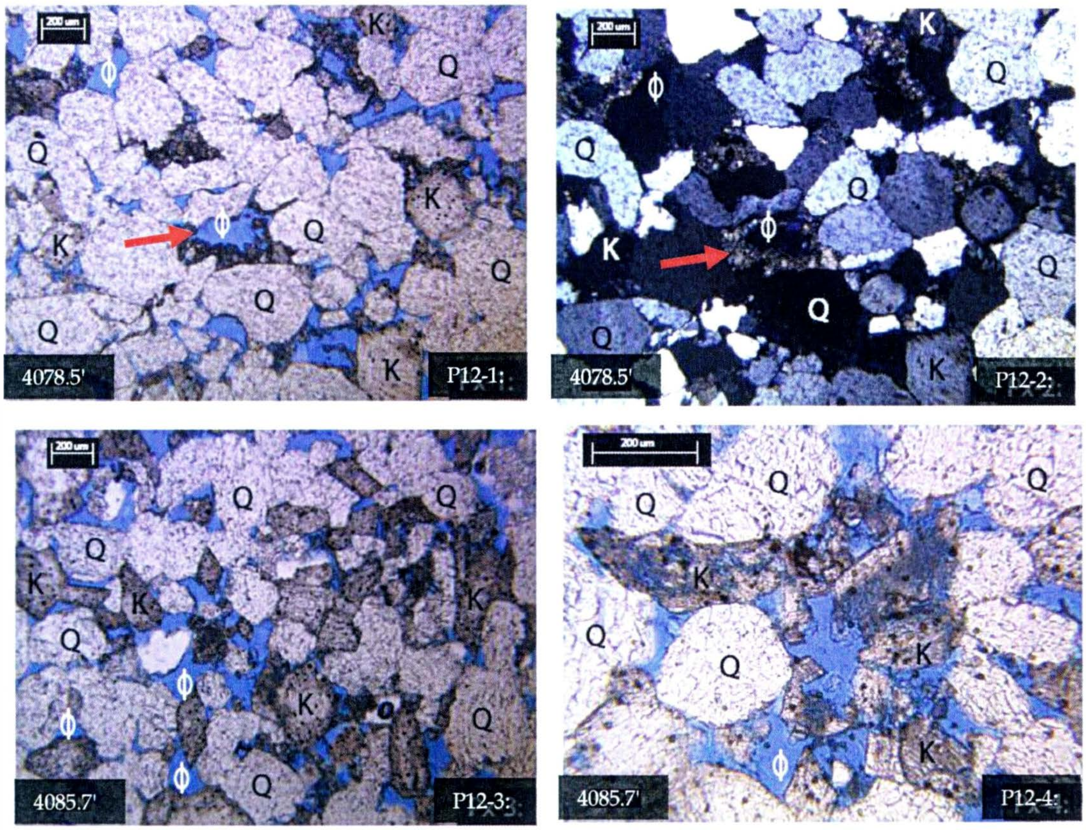

P12-1: PPL and P12-2: XPL – Microcrystalline carbonate is being dissolved above (marked by the arrow). **P12-3: PPL and P12-4: PPL** – K-spar from the same slide; P12-4 has abundant K-spar dissolution and P12-3 has very almost no K-spar dissolution.

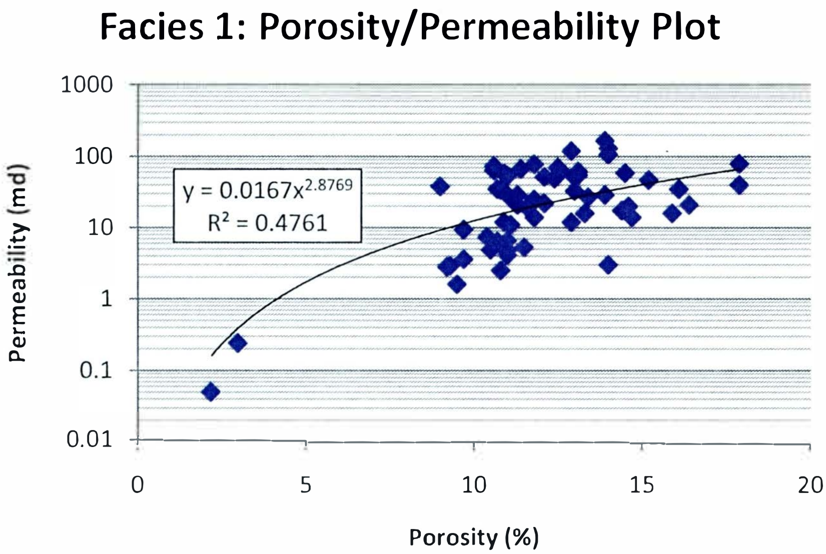
Facies 1: Porosity/Permeability Plot
1000
100
10
1
0.1
0.01
Permeability (md)
y = 0.0167x^2.8769
R² = 0.4761
0
5
10
15
20
Porosity (%)

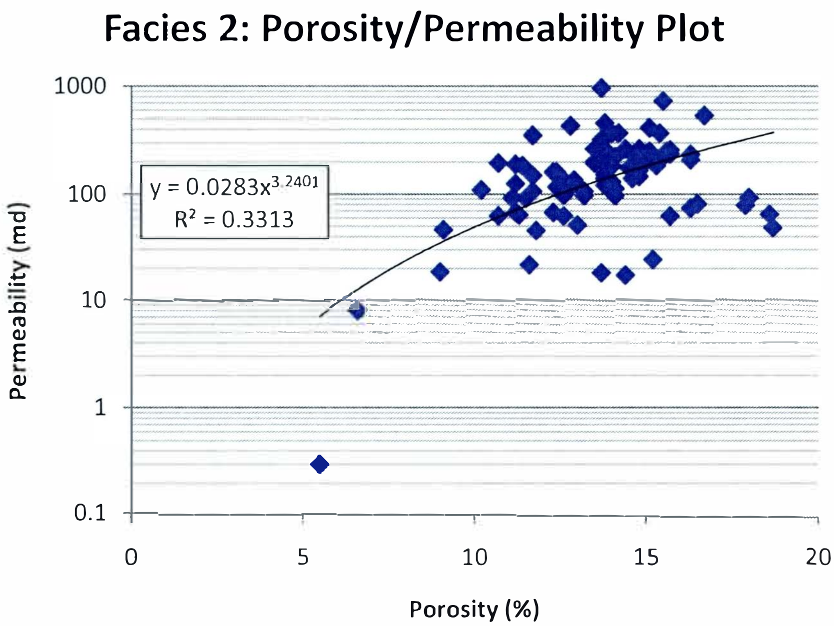
Facies 2: Porosity/Permeability Plot
1000
100
10
1
0.1
Permeability (md)
y = 0.0283x^3.2401
R² = 0.3313
0
5
10
15
20
Porosity (%)

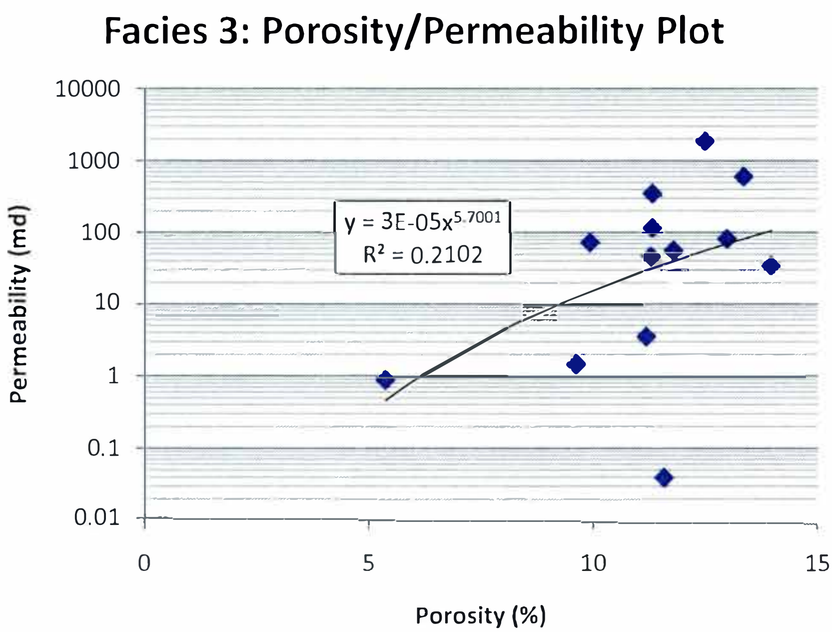
Facies 3: Porosity/Permeability Plot
y = 3E-05x^5.7001
R² = 0.2102
Permeability (md)
10000
1000
100
10
1
0.1
0.01
0
5
10
15
Porosity (%)

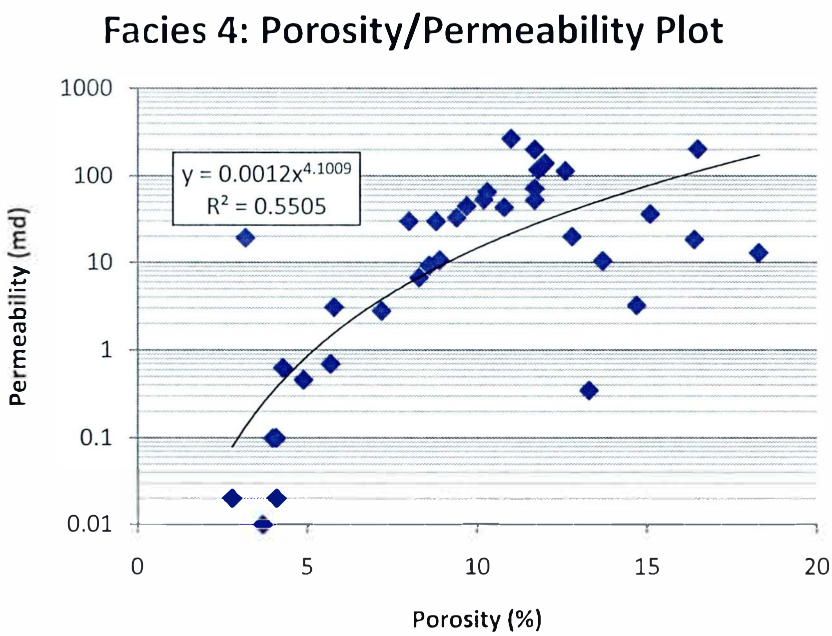
Facies 4: Porosity/Permeability Plot
y = 0.0012x^4.1009
R² = 0.5505
Permeability (md)
1000
100
10
1
0.1
0.01
0
5
10
15
20
Porosity (%)

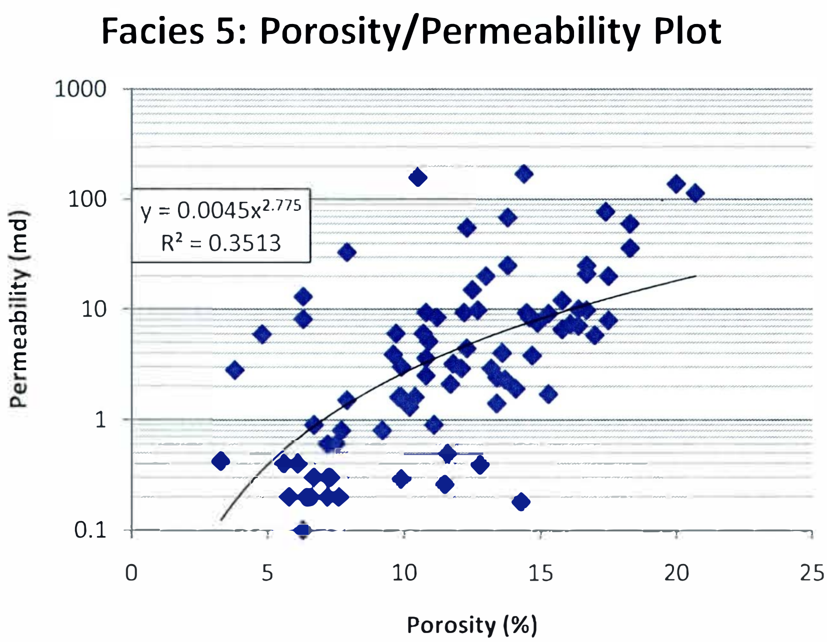
Facies 5: Porosity/Permeability Plot
1000
100
10
1
0.1
Permeability (md)
y = 0.0045x^2.775
R² = 0.3513
0
5
10
15
20
25
Porosity (%)

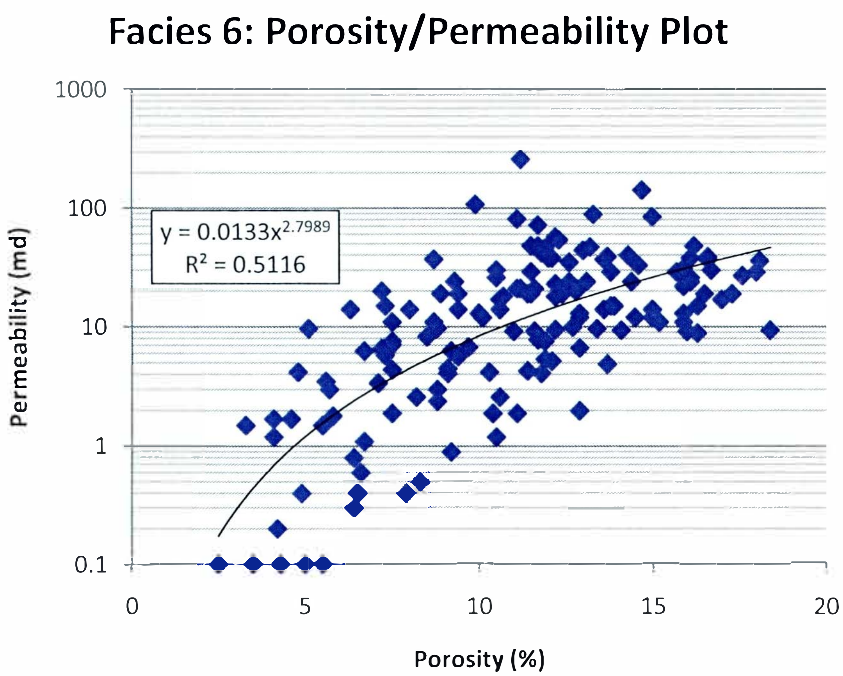
Facies 6: Porosity/Permeability Plot
1000
100
10
1
0.1
Permeability (md)
y = 0.0133x^2.7989
R² = 0.5116
0
5
10
15
20
Porosity (%)

Appendix 4: Core to Wireline Log Correlations: Facies 1 and 2

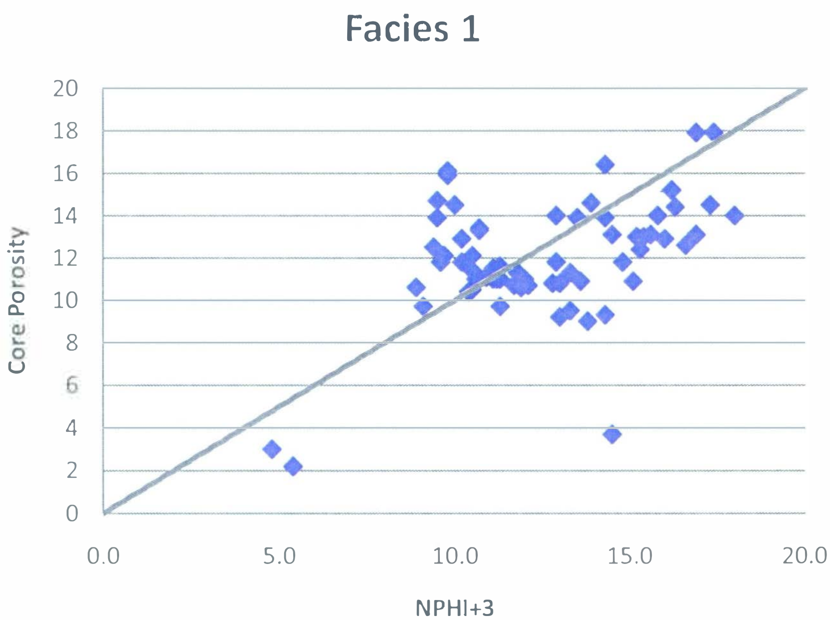

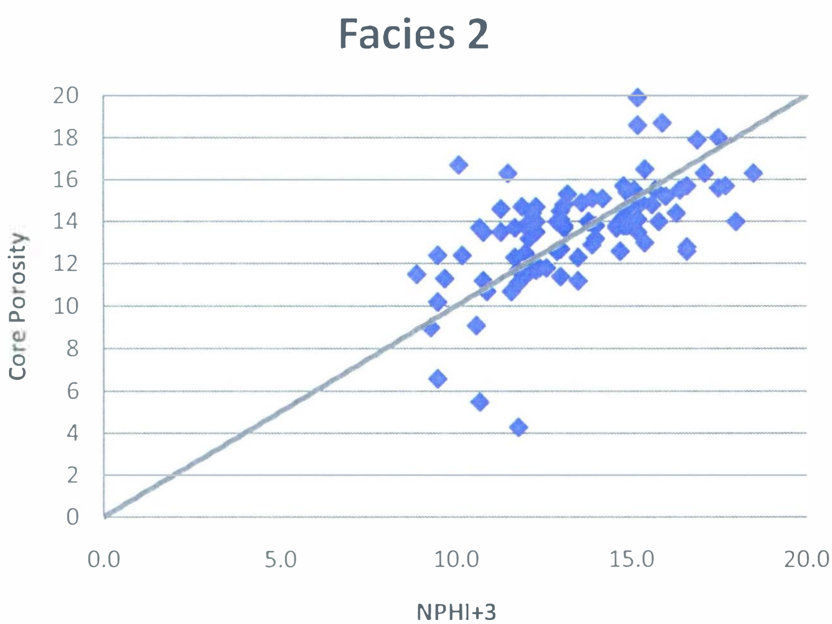

Appendix 5: Core to Wireline Log Correlations: Facies 3 and 4

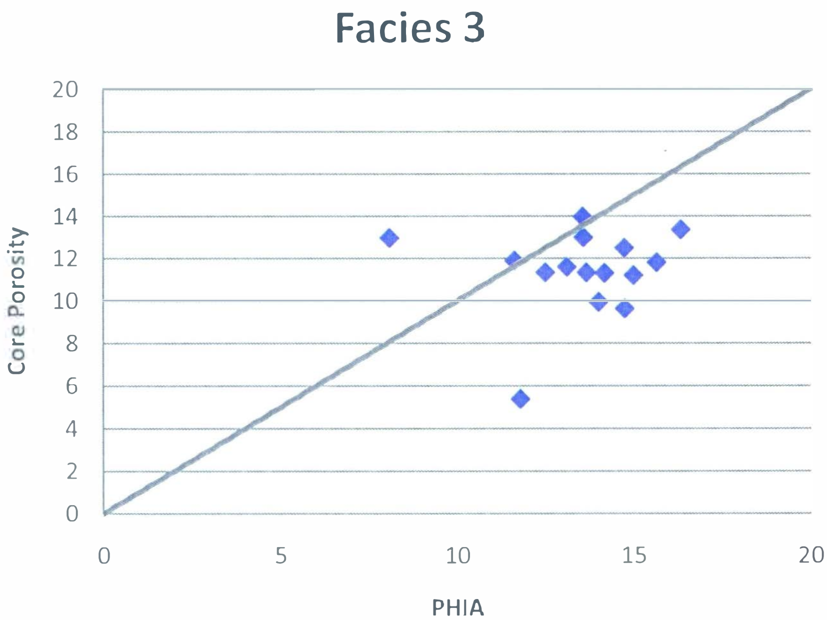

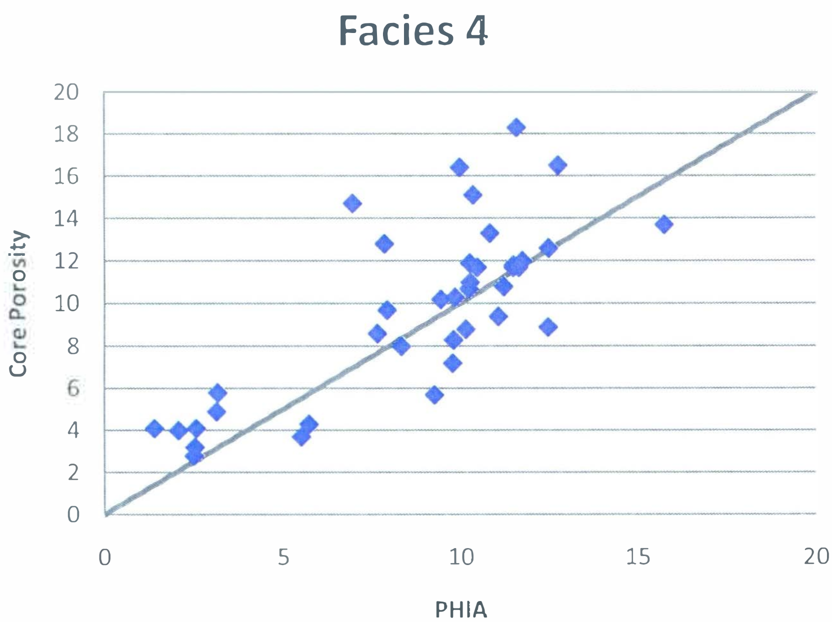

Appendix 6: Core to Wireline Log Correlations: Facies 5 and 6

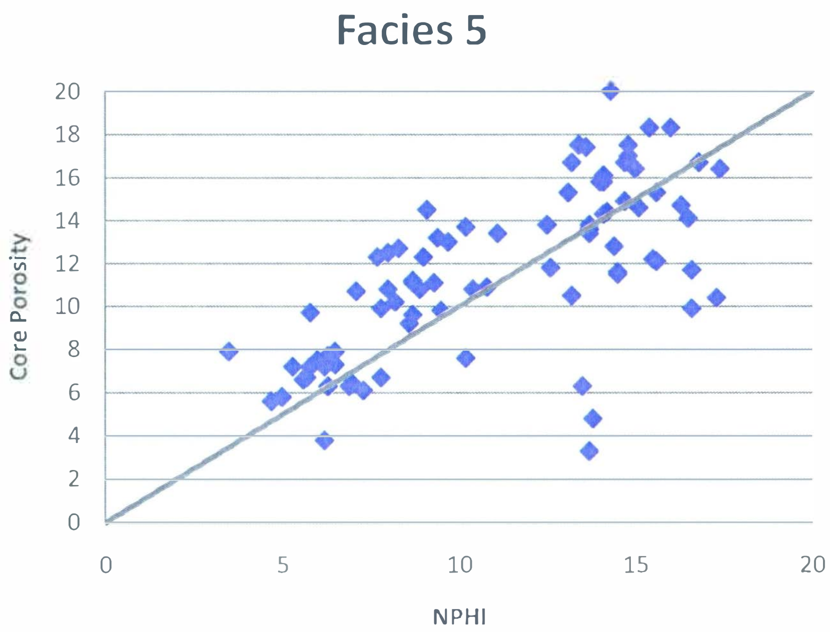

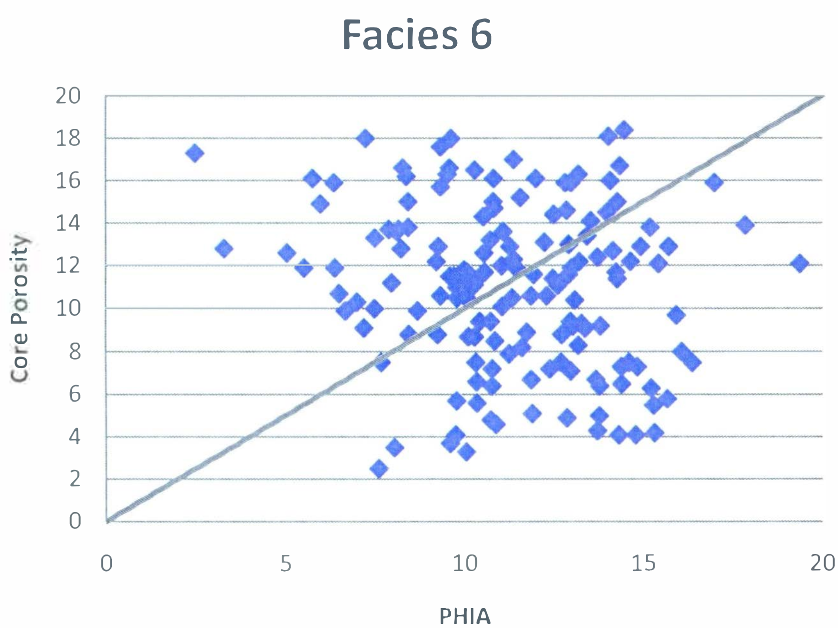

Appendix 7: Infrared Spectroscopy: Angell & Kehrl 5478' White

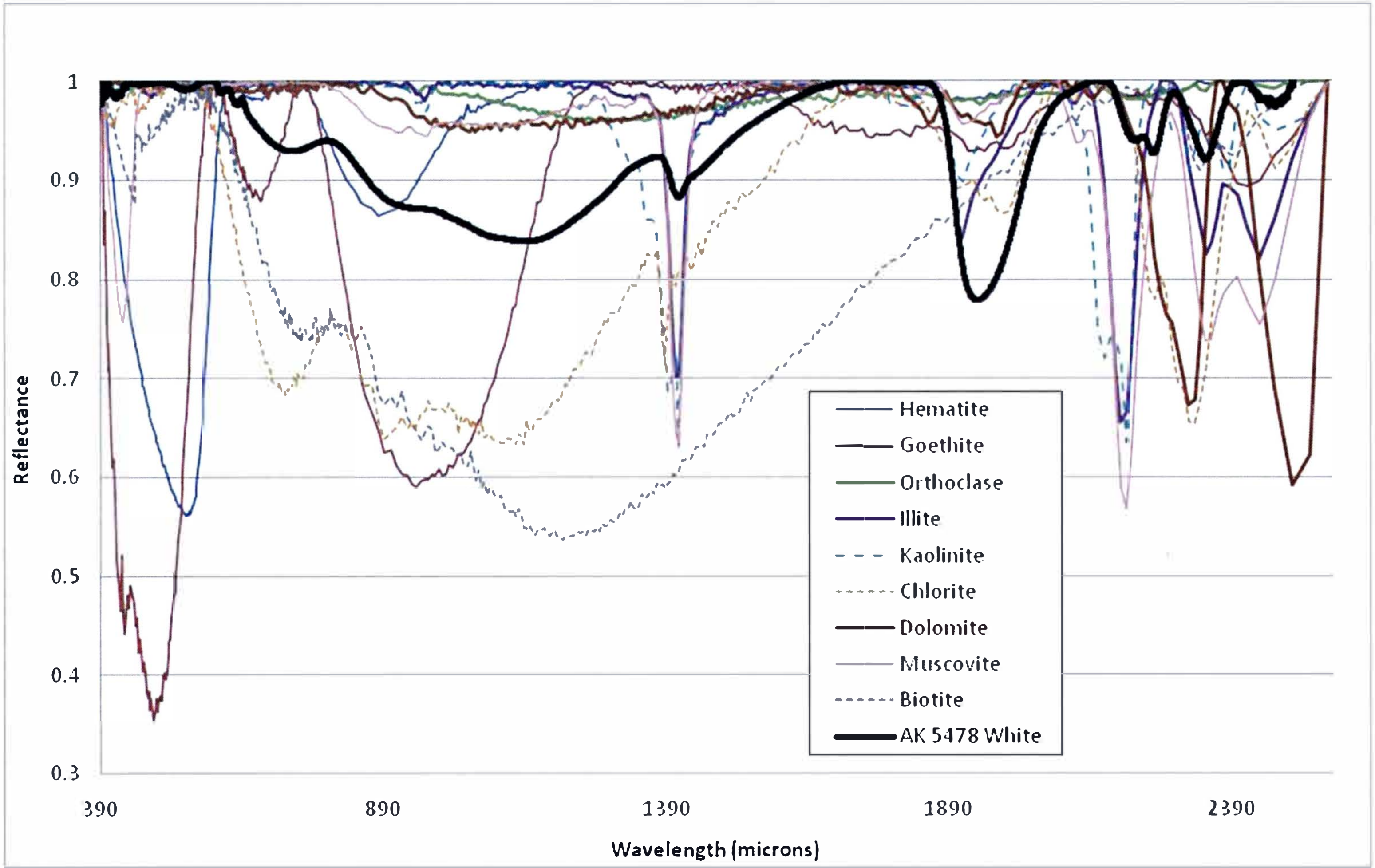

Appendix 8: Infrared Spectroscopy: Angell & Kehrl 5478′ Red

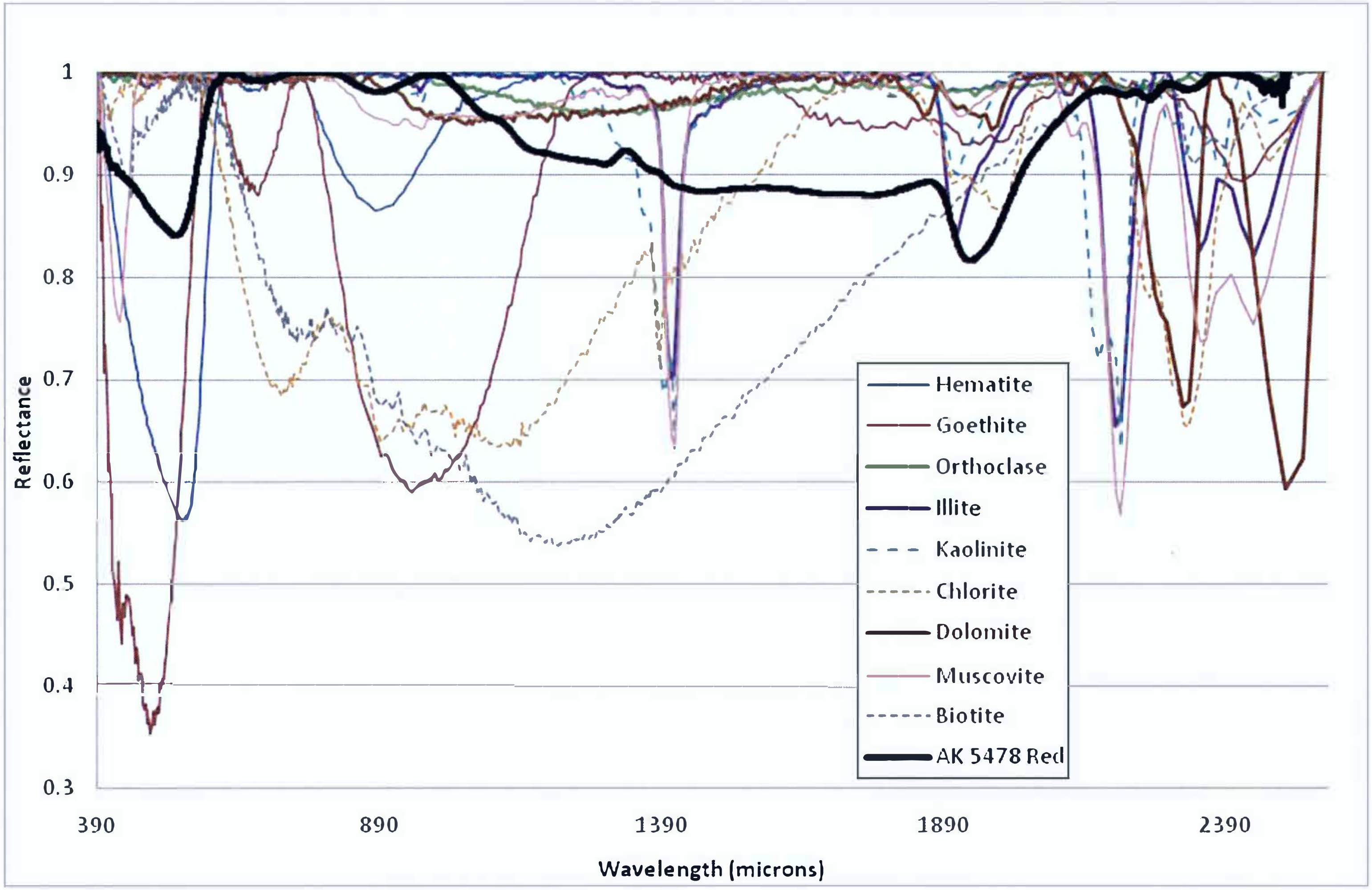

Appendix 9: Infrared Spectroscopy: Angell & Kehrl 5660′

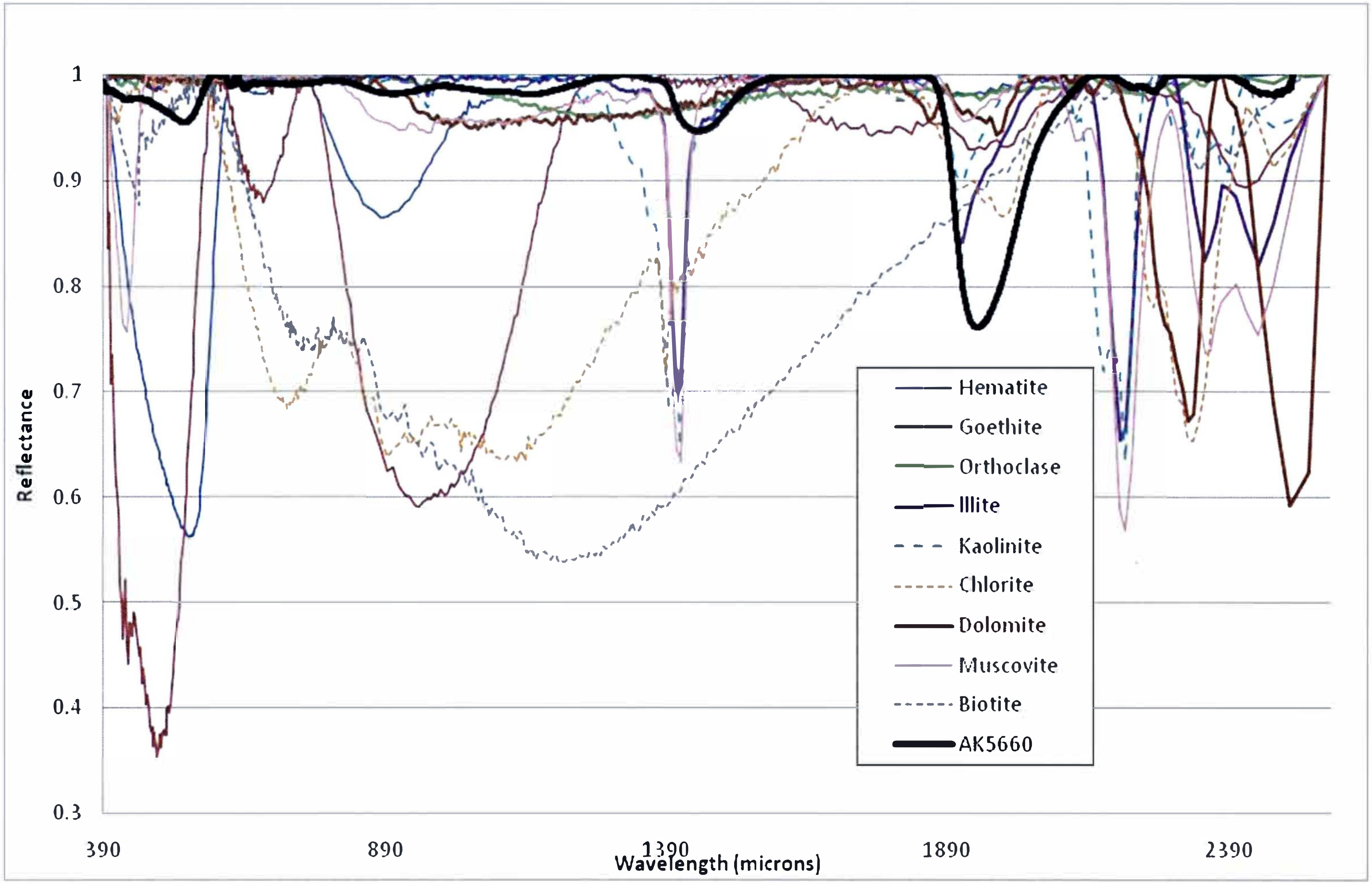

Appendix 10: Infrared Spectroscopy: Angell & Kehrl 5669′

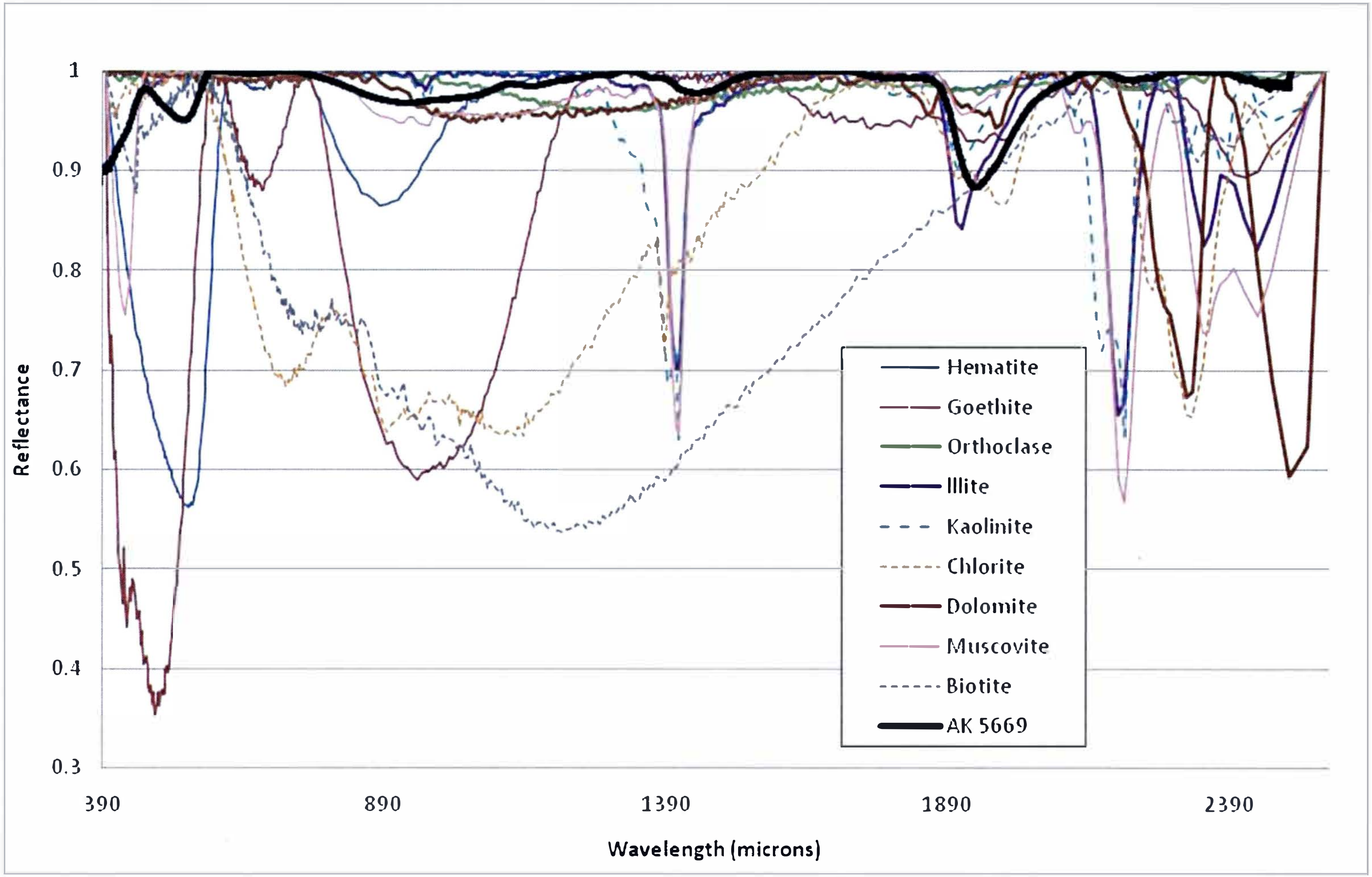

Appendix 11: Infrared Spectroscopy: Semet Solvay 4001′

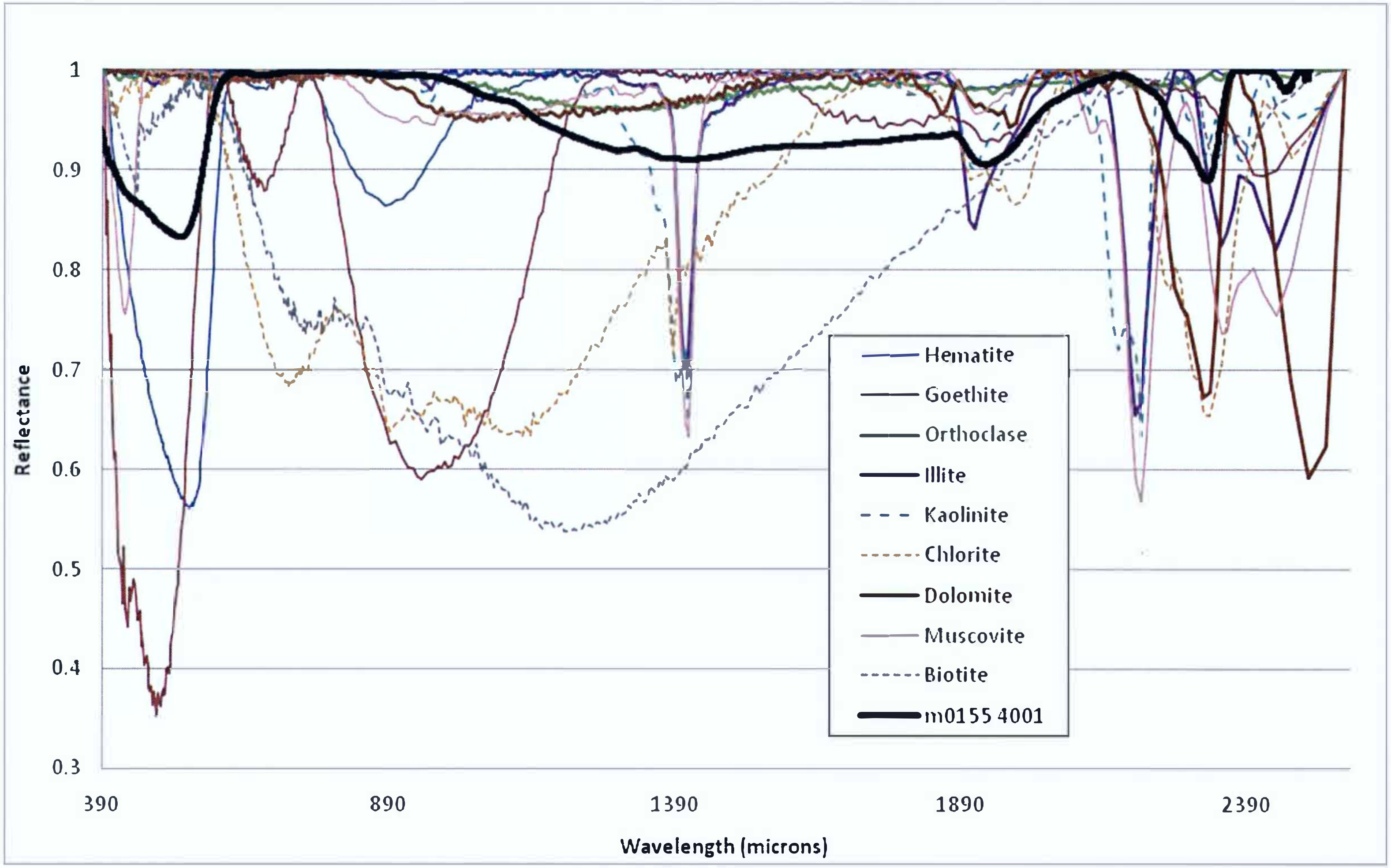

Appendix 12: Infrared Spectroscopy: Semet Solvay 4038.7′

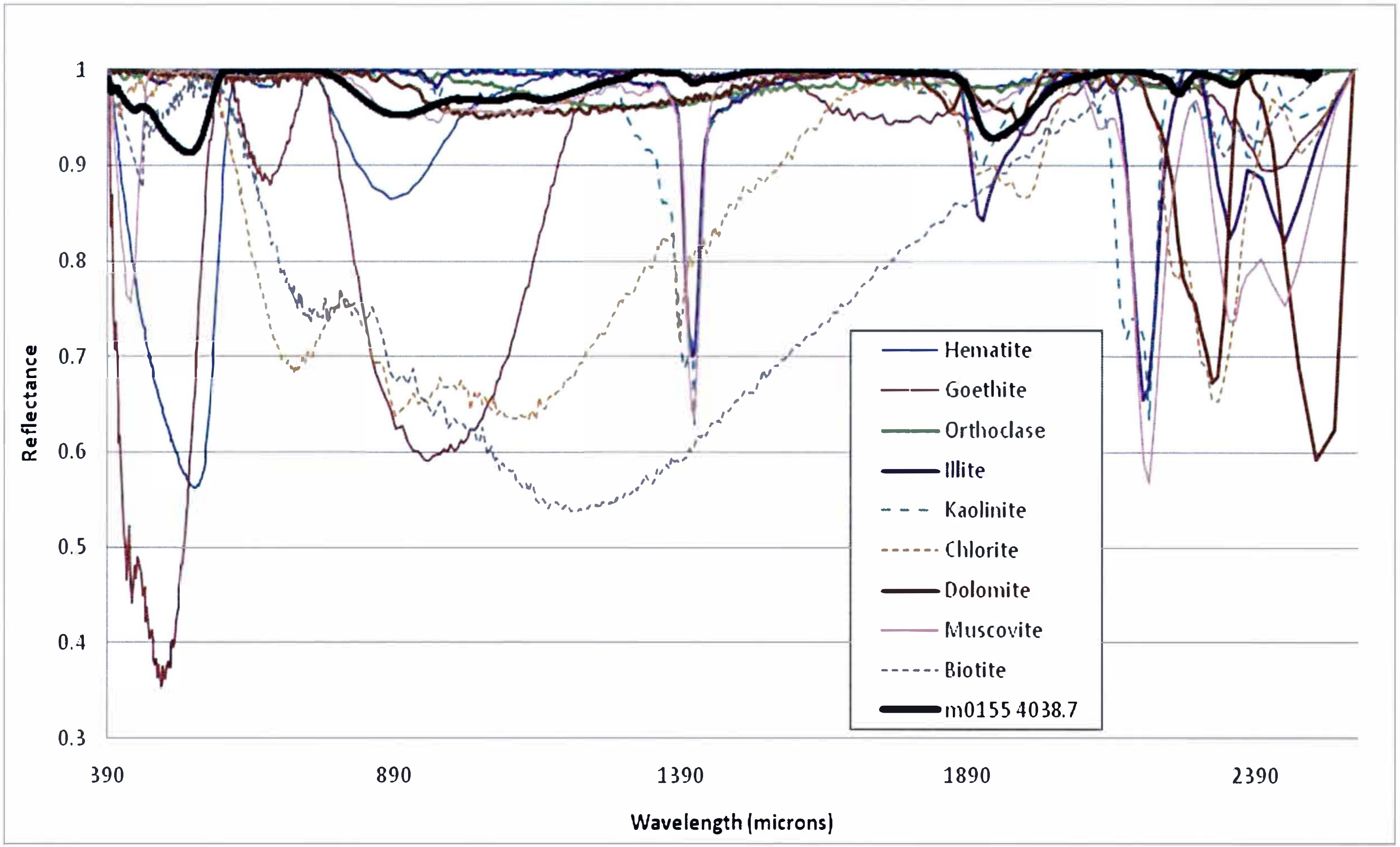

Appendix 13: Infrared Spectroscopy: Semet Solvay 4099′

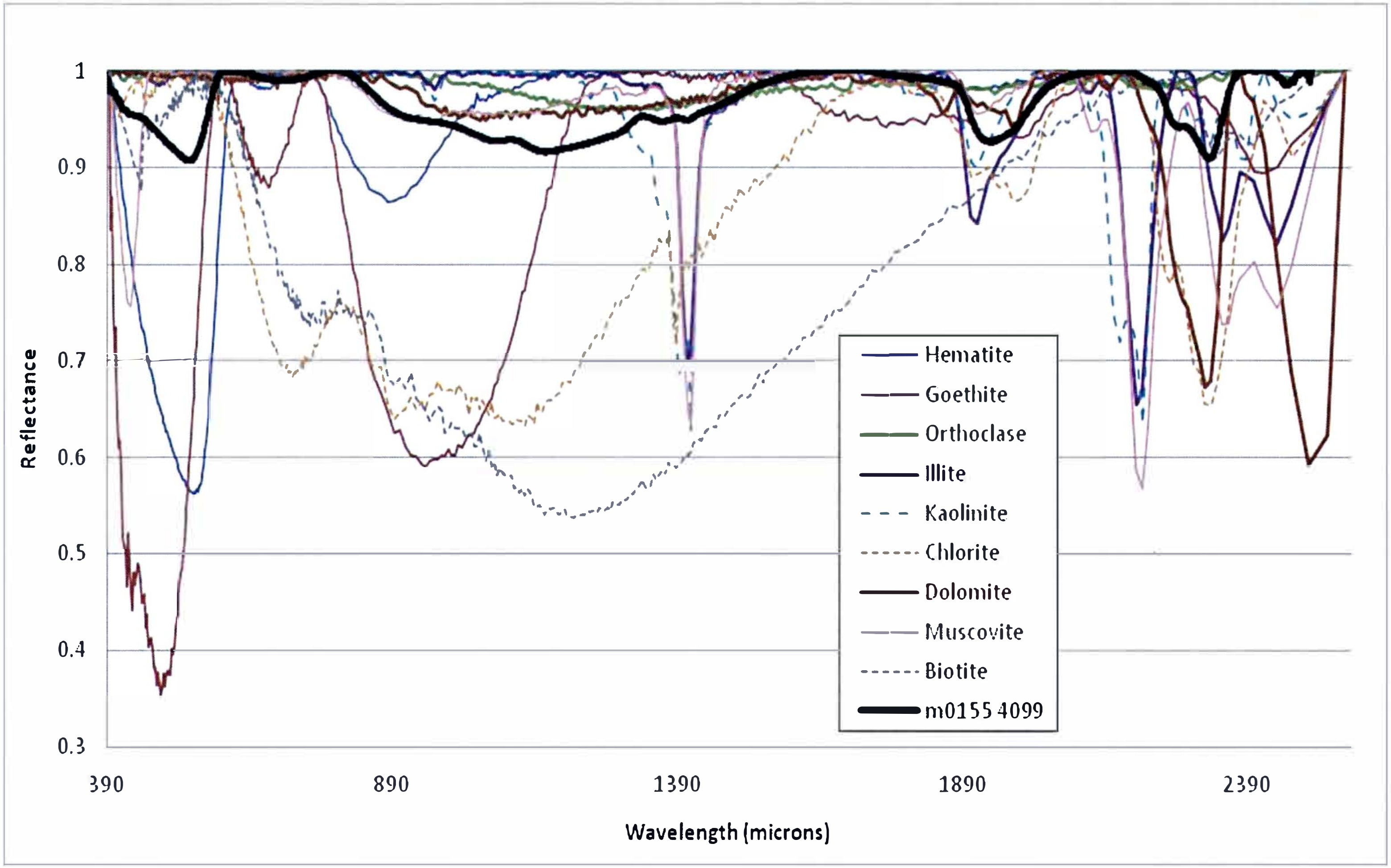

Appendix 14: Infrared Spectroscopy: Lloyd Cupp 5021.5′

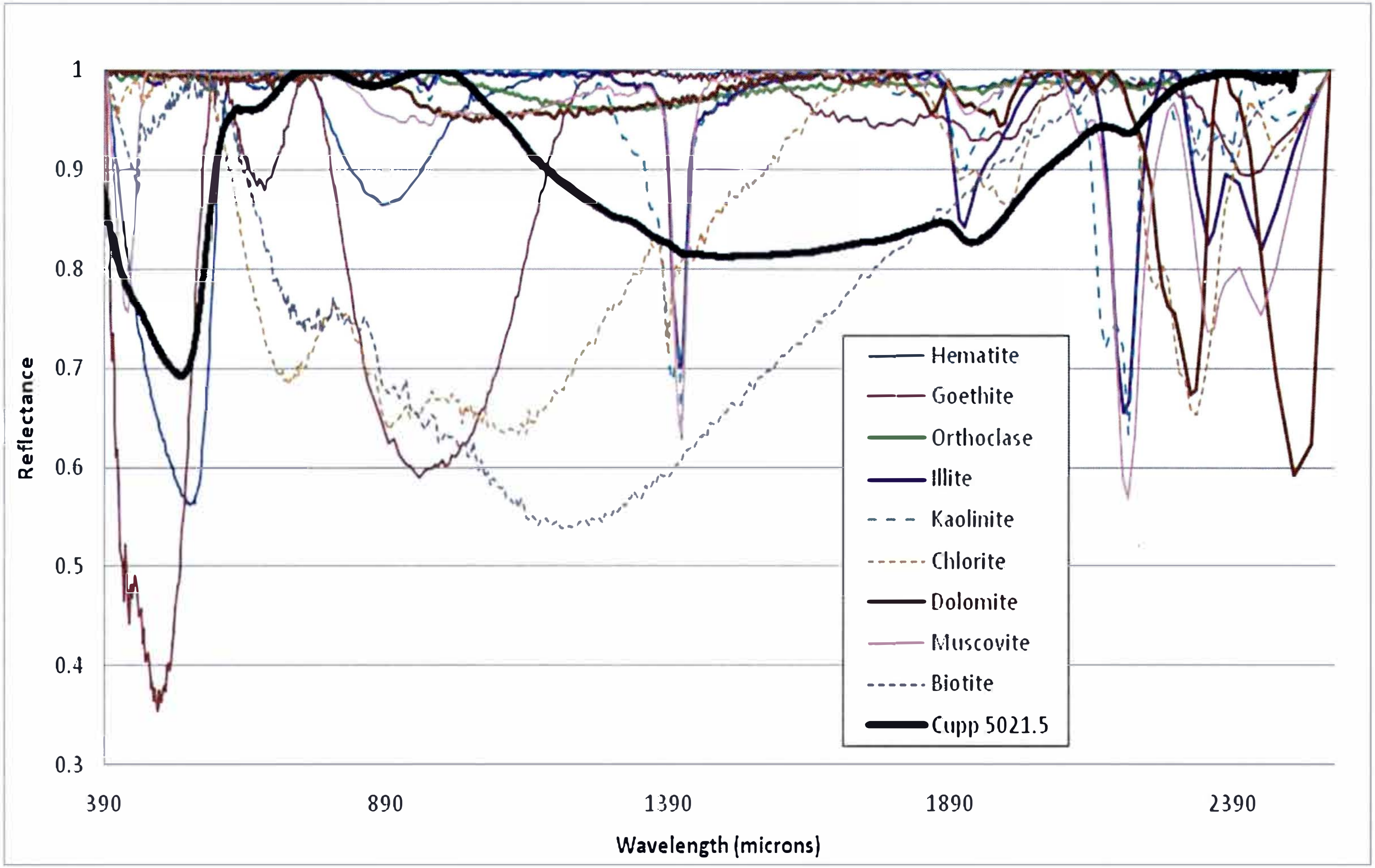

Appendix 15: Infrared Spectroscopy: Lloyd Cupp 5024′

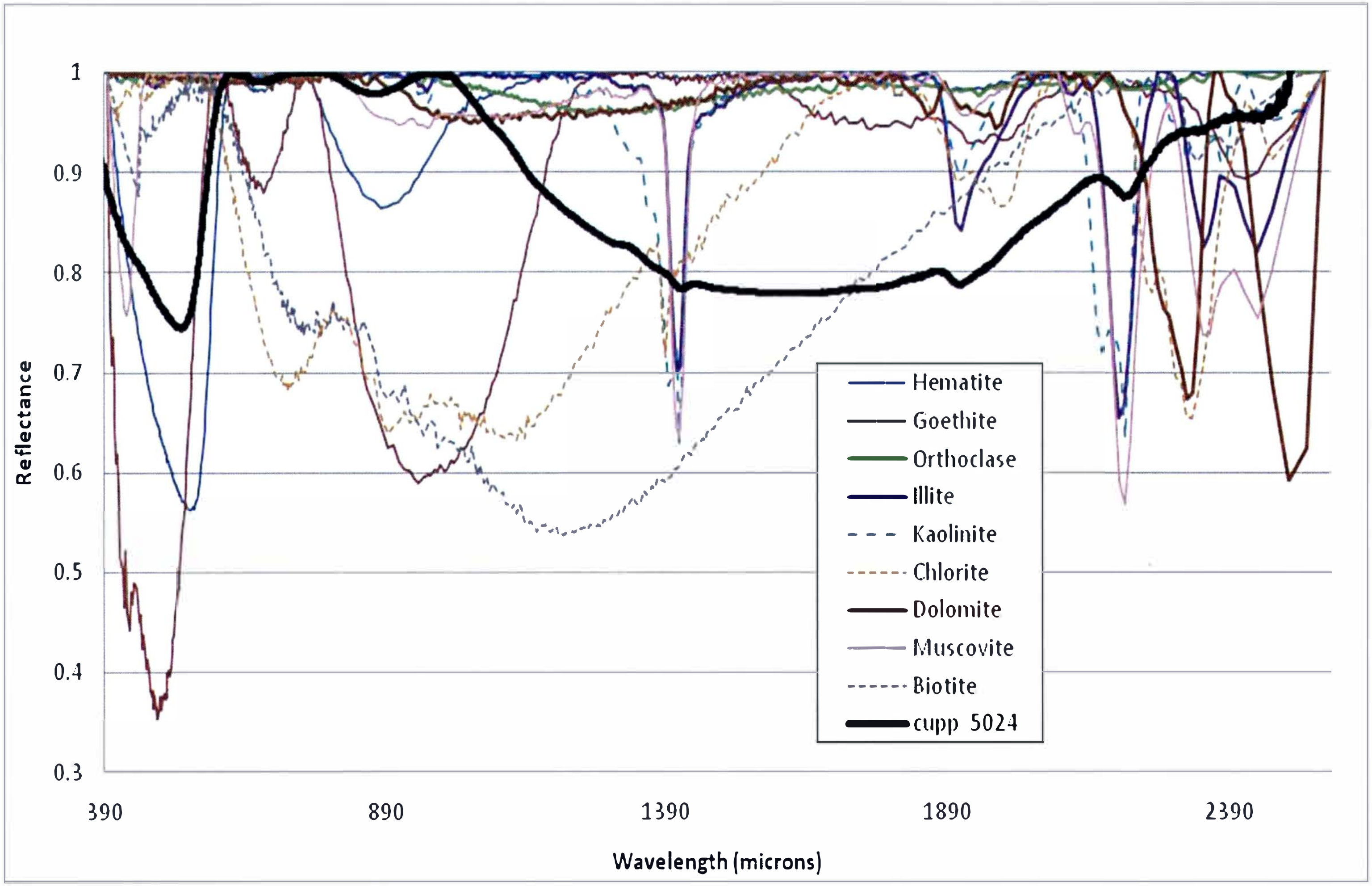

Appendix 16: Infrared Spectroscopy: Lloyd Cupp 5065′

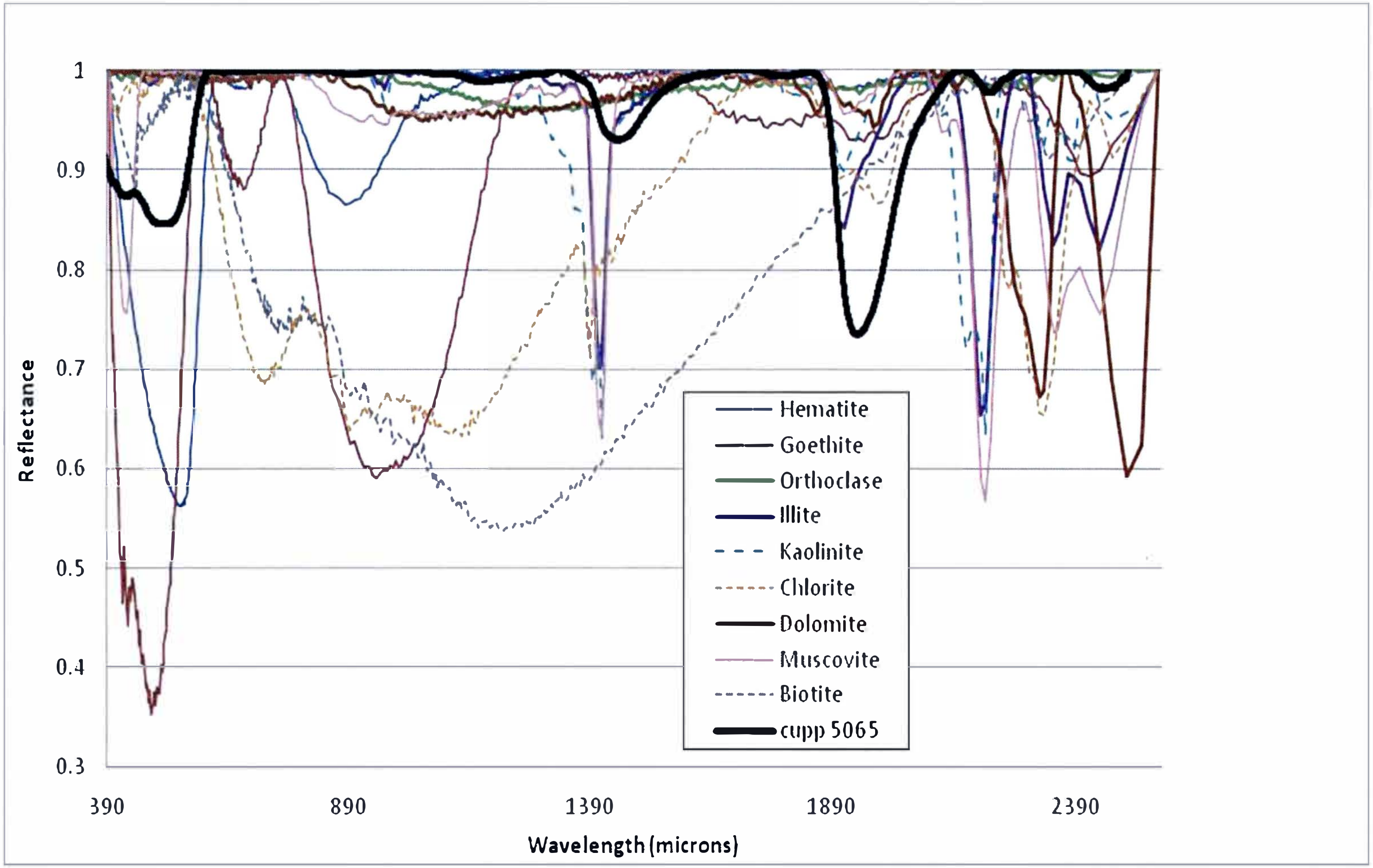

Appendix 17: XRD Analysis: Angell and Kehrl 1-12, 5478'

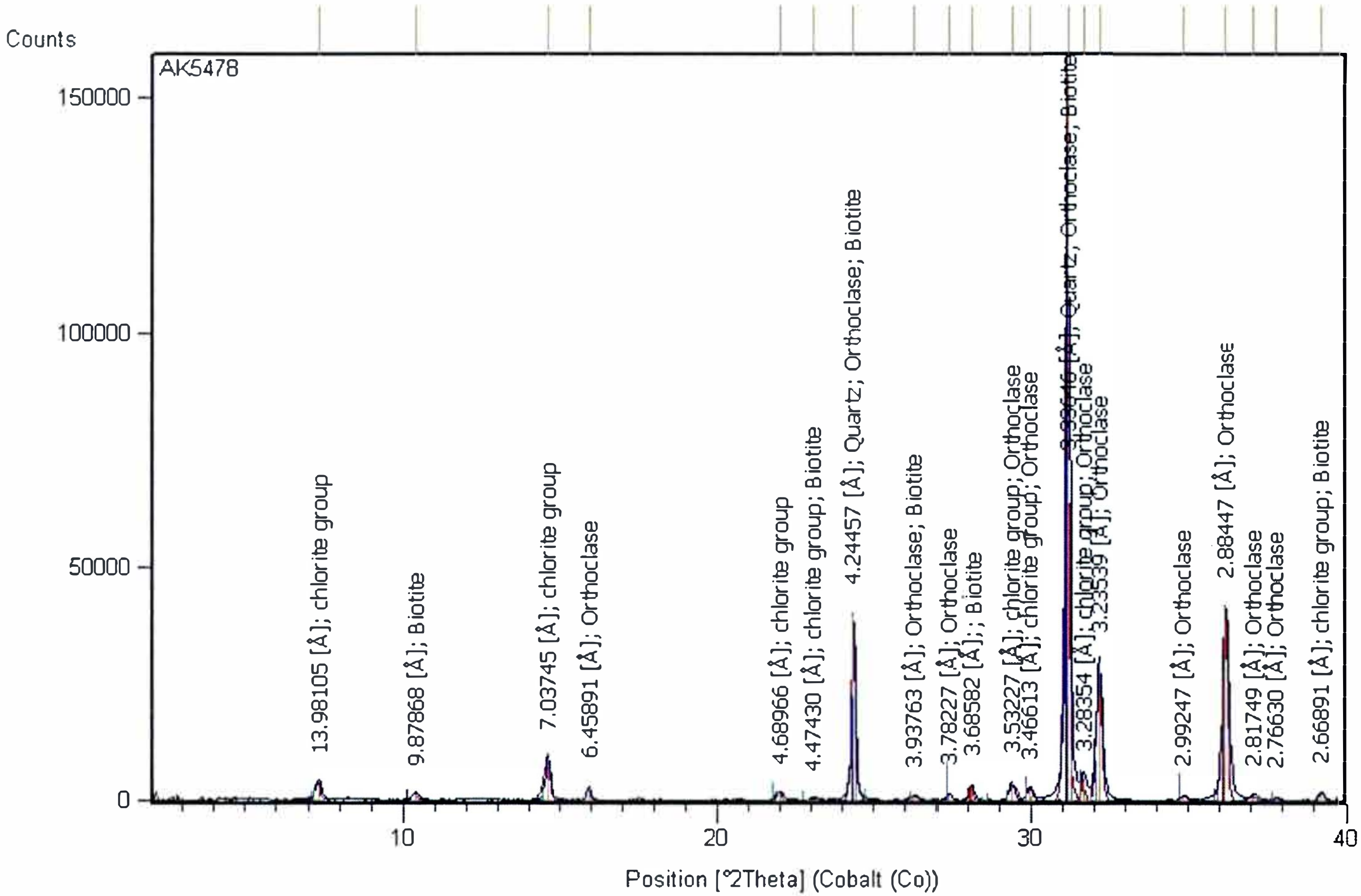

Appendix 18: XRD Analysis: Angell and Kehrl 1-12, 5660'

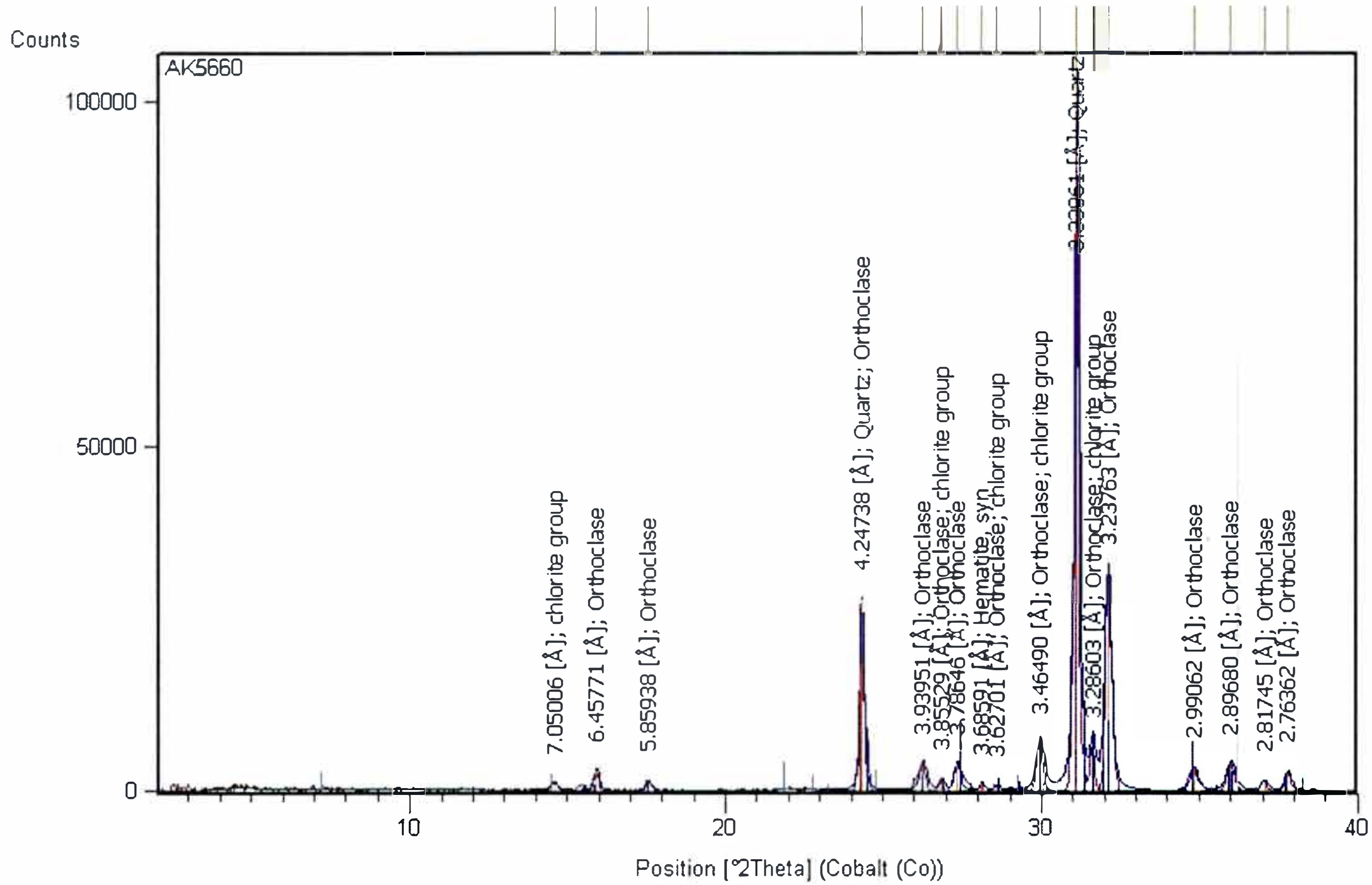

Appendix 19: XRD Analysis: Lloyd Cupp #2, 5021.5'

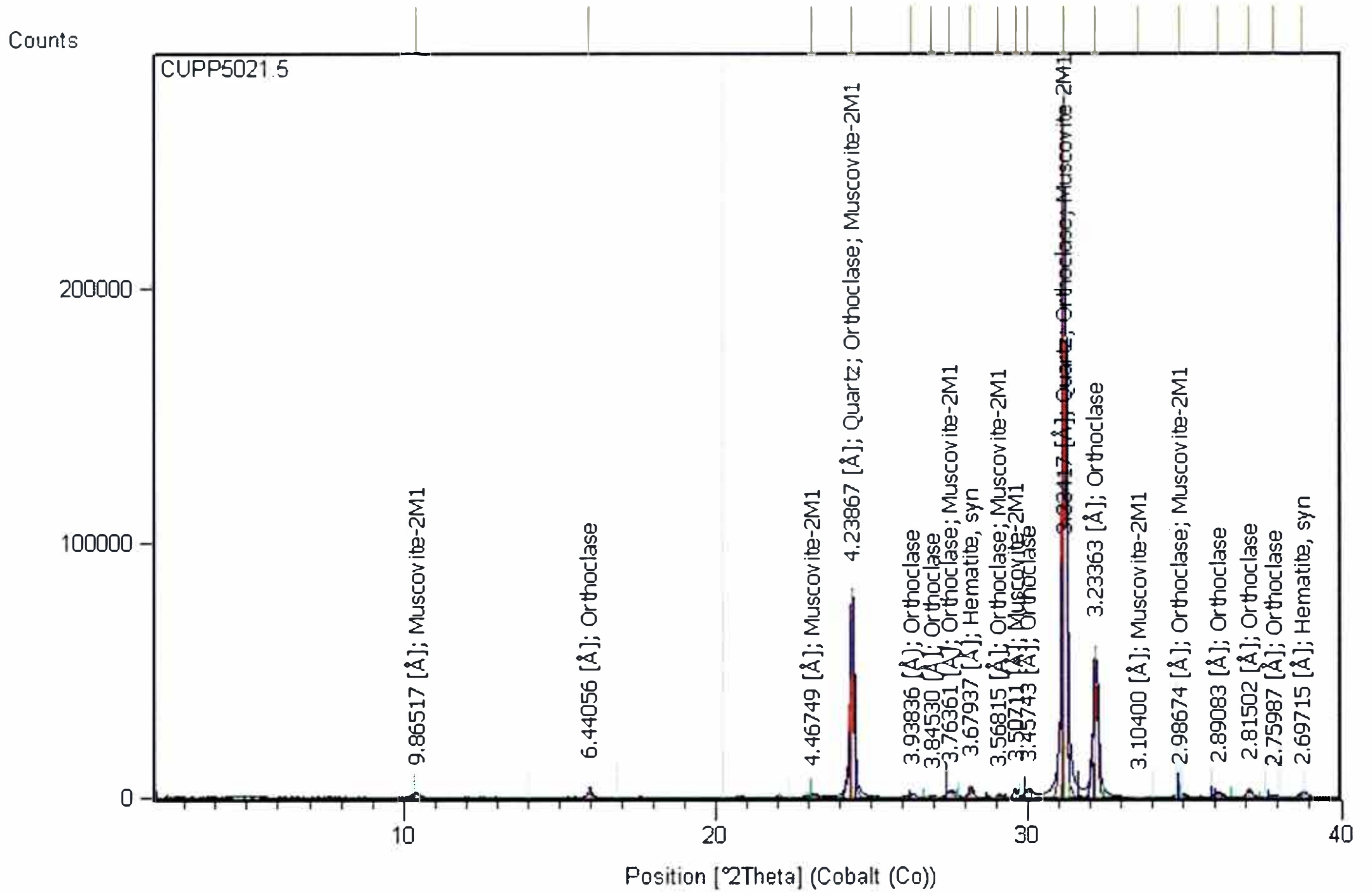

Appendix 20: XRD Analysis: Lloyd and Cupp #2, 5052'

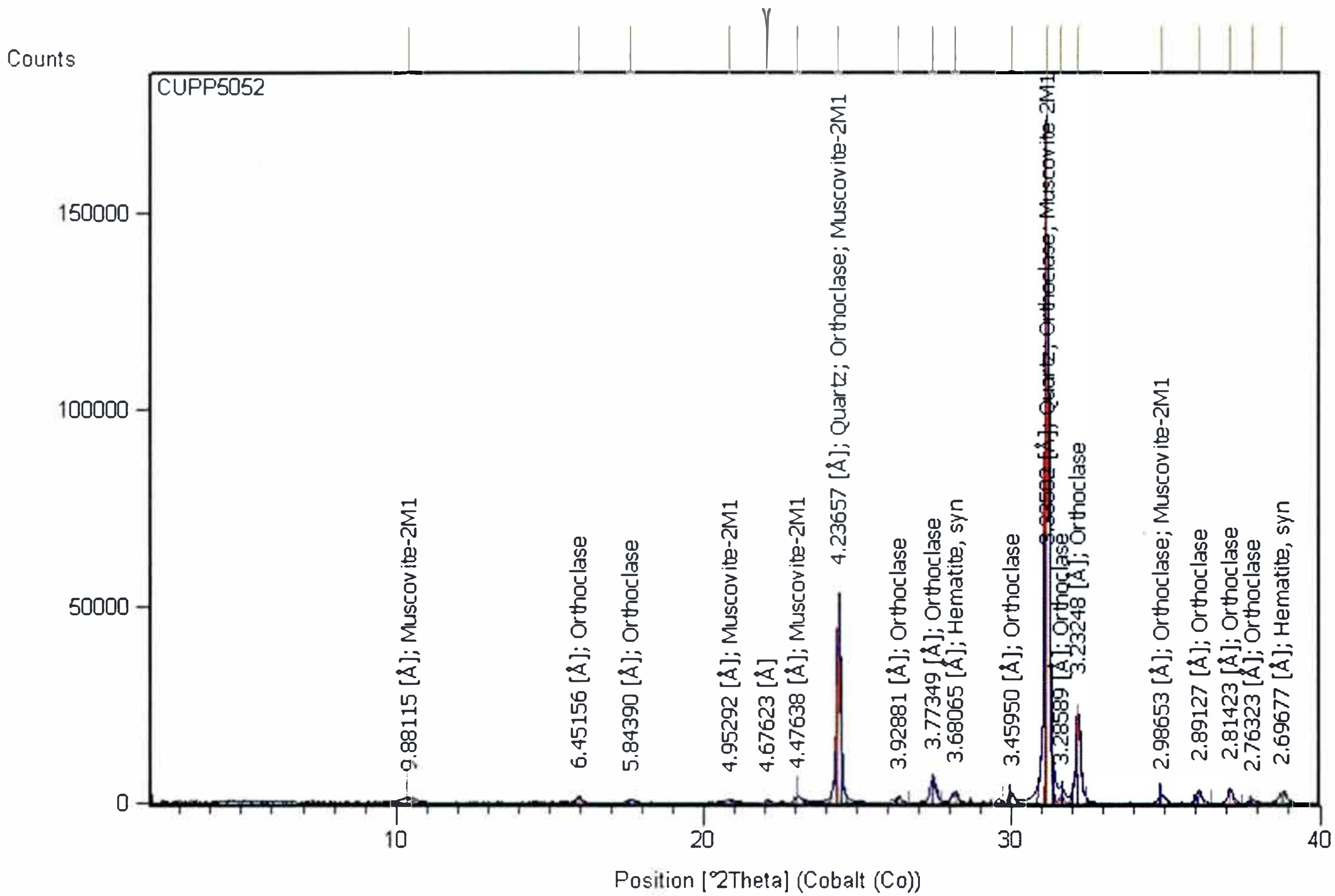

Appendix 21: XRD Analysis: Semet Solvay #2 4001'

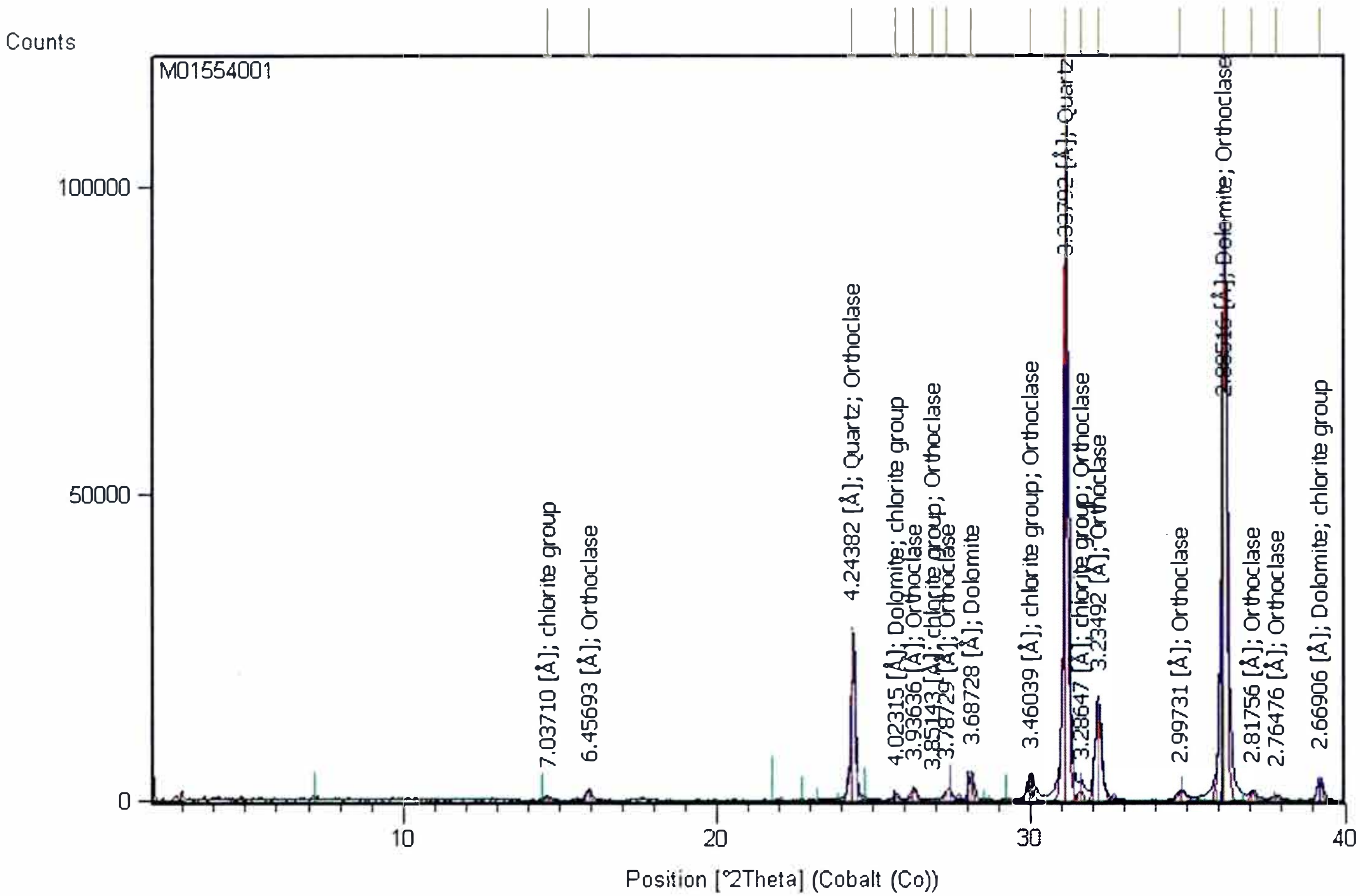

Appendix 22: Model 1 Grid Data

Statistics for 3D grid			
Axis	Min	Max	Delta
X (ft)	17777.5	23578.61	5801.11
Y (ft)	77250.57	83808.86	6558.29
Depth (ft)	-5300	-2600	2700
Cells (nI x nJ x nK)	78 x 88 x 99		
Nodes (nI x nJ x nK)	79 x 89 x 100		
Total number of 3D cells:	679536		
Total number of 3D nodes:	703100		
Number of real horizons:	100		
Number of real layers:	99		
	Facies 1	**Facies 2**	
Major Range	5000	5000	
Minor Range	5000	5000	
Sill	1	1	
Nugget	0.0001	0.0001	
Model Algorithm	Kriging	Kriging	

Appendix 23: Model 1 Permeability Data

Statistics for permeability

Axis	Min	Max	Delta
X	17777.5	23578.61	5801.11
Y	77250.57	83808.86	6558.29
Z	-5300	-2600	2700
Permeability	21.22	874.38	853.16

Description	Value
Unit:	mD
Is upscaled (U)	Yes
Total number of defined cells	679536

Cells (nI x nJ x nK)	78 x 88 x 99

Type of data:	Continuous
Mean:	153.1
Std. dev.	75.87
Variance:	5756.4

Name	Min	Max	Delta	N	Mean	Std	Var	Sum
Logs 1 Ft interval	21.22	874.38	853.16	679536	153.1	75.87	5756.4	1.04E+08
Upscaled	21.22	874.38	853.16	492	142.68	122.96	15118.19	70196.24
Well logs	0.3	2924	2923.7	4206	155.68	150.56	22667.52	654783.4

Appendix 24: Model 1 Porosity Data

Statistics for porosity

Axis	Min	Max	Delta
X	17777.5	23578.61	5801.11
Y	77250.57	83808.86	6558.29
Z	-5300	-2600	2700
Neutron	8.9	28.37	19.47

Description	Value
Unit:	ft3/ft3
Total number of defined cells	679536

Cells (nI x nJ x nK)	78 x 88 x 99

Type of data:	Continuous
Mean:	16.14
Std. dev.	2.87
Variance:	8.22

Name	Min	Max	Delta	N	Mean	Std	Var	Sum
Property	8.9	28.37	19.47	679536	16.14	2.87	8.22	10967311.39
Upscaled	8.9	28.37	19.47	492	15.85	3.84	14.77	7799.75
Well logs	4.3	30.9	26.6	4206	15.19	3.84	14.72	63887

Appendix 25: Model 2 Grid Data

Grid statistics			
Axis	Min	Max	Delta
X	-31.06	3704.58	3735.64
Y	-2651.87	2193.42	4845.29
Depth	-7494.98	-1897.84	5597.14
Cells (nI x nJ x nK)	37 x 48 x 116		
Nodes (nI x nJ x nK)	38 x 49 x 117		
Total number of 3D cells:	206016		
Total number of 3D nodes:	217854		
Number of real horizons:	117		
Number of real layers:	116		
	Facies 1	**Facies 2**	**Facies 3**
Major Range	5000	5000	3000
Minor Range	3000	3000	3000
Depositional Strike	N65E	N65E	--
Sill	1	1	1
Nugget	0.0001	0.0001	0
Model Algorithm	Kriging	Kriging	Gaussian Random

Appendix 26: Model 2 Porosity Data

Statistics for porosity			
Axis	Min	Max	Delta
X	-31.06	3619.33	3650.39
Y	-2651.87	2103.62	4755.49
Z	-7494.98	-1897.84	5597.14
Neutron	0.19	23.42	23.23

Description	Value
Unit:	ft3/ft3
Is upscaled (U)	Yes
Total number of defined cells	118704

Cells (nI x nJ x nK)	37 x 48 x 116

Type of data:	Continuous
Mean:	13.61
Std. dev.	2.03
Variance:	4.13

Name	Min	Max	Delta	N	Mean	Std	Var	Sum
Property	0.19	23.42	23.23	1E+05	13.61	2.03	4.13	2E+06
Upscaled	0.19	23.42	23.23	697	14.03	3.25	10.5	9782
Well logs	0.07	30.3	30.23	6635	14.06	5.28	27.9	93316

Appendix 27: Model 2 Permeability Data

Statistics for permeability

Axis	Min	Max	Delta
X	-31.06	3619.33	3650.39
Y	-2651.87	2103.62	4755.49
Z	-7494.98	-1897.84	5597.14
Permeability	1.62	2007.49	2005.88

Description	Value
Unit:	mD
Is upscaled (U)	Yes
Total number of defined cells	118704

Cells (nI x nJ x nK)	37 x 48 x 116

Type of data:	Continuous
Mean:	136.74
Std. dev.	136.67
Variance:	18679.65

Name	Min	Max	Delta	N	Mean	Std	Var	Sum
Property	1.62	2007.49	2005.88	118704	136.74	136.67	18679.65	16231761.96
Upscaled	1.62	2007.49	2005.88	692	147.69	165.52	27396.98	102202.45
Well logs	1.04	2726.45	2725.41	4553	145.76	148.52	22057.02	663642.86

Appendix 28: Paleotopograhic High – Livingston, County

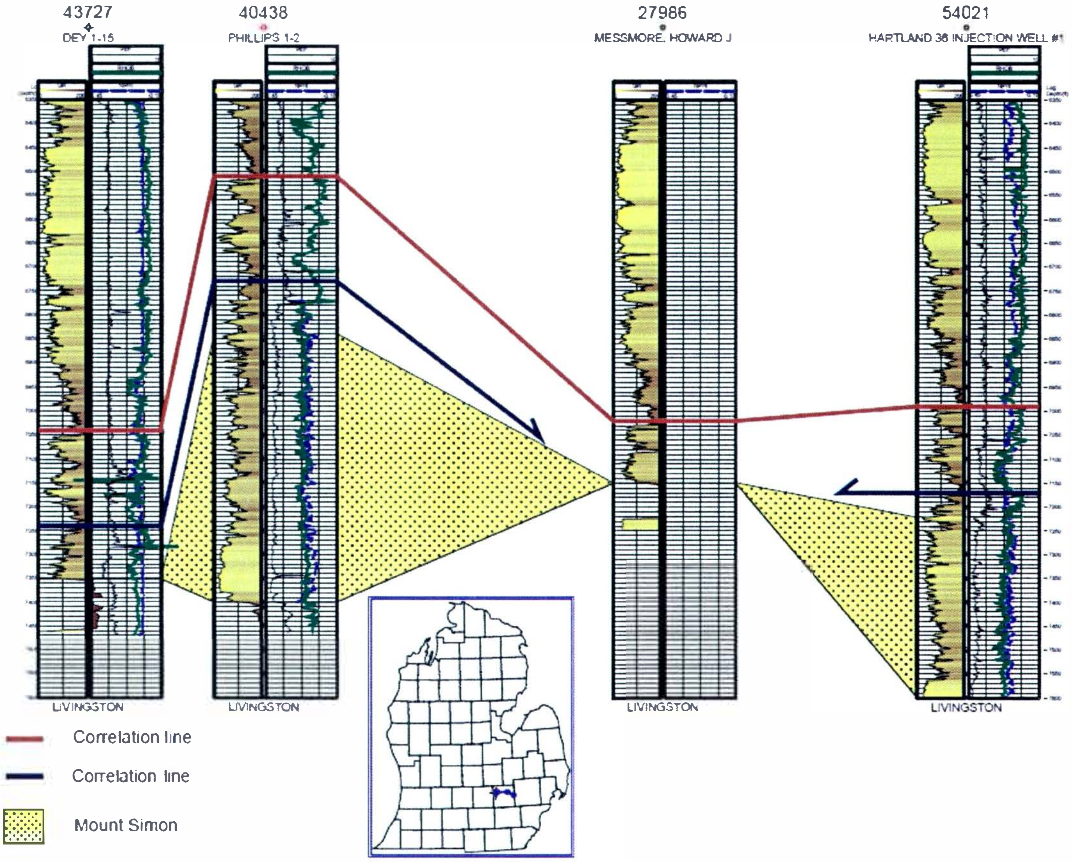

There is an observed paleotopographic high in Livingston, County, which should be considered when CO_2 injection projects. Red and blue correlation lines were used to help demonstrate the onlap of the Mount Simon and above strata on the Paleotopographic high.

Appendix 29: Waste Injection Data

WellAPINo	Total gal of injectate	Equiv tons of CO2	STATUS
21121000027000	47211266	128674	Plugged
21139000517000	956606100	2607227	Active
21139000527000	1029360211	2805518	Active
21139000537000	653436009	1780938	Active
21163000697000	257774260	702563	Plugged
21139000707000	110739844	301821	Plugged
21139000717000	205063274	558899	Plugged
21139001297000	452816909	1234151	Active
21139001307000	450746358	1228508	Active
21077001377000	222021758	605120	Active
21163001557000	169429102	461778	Temporarily abandoned
21163001847000	81525102	222196	Plugged
21139002177000	65218954	177754	Plugged
21163002267000	75334789	205325	Plugged
21077003277000	119562178	325866	Active
21161003287000	150324076	409708	Plugged
21091003577000	266164922	725432	Active
21139003737000	204956496	558608	Active
21091004207000	70014896	190825	Active
21163004527000	1372379	3740	Active
21163004537000	715730	1951	Active
21139004707000	68904979	187800	Active
21139004717000	58583483	159669	Active

Appendix 29: Waste Injection Data

WellAPINo	Permit.WellNAme	WELLNUM
21121000027000	Dupont Montague	1
21139000517000	Heinz	WDW #1
21139000527000	Heinz	WDW #2
21139000537000	Heinz	WDW #3
21163000697000	Disposal Well	1
21139000707000	Deep Well	1
21139000717000		D-2
21139001297000	Mt Simon	3
21139001307000	Mt Simon	4
21077001377000	Upjohn	3
21163001557000	Semet-Solvay	2
21163001847000	Ford Motor	D-2
21139002177000		D-3
21163002267000	Semet Solvay	3
21077003277000	Upjohn	4
21161003287000	Stofer Marshall	1
21091003577000	I.W.	1
21139003737000	Parke-Davis Mt. Simon	5
21091004207000	M.W.	2
21163004527000	EDS	1-12
21163004537000	EDS	2-12
21139004707000	Mirant IW	1
21139004717000	Mirant IW	2

Appendix 29: Waste Injection Data

WellAPINo	OWNER	TWPNUM	LONGITUDE
21121000027000	E.I. DuPont de Nemours & Co., Incorporated	White River	-86.40382667
21139000517000	Heinz North America	Holland	-86.12668583
21139000527000	Heinz North America	Holland	-86.12578794
21139000537000	Heinz North America	Holland	-86.12980867
21163000697000	Detroit Coke Corporation	Detroit	-83.10373311
21139000707000	Chemetron Corp.	Holland	-86.131021
21139000717000	BASF Chemetron	Holland	-86.130987
21139001297000	Pfizer, Incorporated	Holland	-86.11708467
21139001307000	Pfizer, Incorporated	Holland	-86.11661504
21077001377000	Pharmacia and Upjohn Company, LLC	Portage	-85.55238182
21163001557000	Honeywell International, Incorporated	Detroit	-83.10586022
21163001847000	Ford Motor Company	Detroit	-83.15166067
21139002177000	BASF Chemetron	Holland	-86.133581
21163002267000	Honeywell International, Incorporated	Detroit	-83.10785894
21077003277000	Pharmacia and Upjohn Company, LLC	Portage	-85.55276598
21161003287000	Gelman Sciences, Incorporated	Scio	-83.802135
21091003577000	Bio-Lab, Incorporated	Madison	-84.01626014
21139003737000	Pfizer, Incorporated	Holland	-86.11589692
21091004207000	Bio-Lab, Incorporated	Madison	-84.01890566
21163004527000	Environmental Disposal Systems, Incorporated	Romulus	-83.31682614
21163004537000	Environmental Disposal Systems, Incorporated	Romulus	-83.31690369
21139004707000	Mirant Zeeland, LLC	Zeeland	-85.99255493
21139004717000	Mirant Zeeland, LLC	Zeeland	-85.99522293

Appendix 29: Waste Injection Data

WellAPINo	LATITUDE	Injection Top	Injection Bottom
21121000027000	43.39738075	5887	6514
21139000517000	42.78541179	5020	5915
21139000527000	42.78331268	4624	6189
21139000537000	42.78365421	5013	5913
21163000697000	42.29210714	4112	4112
21139000707000	42.796367	5895	5895
21139000717000	42.795566	5910	5910
21139001297000	42.798256	5121	5945
21139001307000	42.79771636	5121	5946
21077001377000	42.20938802	4915	5615
21163001557000	42.29188896	4109	4112
21163001847000	42.30060253	4307	4695
21139002177000	42.796758	4343	5900
21163002267000	42.29114478	3750	4127
21077003277000	42.20713441	4874	5600
21161003287000	42.276798	5460	5804
21091003577000	41.89358006	4241	4856
21139003737000	42.79725036		6027
21091004207000	41.89360776	4480	4850
21163004527000	42.24351573	3662	4645
21163004537000	42.24371402		4550
21139004707000	42.82172318	5170	6775
21139004717000	42.82097047	5151	6632

Appendix 29: Waste Injection Data

WellAPINo	InjectateDescription
21121000027000	Hydrochloric acid (10% - 15%)
21139000517000	Non-hazardous wash water and process water from food products manufacture
21139000527000	Non-hazardous wash water and process water from food products manufacture
21139000537000	Non-hazardous wash water and process water from food products manufacture
21163000697000	
21139000707000	
21139000717000	
21139001297000	Hazardous waste from pharmaceuticals manufacture
21139001307000	Hazardous waste from pharmaceuticals manufacture
21077001377000	Hazardous waste water from pharmaceuticals manufacture
21163001557000	formerly ammonia/phenol hazardous waste water from coke manufacturing
21163001847000	
21139002177000	
21163002267000	formerly ammonia/phenol hazardous waste water from coke manufacturing
21077003277000	Hazardous waste water from pharmaceuticals manufacture
21161003287000	
21091003577000	Non-hazardous waste water from water treatment chemicals manufacture
21139003737000	Hazardous waste from pharmaceuticals manufacture
21091004207000	Non-hazardous waste water from water treatment chemicals manufacture
21163004527000	No injection in this well
21163004537000	No injection in this well
21139004707000	Non-hazardous electric power plant cooling tower condensation water
21139004717000	Non-hazardous electric power plant cooling tower condensation water

Appendix 30: Pressure Fall-off Test Data

WellAPINo	STATUS	Permit.WellNAme	WELLNUM
21121000027000	Plugged	Dupont Montague	1
21139000517000	Active	Heinz	WDW #1
21139000527000	Active	Heinz	WDW #2
21139000537000	Active	Heinz	WDW #3
21163000697000	Plugged	Disposal Well	1
21139001297000	Active	Mt Simon	3
21139001307000	Active	Mt Simon	4
21077001377000	Active	Upjohn	3
21163001557000	Temporarily abandoned	Semet-Solvay	2
21163001847000	Plugged	Ford Motor	D-2
21139002177000	Plugged		D-3
21163002267000	Plugged	Semet Solvay	3
21161003287000	Plugged	Stofer Marshall	1
21091003577000	Active	I.W.	1
21139003737000	Active	Parke-Davis Mt. Simon	5
21163003767000	Plugged	Environmental Disposal Systems	1
21091004207000	Active	M.W.	2
21163004537000	Active	EDS	2-12
21139004707000	Active	Mirant IW	1
21139004717000	Active	Mirant IW	2

Appendix 30: Pressure Fall-off Test Data

WellAPINo	OWNER	LONGITUDE
21121000027000	E.I. DuPont de Nemours & Co., Incorporated	-86.40382667
21139000517000	Heinz North America	-86.12668583
21139000527000	Heinz North America	-86.12578794
21139000537000	Heinz North America	-86.12980867
21163000697000	Detroit Coke Corporation	-83.10373311
21139001297000	Pfizer, Incorporated	-86.11708467
21139001307000	Pfizer, Incorporated	-86.11661504
21077001377000	Pharmacia and Upjohn Company, LLC	-85.55238182
21163001557000	Honeywell International, Incorporated	-83.10586022
21163001847000	Ford Motor Company	-83.15166067
21139002177000	BASF Chemetron	-86.133581
21163002267000	Honeywell International, Incorporated	-83.10785894
21161003287000	Gelman Sciences, Incorporated	-83.802135
21091003577000	Bio-Lab, Incorporated	-84.01626014
21139003737000	Pfizer, Incorporated	-86.11589692
21163003767000	Environmental Disposal Systems, Incorporated	-83.39346415
21091004207000	Bio-Lab, Incorporated	-84.01890566
21163004537000	Environmental Disposal Systems, Incorporated	-83.31690369
21139004707000	Mirant Zeeland, LLC	-85.99255493
21139004717000	Mirant Zeeland, LLC	-85.99522293

Appendix 30: Pressure Fall-off Test Data

WellAPINo	LATITUDE	WELLTYPE	InjInterval Top	InjInterval Bottom	Data from (yr)
21121000027000	43.39738075	Disposal (1W)	5887	6514	1974
21139000517000	42.78541179	Disposal (1I)	5020	5915	2009
21139000527000	42.78331268	Disposal (1I)	4624	6189	2004
21139000537000	42.78365421	Disposal (1I)	5013	5913	2008
21163000697000	42.29210714	Disposal (1W)	4112	4112	1971
21139001297000	42.798256	Disposal (1W)	5121	5945	2004
21139001307000	42.79771636	Disposal (1W)	5121	5946	2006
21077001377000	42.20938802	Disposal (1W)	4911	5615	2006
21163001557000	42.29188896	Disposal (1W)	4109	4112	1995
21163001847000	42.30060253	Disposal (1W)	4307	4695	1976
21139002177000	42.796758	Disposal (1W)	4735	5900	1995
21163002267000	42.29114478	Disposal (1W)	3750	4127	1996
21161003287000	42.276798	Disposal (1I)	5460	5804	1981
21091003577000	41.89358006	Disposal (1I)	4343	4794	2006
21139003737000	42.79725036	Disposal (1W)	5104	6027	1999
21163003767000	42.21249228	Disposal (1W)	4020	4490	1993
21091004207000	41.89360776	Disposal (1I)	4480	4850	2003
21163004537000	42.24371402	Disposal (1W)		4550	2002
21139004707000	42.82172318	Disposal (1I)	5170	6775	2007
21139004717000	42.82097047	Disposal (1I)	5151	6632	2008

Appendix 30: Pressure Fall-off Test Data

WellAPINo	Thickness (uncased to TD)	Thickness (used for calculation)	Diameter of Well	K (md)
21121000027000	627	627	7	186
21139000517000	895	250	9.875 (in)	276.8
21139000527000	1565	250	9.875 (in)	101.8
21139000537000	900	250	9.875 (in)	128.1
21163000697000	0	115	--	35.8
21139001297000	824	740	8.5	162.5
21139001307000	825	740	7.875	163
21077001377000	704	290	12	60
21163001557000	3	123	--	20.96
21163001847000	388	154	9.625	60
21139002177000	1165	1000	10.56	72.2
21163002267000	377	123	4.375	85.3
21161003287000	344	200	--	32
21091003577000	451	300	7.875	5.4
21139003737000		740	7.875	76.42
21163003767000	470	235	8.75	115.4
21091004207000	370	300	7.875	11.7
21163004537000		223	8.76	102
21139004707000	1605	376	6.75	190
21139004717000	1481	376	6.75	66

Appendix 30: Pressure Fall-off Test Data

WellAPINo	Porosity	Compressibility of Fluid (1/psi E-6)	Compressibility of Rock (1/psi E-6)	Total Compressibility	Formation Fluid Viscosity
21121000027000	12	--	--	--	--
21139000517000	12	3.056	4.508	7.564	--
21139000527000	12	3.056	4.508	7.564	--
21139000537000	12	3.056	4.508	7.564	--
21163000697000	--	--	--	--	--
21139001297000	14	--	--	4.5	0.65
21139001307000	14	unknown	--	4.5	0.65
21077001377000	13	3.07	4.36	7.43	--
21163001557000	--	--	--	--	--
21163001847000	13	--	--	7	--
21139002177000	15	--	--	7.4	1
21163002267000	12.4	--	--	6.7	--
21161003287000	--	--	--	--	--
21091003577000	13	2.48	4.23	6.71	--
21139003737000	14	--	--	4.5	0.65
21163003767000	14	--	--	7.2	1.48?
21091004207000	13	2.48	4.23	6.71	--
21163004537000	--	--	--	7.26	1.34
21139004707000	13	--	--	--	0.65
21139004717000	13	--	--	--	0.65

Appendix 30: Pressure Fall-off Test Data

WellAPINo	Specific gravity of injectate	Injectate Viscosity	reservoir pressure	Perforations
21121000027000	0.898	1.5	2671	Yes
21139000517000	1.01	0.87	--	--
21139000527000	1.02	0.93	--	--
21139000537000	1.01	0.88	--	--
21163000697000	--	0.8098	--	--
21139001297000	--	1	--	--
21139001307000	--	1	--	--
21077001377000	0.996	0.96	2144	--
21163001557000	--	--	1755	Yes
21163001847000	--	--	--	Yes
21139002177000	--	1	--	--
21163002267000	--	0.87	--	--
21161003287000	--	1	--	--
21091003577000	1.03	0.91	--	--
21139003737000	--	--	--	--
21163003767000	--	1.48?	--	--
21091004207000	1.03	0.91	--	--
21163004537000	--	--	--	--
21139004707000	--	--	--	--
21139004717000	--	--	--	--

UWI	NPHI	RHOB	GR	DT	Res	NAPI	PEF	Spectral GR	SNP	BITS	CAL	Core	Core porosity	Perm
144410	x	x	x				x							
159232	x	x	x								x			
21005351860000														
21011428580000	x	x	x				x						x	x
21015001538000														
21017377790000	x							x						
21021261120000														
21023299690000	x	x	x								x			
21023330190000														
21023375690000	x	x	x											
21023380450000														
21025404170000			x											
21027229130000														
21027232890000														
21027343040000														
21027354590000	x													
21027359670000	x													
21027369850000														
21029234350000			x	x	x	x				x				
21029234780000														
21029348240000	x	x	x	x	x		x			x	x			
21031306820000	x	x	x								x			
21045291170000	x									x	x			
21051350900000	x	x	x				x				x			
21055342920000	x	x	x	x			x	x						
21057297390000	x	x	x	x	x					x	x			
21059404140000	x	x	x											
21059532680000	x	x	x				x							
21063291910000	x	x	x											
21065286070000														
21075222750000														
21075271370000														
21077001377000		x				x							o	x
21077003277000	x	x	x									x		x
21081001568000														
21091003577000	x	x	x		x		x				x		x	x
21091004207000	x	x	x				x						x	x
21091104480000														
21093279860000	x		x	x	x	x				x	x			
21093404380000	x	x	x		x		x	x		x	x			
21093437270000	x	x	x				x	x						
21093540210000	x	x	x				x							
21097426710000	x	x	x											
21099337370000	x	x	x											
21105399840100	x	x	x				x							
21113343760000	x	x	x				x					x		
21115077020000														
21115112210000														
21115254940000														
21115359480000	x	x	x				x	x						
21121000027000	x	x	x									x	x	x
21123398560100	x	x	x				x	x						
21127331340000	x	x	x											
21127416550000														
21127582490000	x	x	x		x		x				x			
21133398540100	x	x	x											
21139000517000	x	x	x								x			
21139000527000		x	x		x						x			
21139000537000	x	x	x											
21139000707000			x									x	x	x
21139000717000	x	x	x						x		x		x	
21139001297000	x	x	x											
21139001307000	x	x	x								x			
21139002177000														
21139003737000	x	x	x				x				x			
21139004707000	x	x	x				x							
21139004717000														
21139348850000	x	x	x				x				x			
21141271990000														
21147001398000												x	x	x
21147001518000												x	x	x
21147001528000												x	x	x
21147303760000	x		x	x	x					x	x			
21147389640000	x	x	x											
21147407930000	x	x	x				x							
21149313350100	x	x	x									x		
21161003287000	x	x	x								x			
21161101410000														
21161107920000														
21161113410000														
21163001468000	x	x	x							x	x			
21163001557000	x	x	x								x	x	x	x
21163001847000	x	x	x		x						x			
21163003767000	x	x	x	x	x		x				x		x	x
21163004527000	x	x	x				x							
21163004537000													x	x
21163104300000														
21163194960000														
21031350600000														
21163000697000														
21163002267000														

Appendix 31: Well Data

UWI	Thin Section	Cuttings	PET	Inject Data	Wireline logs	ECLR	MNSM
144410						2895.74	3001.84
159232						3776.84	4215.54
21005351860000		x			No logs run	4316	4745
21011428580000					Rasters CNLDT, DMLL, SON	13952.69	14161.3
21015001538000							6193
21017377790000		x			Rasters CNLDT, DMLL, SON, SGR	13693.66	13793
21021261120000		M			Raster GRN	3105.55	3365
21023299690000					Rasters ND, DLL	4463.58	4874
21023330190000					Rasters DENS, RES	4092.19	4500
21023375690000		x			Rasters CNLDT, DMLL, SON	4299.93	4709
21023380450000					Rasters CNLDT, DMLL, SON	4366.19	4749
21025404170000		x			Rasters CNLDT, BTV, FRACID	5768.52	6151
21027229130000		M			Raster not deep enough	3030	3280
21027232890000		M			Raster GRN		3881
21027343040000		o			Raster ND, CNL, FDC, SON, DLL	3470.04	3804
21027354590000					Raster ND		3718
21027359670000		x			Raster CNLDT	2287.78	2582
21027369850000		x			Raster ND, DIL, SON	3327.23	3778
21029234350000		M			Raster LGRN, SON		4330
21029234780000		M			Raster LGRN		4482
21029348240000		M			Rasters CNLDT, DMLL, SON	8184.6	8326
21031306820000					Raster ND, DLL, SON	5394.41	5444.44
21045291170000		x			Raster ND, DLL, SON		6905
21051350900000		M			Rasters CNLDT, DMLL, SON	14860.99	14984
21055342920000					Rasters CNLDT, DMLL, SON	10120.93	10198.16
21057297390000					Rasters SON, DLL,DIP	10820.34	10963.31
21059404140000		x			Rasters CNLDT, DMLL, SON	5111.75	5496
21059532680000		x			Rasters CNLDT, DMLL, SON, CIBL	4390.08	4768
21063291910000		x			Rasters CNLDT, DMLL, SON		8838
21065286070000					not logged below Trenton		7220
21075222750000		M			Rasters GR, NEUT		5826
21075271370000					Rasters GR, NEUT	5399.71	5765
21077001377000			x	x	no State Raster	4542.85	4956.91
21077003277000		x	x	x	no State Raster	4525.44	4939.97
21081001568000					no State Raster		7105
21091003577000			x	x	no State Raster		4474.15
21091004207000			x	x	GR, NEUT, DENS, PEF		4474.81
21091104480000					no State Raster		3611
21093279860000		M			no State Raster		
21093404380000					no State Raster		6952
21093437270000					Rasters CNLDT, DMLL, SON	7282	7319
21093540210000					Rasters CNLDT, DMLL	7150.8	7221.14
21097426710000							2049
21099337370000					Raster ND, SON	5106.91	5166
21105399840100		M			Rasters CNLDT, DMLL, SON	6903.26	6991.5
21113343760000	x				Rasters CNLDT, DMLL	14145.14	14229.3
21115077020000					No logs run		3425
21115112210000		M			No logs run		3176
21115254940000		M			no State Raster		3356
21115359480000					Rasters CNLDT, DMLL, SON	2958.88	3083.47
21121000027000	x		x	x	GR	5687.93	5778.05
21123398560100					Rasters CNLDT, DMLL, SON	9693.65	9866.13
21127331340000					Raster ND, DLL	5713.9	5823
21127416550000					Rasters CNLDT, DMLL, SON	7612.99	7728
21127582490000					GR, RHOB, DT, SPHI	6439.4	6541.59
21133398540100					Rasters CNLDT, DMLL, SON	12199.93	12297
21139000517000			x	x	no State Raster	4830.14	5031
21139000527000			x	x	no State Raster	4845.39	5045
21139000537000			x	x	no State Raster	4800.3	5033
21139000707000	x		x	x	no State Raster	4854.59	5062.66
21139000717000			x	x	no State Raster	4867.53	5057.63
21139001297000			x	x	GR, NEUT, DENS	4890.31	5082
21139001307000			x	x	no State Raster	4876.91	5080
21139002177000			x	x	no State Raster		5219
21139003737000			x	x	no State Raster	4887.14	5090
21139004707000			x	x	no State Raster	5289.96	5474
21139004717000			x	x	no State Raster		
21139348850000					Rasters CNLDT, DIL, SON	6835.93	7014
21141271990000		M			Rasters LGN, SON, DIL, SNP		5541.51
21147001398000	o				no State Raster		4570
21147001518000	?				no State Raster		4679.94
21147001528000					no State Raster		4655
21147303760000					Rasters SNP, DLL		4408
21147389640000					Rasters CNLDT, DMLL, SON		6423
21147407930000					Rasters CNLDT, DMLL	4530.91	4583
211493133S0100	x				Raster ND, DMLL, SON	4081.18	4466
21161003287000			x	x	Raster ND, DLL	5229.53	5316.63
21161101410000		M			No raster		6034
21161107920000		M			No raster		5839
21161113410000		M			No raster		5348
21163001468000					No raster		3569.11
21163001557000	x		x	x	No raster	3902.18	3990.18
21163001847000			x	x	No raster		4129.56
21163003767000			x		No raster		4134.71
21163004527000			x	x	No raster		4368.74
21163004537000			x	x	GR, NEUT, DENS, PEF	4120	4219.08
21163104300000		M			No raster		3774
21163194960000		M			Rarters GRN, MLL, LAT, RES		5292
21031350600000		x			Rasters CNLDT, DMLL, SON		
21163000697000			x	x	No raster		
21163002267000			x	x	No raster		

UWI	PC	EF1	EF2	EF3	Well type	COUNTY	Permit
144410	4496						
159232	4669.87	4213.94	4276.68	4624.3			
21005351860000	5582				DH	ALLEGAN	35186
21011428580000	15494				GAS	ARENAC	42858
21015001538000							
21017377790000		13791.76			GC	BAY	37779
21021261120000	4609.45				DH	BERRIEN	26112
21023299690000	5418	4872.4	5006.36	5347.21	DH	BRANCH	29969
21023330190000					DH	BRANCH	33019
21023375690000	5210	4707.69	4843.88	5183.32	DH	BRANCH	37569
21023380450000	5207				DH	BRANCH	38045
21025404170000					DH	CALHOUN	40417
21027229130000					DH	CASS	22913
21027232890000					DH	CASS	23289
21027343040000					BDW	CASS	34304
21027354590000					DH	CASS	35459
21027359670000					OIL	CASS	35967
21027369850000					DH	CASS	36985
21029234350000	4566				DH	CHARLEVOIX	23435
21029234780000	4718				DH	CHARLEVOIX	23478
21029348240000					DH	CHARLEVOIX	34824
21031306820000		5442.21	5488.31		DH	CHEBOYGAN	30682
21045291170000					DH	EATON	29117
21051350900000		14985.13	15532.68		DH	GLADWIN	35090
21055342920000	10904.36	10195.93	10220.33	10883.11	DH	GRAND TRAVERSE	34292
21057297390000	12175	10962.07	11258.91	12168.12	DH	GRATIOT	29739
21059404140000	5805.49	5495.64	5636.73	5764.83	OIL	HILLSDALE	40414
21059532680000					GAS	HILLSDALE	53268
21063291910000	8872				MNB	HURON	29191
21065286070000	7690				DH	INGHAM	28607
21075222750000					DH	JACKSON	22275
21075271370000					DH	JACKSON	27137
21077001377000	5554	4955.31	5162.19	5472.51	MDW	KALAMAZOO	00137
21077003277000	5594	4939.92	5060.21	5497.59	MDW	KALAMAZOO	00327
21081001568000					BDW	KENT	00156
21091003577000					MDW	LENAWEE	00357
21091004207000					MDW	LENAWEE	M420
21091104480000	3865						
21093279860000	7150				DH	LIVINGSTON	27986
21093404380000	7400				GAS	LIVINGSTON	40438
21093437270000	7351.71				DH	LIVINGSTON	43727
21093540210000	7599				GIW	LIVINGSTON	54021
21097426710000	2088.31						
21099337370000	5362				DH	MACOMB	33737
21105399840100		6988.98	7032.82	7453.77	DH	MASON	39984
21113343760000		14227.07	14262.27		DH	MISSAUKEE	34376
21115077020000	3625				DH	MONROE	07702
21115112210000	3342				DH	MONROE	11221
21115254940000	3637				DH	MONROE	25494
21115359480000	3470				DH	MONROE	35948
21121000027000		5774.44	5818.84	6524.45	MDW	MUSKEGON	00002
21123398560100		9865.21	9952.51		GAS	NEWAYGO	39856
21127331340000	7192	5822.08	5860.04	6133.73	DH	OCEANA	33134
21127416550000					DH	OCEANA	41655
21127582490000		6539.08	6611.79		DH	OCEANA	58249
21133398540100		12297.67	12366.41		GAS	OSCEOLA	39854
21139000517000		5029.81	5190.28		MDW	OTTAWA	00051
21139000527000	6152	5042.39	5194.34	6020.82	MDW	OTTAWA	00052
21139000537000		5031.81	5183.76		MDW	OTTAWA	00053
21139000707000		5062.89	5224.78		MDW	OTTAWA	00070
21139000717000		5057.86	5219.74		MDW	OTTAWA	00071
21139001297000			5237.89		MDW	OTTAWA	00129
21139001307000					MDW	OTTAWA	00130
21139002177000					MDW	OTTAWA	00217
21139003737000					MDW	OTTAWA	00373
21139004707000	6595.4	5470.92	5637.51	6424.89	MDW	OTTAWA	00470
21139004717000					MDW	OTTAWA	00471
21139348850000		7013.11	7199.09		DH	OTTAWA	34885
21141271990000	5877				BDW	PRESQUE ISLE	27199
21147001398000	4599				BDW	SAINT CLAIR	00139
21147001518000	4724.94				BDW	SAINT CLAIR	00151
21147001528000	4685				BDW	SAINT CLAIR	00152
21147303760000	4449				DH	SAINT CLAIR	30376
21147389640000	6545				DH	SAINT CLAIR	38964
21147407930000	4714				BDW	SAINT CLAIR	40793
21149313350100	5074	4466.1	4563.7	4977.07	DH	SAINT JOSEPH	31335
21161003287000					MDW	WASHTENAW	00328
21161101410000	6374				DH	WASHTENAW	10141
21161107920000	6094				DH	WASHTENAW	10792
21161113410000	5670				DH	WASHTENAW	11341
21163001468000	3710				BDW	WAYNE	00146
21163001557000	4092.51				MDW	WAYNE	00155
21163001847000	4258				MDW	WAYNE	00184
21163003767000					MDW	WAYNE	00376
21163004527000					MDW	WAYNE	00452
21163004537000					MDW	WAYNE	00453
21163104300000	3985				DH	WAYNE	10430
21163194960000					GS	WAYNE	19496
21031350600000					DH	CHEBOYGAN	35060
21163000697000					MDW	WAYNE	00069
21163002267000					MDW	WAYNE	00226

UWI	LEASE	WELL #
144410		
159232		
21005351860000	HOWARD HUNT UNIT	1
21011428580000	STATE SIMS	2-7
21015001538000		
21017377790000	PREVOST ET AL	1-11
21021261120000	THALMANN	1
21023299690000	CLARK, HARVEY	1
21023330190000	RENSEL, RICHARD A & ALLEN, ALVA	1-13
21023375690000	ARCO & JOHNSON	1-3
21023380450000	ARCO & GAGLIO	1-13
21025404170000	MARKOVICH, ET AL	1-5
21027229130000	RAYMOND ANDRESEN	1
21027232890000	WOODEN, WARREN	1
21027343040000	LAWSON	1
21027354590000	HOLDEMAN	1-31
21027359670000	HAWKES & ADAMS	1-28
21027369850000	SMITH	1-20
21029234350000	STATE BEAVER ISLAND	1
21029234780000	STATE BEAVER ISLAND	2
21029348240000	NORTH MICHIGAN LAND & OIL CORP.	1-27
21031306820000	STATE WAVERLY	1-24
21045291170000	KELLY, GLADYS UNIT	1
21051350900000	MARTIN	1-15
21055342920000	STATE BLAIR	2-24
21057297390000	SPARKS R&J, & ECKELBARGER K&V, & WHIGHTSIL	1-8
21059404140000	ROWE, W	A-8
21059532680000	HEFFELFINGER	1-25
21063291910000	VOLMERING, C J	1
21065286070000	KRANZ, WALTER JR	1
21075222750000	DANCER, HAROLD	1
21075271370000	SMITH, ALFRED	2
21077001377000	UPJOHN	3
21077003277000	UPJOHN	4
21081001568000	ALTO PROPANE STORAGE FEE	2 SWD
21091003577000	INDUSTRIAL WELL	1
21091004207000	M.W.	2
21091104480000	HARRY TAYLOR	1
21093279860000	MESSMORE, HOWARD J	1
21093404380000	PHILLIPS	1-2
21093437270000	DEY	1-15
21093540210000	HARTLAND 36 INJECTION WELL	1
21097426710000		
21099337370000	GRIERSON	1-24
21105399840100	VICTORY	2-26
21113343760000	DOORNBOS ET AL	5-30
21115077020000	MRS. JAMES SANCRANT	1
21115112210000	CHAPMAN, DELMONT L. & ROSE L.	1
21115254940000	SHIMP, MERLIN	1
21115359480000	COUSINO	1-1
21121000027000	Dupont Montague	1
21123398560100	PATRICK & STATE NORWICH	2-28
21127331340000	SCHILLER UNIT	1-10
21127416550000	DRUM	1-16
21127582490000	ST HART & FUEHRING	4-30
21133398540100	BOYCE	2-19
21139000517000	Heinz	WDW #1
21139000527000	Heinz	WDW #2
21139000537000	Heinz	WDW #3
21139000707000	Deep Well	1
21139000717000	Deep Well	D-2
21139001297000	Mt Simon	3
21139001307000	Mt Simon	4
21139002177000	DISPOSAL WELL	D-3
21139003737000	PARKE-DAVIS MT. SIMON	5
21139004707000	Mirant IW	1
21139004717000	Mirant IW	2
21139348850000	UMLOR ROBERT ET AL	1-3
21141271990000	DRAYSEY, DONALD E.	1 BDW
21147001398000	CONSUMERS POWER COMPANY	BD1
21147001518000	CONSUMERS POWER COMPANY	BD1-7
21147001528000	CONSUMERS POWER COMPANY	BD 2-7
21147303760000	OSTERLAND, ALVIN W & FLORENCE M ET AL	1-14
21147389640000	ARCO & SENYK	1-30
21147407930000	ST. CLAIR NGL	SWD 1-
21149313350100	CUPP, LLOYD	1-11
21161003287000	Stofer Marshall	1
21161101410000	VOSS, WM. F. (COMM.)	1
21161107920000	RODDENBERRY, TROY ET AL COMM.	1
21161113410000	MEINZINGER, VIOLA	1
21163001468000	MARATHON OIL CO. (WOODHAVEN)	BD1
21163001557000	Semet-Solvay	2
21163001847000	Ford Motor	D-2
21163003767000	DISPOSAL WELL	1
21163004527000	EDS #1-12	1-12
21163004537000	EDS #2-12	2-12
21163104300000	THEISON, B. ESTATE	1
21163194960000	DETROIT HOUSE OF CORRECTION	3
21031350600000	SALLING-HANSON CO. TR.	1-11
21163000697000	Disposal Well	1
21163002267000	Semet-Solvay	3

UWI	COMPANY	TD	ELEV
144410			
159232			
21005351860000	MARTIN PROPERTIES INC	6000	687
21011428580000	MATREX LLC	15514	621
21015001538000			
21017377790000	QUICKSILVER RESOURCES INC	14589	621
21021261120000	SECURITY OIL AND GAS CO	5648	804
21023299690000	CONSUMERS POWER CO AND QUINTANA PRODUCTION CO	5475	889
21023330190000	MUTCH J O	4633	1019
21023375690000	ATLANTIC RICHFIELD CO INC		
21023380450000	ATLANTIC RICHFIELD CO INC	5378	958
21025404170000	KULKA AND SCHMIDT INC	6240	947
21027229130000	SPILLER OIL CO.	3300	848
21027232890000	PERRY C A AND SON INC	3950	865
21027343040000	CENTER JUNCTION CORP	3851	967
21027354590000	HALLWELL INC	3800	897
21027359670000	CENTER JUNCTION CORP	2998	929
21027369850000	MANNES OIL CORP	4001	840
21029234350000	MCCLURE OIL CO	5383	678
21029234780000	MCCLURE OIL CO	4803	741
21029348240000	ENERGY ACQUISITION CORP AND WEITZMAN IRVIN	8900	1145
21031306820000	C M S OIL AND GAS CO AND TRIBAL OIL CO	5753	801
21045291170000	EXXONMOBIL OIL CORP	6922	870
21051350900000	HUNT ENERGY CORP	15859	735
21055342920000	SWEPI LP	11020	915
21057297390000	MCCLURE OIL CO	17466	762
21059404140000	MARATHON OIL CO	5917	1107
21059532680000	EDGE PETROLEUM OPERATING CO INC	4866	1114
21063291910000	TALASKI LAVERNE	2320	711
21065286070000	EXXONMOBIL OIL CORP	7866	939
21075222750000	COLLIN C W AND BLACK J OLIVER	6038	997
21075271370000	NANCO INC	5936	1018
21077001377000	PHARMACIA AND UPJOHN	5615	886
21077003277000	PHARMACIA AND UPJOHN	5600	886
21081001568000	PLAINS LPG SERVICES LP	8205	0
21091003577000	GREAT LAKES CHEMICAL	4856	816
21091004207000	Bio-Lab, Inc.	4850	816
21091104480000	Walter Eckert	3902	715
21093279860000	EXXONMOBIL OIL CORP	7589	980
21093404380000	TERRA ENERGY LTD AND SMITH PETROLEUM	7450	940
21093437270000	SWEPI LP	7476	918
21093540210000	K C 5 MICHIGAN RESOURCES INC	7535	1026
21097426710000			
21099337370000	ENERGY ACQUISITION CORP AND WEITZMAN IRVIN	5400	739
21105399840100	MILLER BROTHERS	7485	0
21113343760000	JEM PETROLEUM CORP	14713	1232
21115077020000	JACOB BECK	5495	669
21115112210000	STURMAN JOSEPH W	3377	597
21115254940000	FERGUSON AND GARRISON	3671	680
21115359480000	REEF PETROLEUM CORP	3506	646
21121000027000	DU PONT DE NEMOURS AND CO	6514	656
21123398560100	SAVOY ENERGY LP	10200	1092
21127331340000	AMOCO PRODUCTION CO	7240	752
21127416550000	SPARTON CORP	7920	867
21127582490000	BATTELLE CORP	6874	912
21133398540100	H AND H STAR ENERGY INC DBA PETROSTAR ENERGY	12810	0
21139000517000	H J HEINZ CO	5915	602
21139000527000	H J HEINZ CO	6189	619
21139000537000	H J HEINZ CO	5913	617
21139000707000	CHEMETRON CORP PIGMENTS DIV	5895	623
21139000717000	B A S F CHEMETRON	5910	607
21139001297000	PARKE DAVIS AND CO	5945	604
21139001307000	PARKE DAVIS AND CO	5946	602
21139002177000	B A S F CHEMETRON	5900	617
21139003737000	PARKE DAVIS AND CO	6027	600
21139004707000	MIRANT ZEELAND LLC		
21139004717000	MIRANT ZEELAND LLC		
21139348850000	CHEVRON U S A INC	7245	891
21141271990000	PRESQUE ISLE COUNTY ROAD COMMISSION	5940	809
21147001398000	CONSUMERS ENERGY CO	4634	0
21147001518000	CONSUMERS ENERGY CO	4733	0
21147001528000	CONSUMERS ENERGY CO	4702	0
21147303760000	MICHIGAN CONSOLIDATED GAS CO	4550	603
21147389640000	MILLER BROTHERS AND ATLANTIC RICHFIELD	6696	801
21147407930000	B P PRODUCTS AND DOME PETROLEUM CORP	0	605
21149313350100	MARATHON OIL CO	5283	0
21161003287000	GELMAN SCIENCES INC	5804	935
21161101410000	COLVIN AND ASSOCIATES ELECTRIC STEEL CO	6410	0
21161107920000	CHAMNESS I C	6094	0
21161113410000	COLVIN AND ASSOCIATES ELECTRIC STEEL CO	5692	818
21163001468000	MARATHON OIL CO	3752	0
21163001557000	HONEYWELL INTERNATIONAL INC	4112	600
21163001847000	FORD MOTOR CO	4308	602
21163003767000	ENVIRONMENTAL DISPOSAL SYSTEMS		658
21163004527000	ENVIRONMENTAL DISPOSAL SYSTEMS	4550	
21163004537000	ENVIRONMENTAL DISPOSAL SYSTEMS	4550	
21163104300000	COLVIN AND ASSOCIATES ELECTRIC STEEL CO	4046	0
21163194960000	CONSUMERS ENERGY CO	5483	900
21031350600000	ORYX ENERGY CO	5940	813
21163000697000	DETROIT COKE CORP	4112	587
21163002267000	HONEYWELL INTERNATIONAL INC	4127	600.5

UWI	LONG	LAT
144410		
159232		
21005351860000	-86.19937001	42.56902001
21011428580000	-83.68136001	44.06028001
21015001538000		
21017377790000	-83.95255	43.63590001
21021261120000	-86.26295	41.95783001
21023299690000	-85.27166001	42.05646001
21023330190000	-84.96022001	41.77114
21023375690000	-85.21670001	41.97170001
21023380450000	-85.07784001	41.94246
21025404170000	-85.14550999	42.408
21027229130000	-85.9368	41.7795
21027232890000	-85.96415999	41.88034001
21027343040000	-85.93625002	41.8331
21027354590000	-85.86552002	41.81027
21027359670000	-85.94573001	41.82579001
21027369850000	-85.97139	41.84916
21029234350000	-85.52786999	45.65883002
21029234780000	-85.58503	45.61878001
21029348240000	-84.79477	45.14025001
21031306820000	-84.37411001	45.40923001
21045291170000	-84.61575002	42.55126
21051350900000	-84.33462001	43.88523001
21055342920000	-85.57971999	44.63675
21057297390000	-84.57948002	43.27308001
21059404140000	-84.64054001	42.06351001
21059532680000	-84.71499999	41.82595001
21063291910000	-82.66169002	43.71703002
21065286070000	-84.45330001	42.53110001
21075222750000	-84.45830001	42.1789
21075271370000	-84.70940001	42.17640001
21077001377000	-85.55080001	42.2181
21077003277000	-85.5504	42.2177
21081001568000	-85.36324002	42.85556001
21091003577000	-84.01626014	41.89358006
21091004207000	-84.01890566	41.89360776
21091104480000	-83.85089	41.73512
21093279860000	-83.82509999	42.67375
21093404380000	-84.06345	42.68012
21093437270000	-84.09019999	42.65328
21093540210000	-83.68767001	42.61893
21097426710000		
21099337370000	-82.74440001	42.84390001
21105399840100	-86.31202001	44.00942001
21113343760000	-85.0833	44.2719
21115077020000	-83.6489	41.86
21115112210000	-83.27330001	42.03060001
21115254940000	-83.71110001	41.86580002
21115359480000	-83.5517	41.9056
21121000027000	-86.40382999	43.39738
21123398560100	-85.63152001	43.65835001
21127331340000	-86.44584001	43.53445001
21127416550000	-86.11509	43.69688001
21127582490000		
21133398540100	-85.55108001	44.10857002
21139000517000	-86.12668999	42.78541001
21139000527000	-86.1283	42.7853
21139000537000	-86.12981002	42.78365001
21139000707000	-86.13052999	42.79649
21139000717000	-86.13051999	42.79569
21139001297000	-86.11691	42.79825
21139001307000	-86.11645	42.7977
21139002177000	-86.13308	42.79694
21139003737000	-86.1158969	42.7972504
21139004707000	-85.9925549	42.8217232
21139004717000	-85.9952229	42.8209705
21139348850000	-85.83666001	43.11673001
21141271990000	-84.21386999	45.38252001
21147001398000	-82.7253	42.7203
21147001518000	-82.4964	42.8886
21147001528000	-82.48629999	42.88860001
21147303760000	-82.63095	42.69359
21147389640000	-82.97127002	42.90929001
21147407930000	-82.50676001	42.81261001
21149313350100	-85.43112	41.95679
21161003287000	-83.8097	42.27670002
21161101410000	-83.6214	42.39470001
21161107920000	-83.59000001	42.40560001
21161113410000	-83.54910001	42.32640001
21163001468000	-83.22712001	42.13184
21163001557000	-83.12080001	42.28830001
21163001847000	-83.12080001	42.28830001
21163003767000	-83.3934641	42.2124923
21163004527000	-83.3168261	42.2435157
21163004537000	-83.3169037	42.243714
21163104300000	-83.3656	42.145
21163194960000	-83.51413	42.39822002
21031350600000	-84.52070001	45.35382002
21163000697000	-83.12080001	42.28830001
21163002267000	-83.10785894	42.29114478

			Detrital			
Well ID	Depth	Qtz	K-Spar	Other	total	Bioclasts
327	4966.2	80	3.6		83.6	
327	4995	72	4		76	
31335	5007.6	64.4	9.6	1.6	74	
31335	5016.1	69.5	9	0	78.5	
31335	5021.8	60	11.5	1	72.5	
31335	5024.3	57	11.5	2.5	71	
31335	5035.2	72.15	2.25	0	74.4	
31335	5044.8	68.5	11	1	80.5	
31335	5052.3	68	10.5	0	78.5	
31335	6065.6	68.5	4.5	0.5	73.5	
34376	14234	56	0.4		56.4	3.6
34376	14262	48.4	14.8		63.2	0
34376	14300	55.2	6.8		62	0.4
34376	14312	60.8	12		72.8	0
34376	14355	54	6.4		60.4	0
M002	5635	48.4	0		48.4	
M002	6001	74	0.4		74.4	
M002	6087.5	73.2	2		75.2	
M002	6090.5	75.2	2.4		77.6	
M0070	5302.2	81.2	3.2		84.4	
M0070	5315	80.8	0.8		81.6	2
M0070	5320	72.5	2		75	
M0070	5334	81.6	0.4		82	
M0070	5529	74.4	0		74.4	
M0070	5540	75.2	0.4		75.6	
M0070	5552	78.4	0.8		79.2	
M0070	5567	74.8	0		74.8	
M0070	5572	67.2	5.6		72.8	
M0155	3964.4	42	25		67	
M0155	4000.7	32	9.2		41.2	
M0155	4018.3	60	11.5	0.5	72	
M0155	4038.7	40	32	1.5	73.5	
M0155	4047.5	40.5	9.5	0.5	50.5	
M0155	4053.7	71	0	2.5	73.5	
M0155	4063.7	63.6	13.2	2.8	79.6	
M0155	4078.5	60.5	17	1.5	79	
M0155	4085.7	56	19	0.5	75.5	
M0155	4094	28.5	14.5	3.5	46.5	
M0155	4100.7	52	19.2	0.8	72	
W139	4570	42.5	4.7		47.2	
W139	4577.4	62.4	20.6		83	
W139	4584.3	88.5	7.7		96.2	
W139	4589.4	32.4	15.7		48.1	
W139	4590.3	63.8	29.9		93.7	
W139	4595.4	79.7	17.5		97.2	
W139	4596.2	64.4	30.6		95	
W139	4599.2	46	4.6		50.6	
W139	4600.3	24.3	18.7		43	
W139	4602.2	70.5	17.1		87.6	
AK	5465.1	60	5	1	66	
AK	5467.8	44	17.5		61.5	
AK	5478	58.5	17.5	0.5	76.5	
AK	5487.2	63	14.5	0.5	78	1
AK	5492.1	57	21.5	1.5	80	
AK	5497.7	50	27	2.5	79.5	1
AK	5640	45	28.5	1	74.5	
AK	5648.4	36.5	36.5		73	
AK	5660.3	42.5	35.5	0.5	78.5	
AK	5669.3	30	45.5		75.5	

		Authigenic				
Well ID	Depth	Quartz	Iron Oxide	Feldspar	Carbonate	Clay
327	4966.2	0.4		1.2		0.4
327	4995	1	0.5	2.5		1
31335	5007.6	8.8	4.8	0.4		4
31335	5016.1	0.5	7	0		6.5
31335	5021.8	0	20	0		5.5
31335	5024.3	0	17	0		10
31335	5035.2	7.45	5.25	0		1.25
31335	5044.8	3.5	8.5	0		1
31335	5052.3	1	6.5	0		11
31335	6065.6	7	0	1		7.5
34376	14234	0.8	0	0	9.2	26.4
34376	14262	10.8	0	0	0	19.2
34376	14300	11.6	0	2.4	3.2	14.4
34376	14312	17.2	0	6.4	0	0.4
34376	14355	35.2	0	2.8	0.4	1.2
M002	5635	1.6			47.6	0.8
M002	6001	10				0.4
M002	6087.5	0.8				16.8
M002	6090.5	2.8				0.8
M0070	5302.2	0.4		0.8		8.4
M0070	5315	0.8				0
M0070	5320	7.5				0
M0070	5334	0				9.2
M0070	5529	1.6				0
M0070	5540	6		0.4		0
M0070	5552	1.2				0
M0070	5567	1.6				1.2
M0070	5572	6		4.4		2.4
M0155	3964.4	1.5	0.5		4	9
M0155	4000.7	1.2	2.8	2.8	38.4	
M0155	4018.3	5	4.5	2.5		3
M0155	4038.7		4	0.5		11
M0155	4047.5	0.5			39	6
M0155	4053.7	0.5		1	6.5	12.5
M0155	4063.7	0.4		4.4		8.8
M0155	4078.5	0.5	0.5		7	2
M0155	4085.7	1			7.5	0.5
M0155	4094	0.5	2	0.5	34	3.5
M0155	4100.7	0.8	1.6	6.4		7.6
W139	4570	0.3		0.6	51.2	
W139	4577.4	7.7		2.1	7.1	
W139	4584.3	1.1		0.9	1.8	
W139	4589.4	0.7		0	50.5	
W139	4590.3	0.7		0.4	0.4	
W139	4595.4	0		1.7	1	
W139	4596.2	2.2		0	3.6	
W139	4599.2	0		0	39.4	
W139	4600.3	1		0	56	
W139	4602.2	7.8		4.1	0.4	
AK	5465.1	2	2		20	3.5
AK	5467.8		0.5		32.5	1
AK	5478	2	8		4.5	2
AK	5487.2	3.5	2.5	0.5		2
AK	5492.1					10.5
AK	5497.7	0.5	0.5		0.5	9
AK	5640	1	3.5	0.5		10.5
AK	5648.4				1.5	25.5
AK	5660.3	2.5				9
AK	5669.3		0.5		9	4.5

		Pore Space				
Well ID	Depth	Inter GranularPorosity	Dissolution	Disconnected Pore	Total	Artifact
327	4966.2	12.8	0.8		13.6	0.8
327	4995	9.5			9.5	
31335	5007.6	6.4		0	6.4	
31335	5016.1	4		3.5	7.5	
31335	5021.8	0.5		1.5	2	
31335	5024.3	0		2	2	
31335	5035.2	10.7		0	10.7	
31335	5044.8	5		0.5	5.5	
31335	5052.3	2.5		0.5	3	
31335	6065.6	9.5		0	9.5	
34376	14234	2.4		0	2.4	1.2
34376	14262	2.8		0	2.8	0
34376	14300	4.4		0	4.4	1.6
34376	14312	3.2		0	3.2	24
34376	14355	0		0	0	0.4
M002	5635	0			0	1.6
M002	6001	14.4			14.4	
M002	6087.5	6.8			6.8	0.4
M002	6090.5	17.2			17.2	1.6
M0070	5302.2	5.2			5.2	0.4
M0070	5315	15.6			15.6	
M0070	5320	17			17	0.5
M0070	5334	8.8			8.8	
M0070	5529	23.6			23.6	0.4
M0070	5540	17.2			17.2	0.4
M0070	5552	19.6			19.6	
M0070	5567	22			22	0.4
M0070	5572	14			14	
M0155	3964.4	14	4		18	
M0155	4000.7	9.2	2.8		12	1.6
M0155	4018.3	12	1		13	
M0155	4038.7	7.5	3.5		11	
M0155	4047.5	3.5	0.5		4	
M0155	4053.7	4	2		6	
M0155	4063.7	5.2	1.6		6.8	
M0155	4078.5	9.5	1		10.5	0.5
M0155	4085.7	14.5	1		15.5	
M0155	4094	21	1		22	
M0155	4100.7	9.2	2.4		11.6	
W139	4570	9			9	
W139	4577.4	21.1			21.1	
W139	4584.3	12.6			12.6	
W139	4589.4	10			10	
W139	4590.3	15.4			15.4	
W139	4595.4	14.2			14.2	
W139	4596.2	14.8			14.8	
W139	4599.2	8			8	
W139	4600.3	6.6			6.6	
W139	4602.2	14.3			14.3	
AK	5465.1	7.5			7.5	
AK	5467.8	4.5			4.5	
AK	5478	7			7	
AK	5487.2	11	1.5		12.5	
AK	5492.1	6.5	3		9.5	
AK	5497.7	6	3		9	
AK	5640	6.5	3.5		10	
AK	5648.4	0	0		0	
AK	5660.3	3.5	6.5		10	
AK	5669.3	4	6.5		10.5	

		Grain Size			
Well ID	Depth	Average	Mode	Largest	Standard Deviation
327	4966.2	0.26	0.07	0.96	0.16
327	4995	0.26	0.23	0.52	0.11
31335	5007.6	0.34	0.09	1.37	0.26
31335	5016.1	0.49	0.19	1.47	0.37
31335	5021.8	0.35	0.10	2.07	0.35
31335	5024.3	0.26	0.10	0.98	0.22
31335	5035.2	0.35	0.20	0.74	0.17
31335	5044.8	0.36	0.16	2.69	0.47
31335	5052.3	0.35	0.12	1.34	0.29
31335	6065.6	0.35	0.17	1.32	0.23
34376	14234	0.33	0.31	0.70	0.19
34376	14262	0.21	0.14	0.76	0.15
34376	14300	0.27	0.10	1.02	0.18
34376	14312	0.27	0.12	0.87	0.18
34376	14355	0.16	0.14	0.87	0.07
M002	5635	0.22	0.12	0.60	0.11
M002	6001	0.20	0.09	0.82	0.14
M002	6087.5	0.19	0.06	0.73	0.14
M002	6090.5	0.21	0.16	0.58	0.12
M0070	5302.2	0.25	0.11	0.48	0.12
M0070	5315	0.24	0.23	0.89	0.14
M0070	5320	0.20	0.20	0.35	0.07
M0070	5334	0.24	0.15	0.63	0.12
M0070	5529	0.22	0.14	0.59	0.12
M0070	5540	0.18	0.15	0.79	0.13
M0070	5552	0.18	0.13	0.57	0.08
M0070	5567	0.09	0.08	0.22	0.04
M0070	5572	0.17	0.08	0.52	0.10
M0155	3964.4	0.12	0.14	0.21	0.04
M0155	4000.7	0.25	0.17	0.51	0.11
M0155	4018.3	0.33	0.38	0.56	0.11
M0155	4038.7	0.22	0.21	0.99	0.15
M0155	4047.5	0.42	0.27	1.91	0.36
M0155	4053.7	0.28	0.22	0.99	0.17
M0155	4063.7	0.42	0.37	1.23	0.25
M0155	4078.5	0.30	0.20	0.97	0.16
M0155	4085.7	0.30	0.31	0.63	0.14
M0155	4094	0.15	0.09	0.53	0.12
M0155	4100.7	0.27	0.10	1.13	0.21
W139	4570	0.18			0.20
W139	4577.4	0.32			0.30
W139	4584.3	0.45			0.40
W139	4589.4	0.23			0.15
W139	4590.3	0.34			0.33
W139	4595.4	0.60			0.60
W139	4596.2	0.62			0.35
W139	4599.2	0.63			0.75
W139	4600.3	0.23			0.10
W139	4602.2	0.48			0.55
AK	5465.1	0.37	0.24	0.90	0.21
AK	5467.8	0.23	0.21	0.74	0.15
AK	5478	0.24	0.20	0.73	0.13
AK	5487.2	0.22	0.21	0.42	0.08
AK	5492.1	0.20	0.14	0.44	0.08
AK	5497.7	0.18	0.20	0.43	0.08
AK	5640	0.22	0.13	0.73	0.13
AK	5648.4	0.16	0.11	0.48	0.08
AK	5660.3	0.20	0.19	0.54	0.10
AK	5669.3	0.15	0.11	0.35	0.06

Comment The 1 degree antiscatter slit will be removed at about 12 deg. 2 theta. Configuration=Bracket Flat Stage, Owner=User-1 Goniometer=PW3050/60 (Theta/Theta); Minimum step size Sample stage=PW3071/xx Bracket Diffractometer system=XPERT-PRO	
Used wavelength	
Intended wavelength type:	$K\alpha_1$
$K\alpha_1$ (Å):	1.78901
$K\alpha_2$ (Å):	1.7929
$K\alpha_2/K\alpha_1$ intensity ratio:	0.5
$K\alpha$ (Å):	1.790307
$K\beta$ (Å):	1.62083
Incident beam path	
Radius (mm):	240
X-ray tube	
Name:	PW3376/00 Co LFF DK194062
Anode material:	Co
Voltage (kV):	45
Current (mA):	40
Focus	
Focus type:	Line
Length (mm):	12
width (mm):	0.4
Take-off angle (°):	6.0
Filter	
Name:	Iron
Material:	Fe
Thickness (mm):	0.016
Soller slit	
Name:	Soller 0.04 rad.
Opening (rad.):	0.04
Mask	
Name:	Inc. Mask Fixed 15 mm (MPD/MRD)
Width (mm):	11.6
Anti-scatter slit	
Name:	Slit Fixed 1°
Type:	Fixed
Height (mm):	1.52

Divergence slit	
Name:	Prog. Div. Slit
Distance to sample (mm):	140
Type:	Automatic
Irradiated length (mm):	20
Offset (mm):	0
Diffracted beam path	
Radius (mm):	240
Anti-scatter slit	
Name:	Prog. AS Slit
Type:	Automatic
Observed length (mm):	20
Offset (mm):	0
Soller slit	
Name:	Soller 0.04 rad.
Opening (rad.):	0.04
Detector	
Name:	X'Celerator
Type:	RTMS detector
PHD - Lower level (%):	42
PHD - Upper level (%):	80
Mode:	Scanning
Active length (°):	2.122
Source	
Created by:	XPertUser
Application SW:	X'Pert Data Collector
	vs. 2.2
Instrument control SW:	XPERT-PRO
	vs. 1.9E
Instrument ID:	13030654
Scan	
Scan axis:	Gonio
Scan range (°):	2.0250 - 79.9994
Step size (°):	0.0334
No. of points:	2333
Scan mode:	Continuous
Counting time (s):	59.69

Analytical Spectral Device FieldSpec3

Spectral Range	350-2500 nm
Spectral Resolution	3 nm @ 700 nm 10 nm @ 1400/2100 nm
Sampling Interval	1.4 nm @ 350-1050 nm 2 nm @ 1000-2500 nm
Scanning Time	100 milliseconds
Detectors	One 512 element Si photodiode array 350-1000 nm Two separate, TE cooled, graded index InGaAs photodiodes 1000-2500 nm
Input	1.5 m fiber optic (25º field of view) Optional foreoptics available
Noise Equivalent Radiance (NEdL)	UV/VNIR 1.1 x 10^{-9} W/cm^2/nm/sr @700 nm NIR 2.4 x 10^{-9} W/cm^2/nm/sr @ 1400 nm NIR 4.7 x 10^{-9} W/cm^2/nm/sr @ 2100 nm
Weight	12 lbs (5.2 kg)
Calibrations	Wavelength, reflectance, radiance*, irradiance* All calibrations are NIST traceable (*radiometric calibrations are optional)

http://www.asdi.com/products/fieldspec-3-portable-spectroradiometer

Hi-Bright Contact Probe

Length	10" (25.4 cm)
Weight	1.5 lbs (.7 kg)
Power requirements	12-18 VDC, 6.5 W
Lightsource type/Life (approx.)	Halogen bulb/1500 hours
Halogen bulb color temperature	2901 +/- 10º% K
Spot size	10 mm

http://www.asdi.com/accessories/hi-brite-contact-probe